CHAPTER 1 INTRODUCTION

In this chapter, a review of some electrochemical principles necessary to be considered when one is performing an electrochemical experiment (i.e. mass transport and its modes, and double layer structure) is presented. A review of the theory on electrochemical studies of cobalt inorganic and organometallic compounds, electrochemical flow cells, and a theory of electrocatalysis is also presented.

1.1 PRINCIPLES OF ELECTROCHEMISTRY

The electrochemical reaction is a heterogeneous electron transfer. It takes place at the interface between the electrode and the solution. Only redox active species present at the interface can undergo this electron transfer. The electrochemical reaction at the interface makes the composition in the nearby solution different from the bulk of the solution further away. Because the solution tends to become homogeneous, redox active species diffuse between the bulk and the perturbed zone, in which the reactant is depleted, widens. Convection due to heating or stirring makes the solution rapidly more homogeneous, thus reducing this zone from about 100 μm to less than 1 μm [1].

Unlike most spectroscopic methods, electrochemical measurements are actually made on only a minute fraction of the sample confined to a highly inhomogeneous environment, the electrode-solution interface. The coupling and interplay within this region of such phenomena as interfacial charge transfer, diffusional mass transfer, adsorption, chemisorptions, homogeneous phase chemical reaction, convection and dissolution can cloud the interpretation of electrochemical data and discourage the practically minded analyst. On the other hand, electrochemistry offers an invaluable tool for fundamental investigation of these processes, each of importance in its own right. In either case, the ultimate success of the experimenter will depend on a firm grasp of the underlying physical principles [2].

The interface between an electrolyte solution and an electrode has come to be known as the electrical double layer [2]. The double layer is much thinner than the diffusion layer because it is only a few molecular layers thick. Under the applied potential, the liquid and solid

layers are charged at their interface. Heterogeneity is a common thread binding all electroanalytical methods. The act of placing an electrode in contact with a solution creates a phase boundary that differentiates identical solute molecules into two types; those at a distance from the electrode and those close enough to participate in the fascinating mutual interactions known collectively as electrochemistry. This is not a trivial distinction, for often it is the bulk-phase properties alone which are of analytical concern [2].

Imagine, for example, a positively polarized mercury surface immersed in a solution of sodium chloride. In this case, the positive electrode surface attracts the negative chloride ions because of electrostatic action, van der Waals' forces, and specific chemical effects. As a result, a layer of essentially non-hydrated chloride ions will accumulate very close to the electrode surface, forming what is known as the *inner Helmholtz layer*. Because of the presence of this negatively charged chloride ions, a double layer is said to exist. Just beyond this layer is a second layer of tightly held hydrated chloride ions, a layer that marks the boundary of the *outer Helmholtz layer*. Beyond this a *diffuse layer* extends with a net charge whose ionic atmosphere contains ions of one sign in excess of their normal concentration and those of the other sign in defect [3]. This assemblage of charged layers is commonly referred to as simply the double layer (Fig. 1.1).

The simplest reactions involve only mass transfer of a reactant to the electrode, heterogeneous electron transfer involving non adsorbed species and mass transfer of the product to the bulk solution. Mass transfer, the movement of material from one location in solution to another arises either from differences in electrical or chemical potential at the two locations or from movement of a volume element of solution. The modes of mass transfer are [4]:

1. Migration: movement of a charged body under the influence of an electric field (a gradient of electrical potential).
2. Diffusion: movement of a species under the influence of a gradient of chemical potential (i.e. a concentration gradient).
3. Convection: stirring or hydrodynamic transport. Generally fluid flow occurs because of natural convection (convection caused by density gradients) and forced convection, and may be characterized by stagnant regions, laminar flow, and turbulent flow.

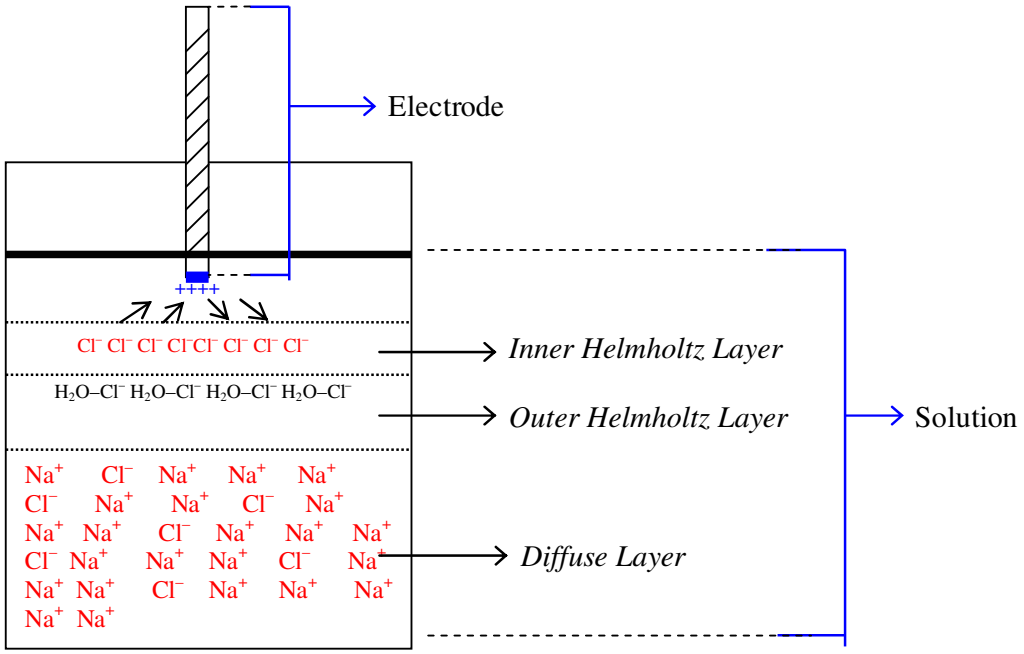

Figure 1.1 Structure of an electrical double-layer.

Mass transfer to an electrode is governed by the Nernst-Planck equation, written for one-dimensional mass transfer along the x-axis as [4]:

$$J_i(x) = -D_i \frac{\delta C_i(x)}{\delta x} - \frac{z_i F}{RT} D_i C_i \frac{\delta \phi(x)}{\delta x} + C_i v(x) \qquad (1.1)$$

where $J_i(x)$ is the flux of species i (mol $s^{-1}cm^{-2}$) at distance x from the surface, D_i is the diffusion coefficient (cm^2 s^{-1}), $\delta C_i(x)/\delta x$ is the concentration gradient at distance x, $\delta \phi(x)/\delta x$ is the potential gradient, z_i and C_i are the charge (dimensionless) and the concentration (mol.cm^{-3}) of species i, respectively, and $v(x)$ is the velocity (cm s^{-1}) with which a volume element in solution moves along the axis. The three terms on the right-hand side represent the contributions of diffusion, migration, and convection, respectively, to the flux [4].

A rigorous solution is generally not very easy when all three forms of mass transfer are in effect; hence electrochemical systems are frequently designed so that one or more of the contributions to mass transfer are negligible. For example, the migrational component can be reduced to negligible levels by addition of an inert electrolyte (a supporting electrolyte)

at a concentration much larger than that of the electroactive species. Convection can be avoided by preventing stirring and vibrations in the electrochemical cell [4].

In the bulk of solution (away from the electrode), concentration gradients are generally small, and the total current is carried mainly by migration [4] where all charged species contribute. For species *j* in the bulk region of a linear mass-transfer system having a cross-sectional area *A*, $i_j = i_{m,j}$

$$i_j = \frac{z^2{}_j F^2 A D_j C_j}{RT} \cdot \frac{\delta\phi}{\delta x} \tag{1.2}$$

where i_j is the current component at any value of *x* arising from a flow of species *j* and $i_{m,j}$ is the migration current of species *j*.

In migration, the driving force responsible for moving the species to (or away from) the electrode surface is the force exerted on a charged particle by a potential gradient existing in the body of the solution. Thus, for example, a potential gradient in an electrolytic solution will cause a current to flow within the body of the solution such that negative species will move one way, positive the other, and neutral species will remain unaffected. The rate of movement of a charged particle depends upon the magnitude of its charge, size, degree of hydration, etc. In conductometric measurements, migration is the sole factor that limits the current. In other cases, such as polarography, it is desirable to eliminate the contribution of migration, and this is accomplished by addition of an excess (about 100-fold) of an inert electrolyte that, in turn, decreases the potential gradient to a value sufficiently small so that diffusion and/ or convection processes becomes current-limiting [3]. In general, it simplifies the mathematical treatment of electrochemical systems by elimination of the $\delta\phi/\delta x$ term in the mass transport equation [4].

Although migration carries the current in the bulk solution during electrolysis, diffusional transport occurs in the vicinity of the electrodes, because concentration gradients of the electroactive species arise there. Indeed, under some circumstances, the flux of electroactive species to the electrode is due almost completely to diffusion [4].

In many respects, the simplest and best understood process influencing electrochemistry is diffusion. Diffusion is a factor virtually in every type of electroanalytical measurement, yet it is most often introduced as a set of elemental laws, devoid of physical significance [2]. This transport mode has its origin in a gradient of chemical potential or, more simply, in a concentration gradient. Thus, if the concentration of the species in the bulk of the solution is greater than its concentration at the electrode surface (because of the electrode reaction), the species will tend to diffuse from the bulk of the solution towards the electrode surface. Whereas the direction of diffusion is from the regions of larger to smaller concentrations, its rate is proportional to the magnitude of the concentration differences and to certain characteristic properties of the diffusing species and medium. Three types of diffusion transport exist, mainly linear, cylindrical and spherical diffusion. Diffusion that takes place in a single direction (diffusion to a plane surface) is termed linear diffusion and is mathematically and experimentally the simplest case [3].

Depending on the size of the electrode and the volume of electrolytic solution used, one can distinguish between three limiting cases of diffusion. The simplest case is an electrode in a thin-layer cell with a very low ratio of cell volume to electrode surface. Under these conditions mass transport within the cell is negligible and diffusion is the only mode of mass transport. By reducing the ratio between the electrode surface and the electrolyte volume, one approximates the normal situation of a voltammetric experiment with semi-infinite planar diffusion. With the transition to extremely small electrode surfaces, the conditions change yet again, and the diffusion process becomes dependent on the size and geometry of the electrode [5].

As one might expect, the voltammetric current-voltage curves of these three cases differ markedly. In the case of a thin electroactive layer, the cathodic and anodic waves appear as perfect mirror images. “Normal” electrodes produce the characteristic cyclic voltammograms, and extremely small electrodes (ultramicroelectrodes) yield steady-state current-voltage curves, which resemble the classic polarograms as well as the current-voltage curves of rotating electrodes (Figure 1.2) [5].

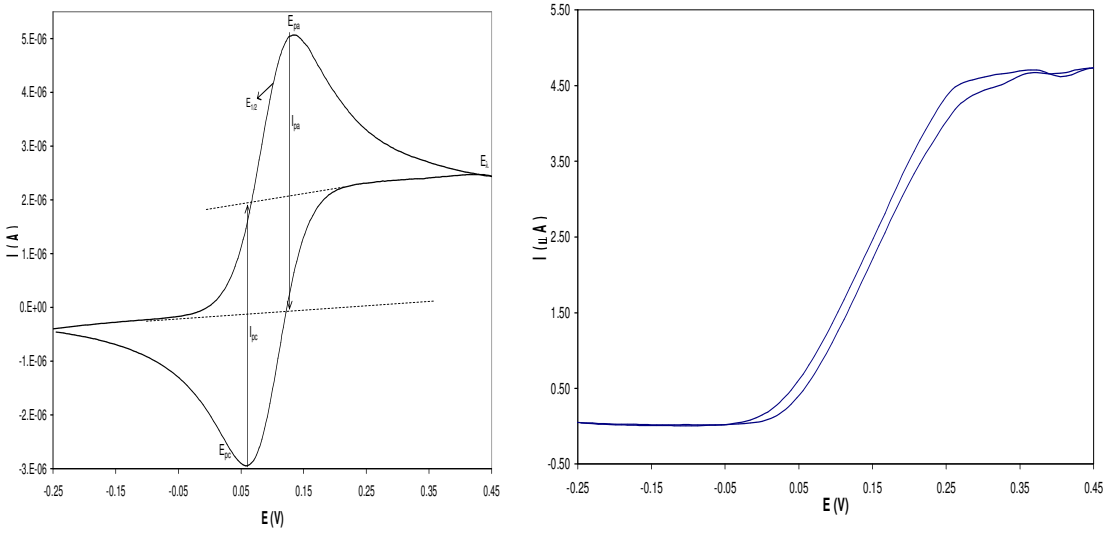

Figure 1.2 Typical voltammetric current-voltage curves. Left: for a semi-infinite diffusion obtained using a "normal" electrode; right: for semi-infinite hemispheric diffusion obtained using extremely small electrodes (ultramicroelectrodes). E_λ = switching potential, $E_{1/2}$ = half-wave potential, E_{pa} and E_{pc} = anodic and cathodic peak potential, I_{pa} and I_{pc} = anodic and cathodic peak current. A typical curve obtained in thin-layer solution can be obtained from Ref [5].

Convection is accomplished whenever the solution bearing the species is stirred into the path of the electrode. This is often called hydrodynamic transport. This stirring action increases the rate of transport of the species to the electrode and quantitative treatment of this mode of mass transport is exceedingly difficult. Convection is frequently employed in electroanalytical techniques (examples include the rotating electrode, mercury electrodes, vibrating electrodes, and even the stirring action employed at the working electrode in coulometric titrations, etc.), because of its increased sensitivity. Frequently one must resort to the use of empirical expressions in the interpretation of these techniques [3].

1.2 ELECTROCHEMISTRY OF COBALT INORGANIC AND ORGANOMETALLIC COMPOUNDS

Most electrochemical studies of cobalt were mainly for analytical purposes; simultaneous determinations of cobalt, nickel, copper and so on were shown to be possible by using complexing agents. The modern trend in the field of polarography of cobalt was to establish the relationship between the structures or bonding types of cobalt complexes and their electrode processes; this was because cobalt complexes, among transition metal complexes, are large in number and exhibit substantial variety in their bonding nature from compound

to compound. In these studies, non-aqueous polarography attracted special attention and promised to provide clues for the elucidation of electron transfer mechanisms of the electrode reactions and their correlation to the electronic configuration of a great variety of mixed ligand complexes [6].

The most striking feature of non-aqueous polarography is that, by adopting aprotic non-aqueous solvents, the Co(III) complexes, which would otherwise lead to a loss of ligands in the lower oxidation states of cobalt, are reduced in a stepwise fashion with a complete retention of the original configuration. For example, the pathway Co(III) → Co(II) → Co(I) → Co(0) takes place without a loss of ligands in aprotic solvents, although the appropriate valence orbital are, of course, delocalized over the entire complex molecule [6].

Voltammetric techniques such as current-controlled oscillopolarography, cyclic voltammetry, controlled-current or –potential electrolytic studies, and investigations of anodic oxidation have attracted much attention in the field of electrochemistry of cobalt as powerful tools, along with classical or conventional polarographic and chronopotentiometric studies, for probing the redox processes of the Co(III)/Co(II) and Co(II)/Co(I) couples in solution. This is partly because a number of electrode processes of an inert-inert type with π-electron systems, which were recently discovered for π-bonded cobalt complexes in organic solvents, made it possible to follow structurally the fate of the electrolyzed cobalt complexes in solution, not only in the reduction process but also in the counter process of oxidation with auxiliary instrumental methods of measurements such as ESR, NMR and magnetic susceptibility [6].

The electrode processes of the completely “inert-inert” or “inert-labile” types are the ones in which it is easiest and simplest to determine the assignments of the polarographic waves. The terms “inert” and “labile” are used with regard to the “lability” of ligands bound to the cobalt towards solvolysis, i.e., the ligand exchange reactions with solvent molecules, whilst the terms as defined by Taube [7] are independent of the nature of the medium. For either extreme case this consists of the complex remaining structurally intact or, alternatively, undergoing a rapid dissociative equilibrium upon reduction. Moreover, the complete retention of the structures in non-aqueous media makes it possible to relate the structures in both the oxidized and reduced forms to the redox reaction of the electrode processes. For this reason cyclic voltammetry or controlled-current oscillopolarography are powerful

methods not only for the examination of the reversibility of the electrode reaction, but also for the identification of the cobalt species responsible for the conventional polarographic waves. Here the interpretation is facilitated because the cathodic reductions can be observed and compared with the anodic oxidations in the same experiment [6].

The electrochemical studies of cobalt complexes with tetraphenylporphirins (TPP) are well documented in the literature [6, 8–13]. The electrochemical behaviour of cobalt (II) complexes with tetraphenylporphirins was studied by cyclic voltammetry. The [Co^{II}TPP] complex and its products, which were obtained by its controlled-potential electrochemical oxidation, were studied by electrochemical spin resonance (ESR) spectra. The first oxidation occurred at E_p = + 0.52 V, on the central Co(II) atom and all subsequent oxidations occurred at the TPP ligand. The potentials of the central cobalt (II) oxidation showed a linear dependence on the third ionization potential of the ion, whereas the ligand oxidation potentials were approximately independent of the cobalt (II) ion. This distinguishes between the cobalt oxidation change and ligand oxidation [6, 8]. Cyclic voltammogram distinctly showed three one-electron reversible steps [8]:

$$[Co^{II}(TPP)] \xleftrightarrow{+0.52\,V} [Co^{III}(TPP)]^{+} \quad (1.3)$$

$$[Co^{III}(TPP)]^{+} \xleftrightarrow{+1.19\,V} [Co^{III}(TPP)]^{2+} \quad (1.4)$$

$$[Co^{III}(TPP)]^{2+} \xleftrightarrow{+1.42\,V} [Co^{III}(TPP)]^{3+} \quad (1.5)$$

On the other hand, the free ligand H_2TPP gave two one-electron irreversible oxidation steps [8]:

$$[H_2TPP] \xleftrightarrow{+1.00\,V} [H_2TPP]^{+} \xleftrightarrow{+1.20\,V} [H_2TPP]^{2+} \quad (1.6)$$

The voltammetric behaviour of cobalt (II) with chloro-N-methyl-$\alpha,\beta,\gamma,\delta$-tetraphenylporphirins ($ClNCH_3TPP$) was studied by cyclic voltammetry [9]. The half-wave potentials for the reversible metal oxidation in acetonitrile occurred at 0.77 V for Co(II) – Co(III) (all $E_{1/2}$ values were reported vs. Ag | AgCl). Following the oxidation of the metal centre, the porphirin ligands were oxidized. The half-wave potentials for oxidation of the tetraphenylporphirin ligand in $ClNCH_3TPP$ occurred at 1.30 and 1.60 V. The ligand oxidations for the N-methyltetraphenylporphirin complexes in general were found at E_p

values of 1.2 – 1.3 and 1.4 – 1.6 V. The cyclic voltammogram of the corresponding zinc (II) complex was recorded to verify the assignment of metal centre and ligand oxidation. The oxidation of the ClZnN-CH_3TPP complex occurred at 1.05 and 1.5 V with no wave appearing in the region 0.0 – 0.9 V. Cyclic voltammetry of $\alpha,\beta,\gamma,\delta$-tetraphenylporphinatocobalt (II) in benzonitrile with 0.10 M tetraphenyl ammonium perchlorate gave the values $E_{1/2}$ = 0.50 V [Co(II) – Co(III)], 1.19 V (ligand oxidation), and 1.6 V (ligand oxidation) [9], agreeing reasonably with the literature values of 0.52 V, 1.19 V and 1.42 V [8].

The electrochemistry of five- and six-coordinate cobalt (III) δ-bonded porphyrins was reported in pyridine (py), tetrahydrofuran (THF), and methylene chloride (CH_2Cl_2) containing 0.1 M tetrabutyl ammonium perchlorate (TBAP) or 0.1 M tetrabutyl ammonium hexafluorophosphate ($TBAPF_6$) as supporting electrolyte [10]. Each complex undergoes up to two reductions and two oxidations, all of which occur at the porphyrin π ring system. Cyclic voltammogram of (TPP)Co(CH_3) and (TPP)Co(CH_2Cl_2) each revealed two reversible one-electron oxidations and a single one-electron or multi-electron reduction within the potential range of the solvent. The singly reduced (TPP)Co(CH_2Cl) and (TPP)Co(C_2H_5) complexes were stable in THF, but this was not the case for (TPP)Co(CH_3), which revealed two one-electron waves in this solvent. Electrooxidized, (TPP)Co(CH_3) and (TPP)Co(CH_2Cl) were relatively stable in CH_2Cl_2 on the conventional cyclic voltammetry time scale, and both neutral derivatives were characterized by two well-defined one-electron oxidations at potentials of 0.96 and 1.19 V. Cyclic voltammogram of (TPP)Co(C_2H_5)(py) in pyridine showed one irreversible oxidation at E_p = 0.81 V and one irreversible reduction at E_p = – 1.49 V leading to the formation of $[(TPP)Co(py)_2]^+$ and $[C_2H_5N(C_2H_5)]^+$ [10].

Cyclic voltammetry and controlled-potential electrolysis were used to investigate the electrochemical reduction of $CoBr_2$ in dimethylformamide (DMF) and DMF + pyridine mixtures [14]. Cyclic voltammogram of $CoBr_2$ at a platinum electrode displayed an irreversible reduction wave at – 1.17 V versus SCE. The reduction of Co(II) led to a Co(I) species at – 1.4 V. On the time scale of slow cyclic voltammetry or of an electrolysis, Co(I) led to solid Co(0) and Co(II) by disproportionation. The regeneration of Co(II) was effective until its total consumption, which required two electrons per molecule. After the scan rate was increased, a second reduction wave appeared at – 1.75 V, and it was assigned to the product generated at – 1.4 V. As the scan rate was increased, the disproportionation reaction

was progressively kinetically frozen and more Co(I) remained in the diffusion layer when its reduction potential was reached (E = – 1.75 V), the reduction of Co(I) also led to solid Co(0). The electrochemical reactions were as follows [14]:

E = – 1.4 V: E $Co^{II}X_2 + e^- \leftrightarrow Co^{I}X + X^-$ (1.7)

C $2Co^{I}X \rightarrow Co(s) + Co^{II}X_2$ (1.8)

E $Co^{II}X_2 + e^- \leftrightarrow Co^{I}X + X^-$ (1.9)

E = – 1.75 V: $Co^{I}X + e^- \rightarrow Co(s) + X^-$ (1.10)

The electrochemical behaviour of $CoBr_2$ was also studied in acetonitrile and pyridine mixtures in the presence of allyl acetate (1 molar equivalent vs. $CoBr_2$) and increasing amounts of ethyl 4-iodobenzoate [15]. In the absence of aromatic halide the voltammogram exhibited two successive reduction waves. The first wave occurred at -1.3 V ascribed to the reduction of Co(II) to Co(I) followed by fast complexation with allyl acetate which led to (η^2-allylOAc)cobalt(I), the latter complex being more stable than the original Co(I) and giving rise to a reoxidation wave Co(II). The resulting (η^2-allylOAc)cobalt(I) was reduced at the second reduction wave E_p = -1.5 V to (η^2-allylOAc)cobalt(0). In the presence of ethyl 4-iodobenzoate, the intensity of the wave at -1.3 V increased and reached a maximum (twice the initial intensity), and the oxidation wave for Co(II) decreased [15].

The first oxidative electrochemistry of cobalt (III) corroles was reported in THF, DMF, benzonitrile (PhCN), and CH_2Cl_2 containing 0.10 M TBAP as supporting electrolyte [16]. The investigated compound was represented as (OMC)Co(PPh_3) where OMC was the trianion of 2,3,7,8,12,13,17,18-octamethyl corrole. The CV of the complex revealed up to three oxidations and two reductions waves depending upon solvent. The (OMC)Co(PPh_3) complex revealed three one-electron reversible oxidations in PhCN at high scan rate, the number of abstracted electrons was calculated by controlled-potential coulometry as well as by analysis of the current-voltage curves obtained by cyclic voltammetry. The first oxidation occurred at 0.19 V in PhCN while the latter two processes occurred at 0.76 and 1.54 V. The first two one-electron waves were reversible at all scan rates, but the third oxidation became irreversible at lower scan rates (0.5 V/s). (OMC)Co(PPh_3) complex showed three one-electron oxidations in CH_2Cl_2, at 0.18 V, 0.80 V and 1.68 V. (OMC)Co(PPh_3) complex showed two one-electron oxidations in THF and DMF at 0.30 V,

0.80 V (THF) and 0.25 V, 0.83 V (DMF) respectively. The electrochemical reactions were as follows [16]:

$$(OMC)Co^{III}(PPh_3) \leftrightarrow [(OMC)Co^{III}(PPh_3)]^{+} + e^{-} \quad (1.11)$$

$$[(OMC)Co^{III}(PPh_3)]^{+} \leftrightarrow [(OMC)Co^{III}(PPh_3)]^{2+} + e^{-} \quad (1.12)$$

$$[(OMC)Co^{III}(PPh_3)]^{2+} \leftrightarrow [(OMC)Co^{III}(PPh_3)]^{3+} + e^{-} \quad (1.13)$$

Complexes of (5,10,15-tri-X-phenyl-2,3,7,8,12,13,17,18-octamethylcorrolato)cobalt(III) triphenylphosphine, (OMTX-PC)Co(PPh_3), where X = *p*-OCH_3, *p*-CH_3, *p*-Cl, *m*-Cl, *m*-F, *o*-Cl, *o*-F, or H, were synthesized and characterized in non-aqueous media using electrochemical, spectroelectrochemical, and EPR techniques [17]. Each cobalt (III) derivative showed two one-electron reductions, the first of which involved a Co(III)/Co(II) conversion and concomitant loss of the bound PPh_3 ligand. Four one-electron oxidations were also observed for the investigated compounds, and this contrasts with the oxidative properties of related cobalt (II) porphyrins which revealed a maximum of three one-electron oxidation waves under similar conditions. The first one-electron oxidation of each cobalt(III) corrole was metal-centred and resulted in formation of Co(IV) corrole as ascertained by EPR spectroscopic characterization of the electrogenerated species [17].

The fact that Co(III) corroles can undergo four one-electron oxidations was not previously reported, but presumably this reaction might also occur for (OMC)Co(PPh_3) at very positive potentials, i.e., at values of $E_{1/2}$ greater than 1.9 V vs. SCE in 0.2 M TBAP in PhCN [17]. The fourth oxidation of (OMTXPC)Co(PPh_3) was quasi-reversible for all eight compounds investigated in that study, and this reaction was not examined in detail due to its proximity to the anodic potential limit of the solvent. However, comparison of cyclic voltammograms of (OMT*p*-ClPC)Co(PPh_3) [$E_{½}$ = 0.31, 0.85, 1.45, and 1.8 V] and (T*p*-ClPP)Co(PPh_3) [$E_{½}$ = 0.30, 1.2, and 1.5 V] seemed to rule out the forth oxidation state as involving the bound phosphine ligand, since the fourth oxidation state was not present on a cyclic voltammogram of (T*p*-ClPP)Co(PPh_3). Further comparison of the (OMT*p*-ClPC)Co(PPh_3) and (T*p*-ClPP)Co(PPh_3) voltammograms showed that the first one-electron oxidation of both macrocycles occurred at virtually the same potential, i.e., + 0.31 V for the corrole and + 0.30 V for the porphyrin. The first oxidation of the neutral porphyrin corresponded to the

Co(II)/Co(III) electrode reaction, while that of the corrole was assigned to the Co(III)/Co(IV) reaction [17].

Complexes of the type [Co(CO)L(η-C_5H_5)] (where L = $P(C_6H_{11})_3$ or PPh_3) were studied by cyclic voltammetry and shown to undergo one-electron oxidation to the radical cations $[Co(CO)L(\eta\text{-}C_5H_5)]^+$. The CV of the complex [Co(CO){$P(C_5H_{11})_3$}(η-C_5H_5)] showed a reversible one-electron oxidation in CH_2Cl_2 at a platinum electrode [18]. The other compounds studied were similarly well behaved except for [Co(CO)(PPh_3)(η-C_5H_5)] which displayed a tendency to deposit a film on the platinum electrode during oxidation in CH_2Cl_2. For this compound the electrode had to be cleaned after every scan; the oxidation potential, $E°$, was estimated at 0.13 V. In THF the voltammetry was cleaner ($E°$ = 0.21 V) but the oxidation was not as chemically reversible. In addition, there was a second irreversible wave at 0.75 V, which was not present in CH_2Cl_2. Since the new wave was peculiar to THF it was believed to be due to the oxidation of the solvated radical cation $[Co(CO)(PPh_3)(THF)(\eta\text{-}C_5H_5)]^+$ to the diamagnetic dication [18].

The compound $[Co(CO)_2(\eta\text{-}C_5H_5)]$, was also studied in the presence of added $[Fe(\eta\text{-}C_5H_5)_2][PF_6]$. When $[Fe(\eta\text{-}C_5H_5)_2][PF_6]$ ($E°$ = 0.43 V) was added to $[Co(CO)_2(\eta\text{-}C_5H_5)]$ ($E°$ ~ 0.97 V) in CH_2Cl_2, no reaction occurred on the basis of $E°$ values [18]. In the presence of PPh_3, however, rapid oxidation occurred at room temperature to give $[Co(PPh_3)_2(\eta\text{-}C_5H_5)][PF_6]$. It must be noted that neither the ferricinium ion nor the dicarbonyl undergone detectable reactions with PPh_3 at room temperature. This means that the formation of $[Co(PPh_3)_2(\eta\text{-}C_5H_5)][PF_6]$ must, therefore, occur via the mechanism shown in equation 1.14 to 1.16 below [18].

$$[Co(CO)_2(\eta - C_5H_5)] + PPh_3 \leftrightarrow [Co(CO)(PPh_3)(\eta - C_5H_5)] + CO \quad (1.14)$$

$$[Co(CO)(PPh_3)(\eta - C_5H_5)] \leftrightarrow [Co(CO)(PPh_3)(\eta - C_5H_5)]^+ \quad (1.15)$$

$$[Co(CO)(PPh_3)(\eta - C_5H_5)]^+ + PPh_3 \leftrightarrow [Co(PPh_3)_2(\eta - C_5H_5)]^+ + CO \quad (1.16)$$

Electrochemical behaviour of $[\{Co(\mu\text{-}NO)(\eta\text{-}C_5H_5)\}_2][PF_6]$ was obtained in CH_2Cl_2 by cyclic voltammetry [19]. The compound was reduced to $[\{Co(\mu\text{-}NO)(\eta\text{-}C_5H_5)\}_2]$ at 0.34 V, and oxidized to $[\{Co(\mu\text{-}NO)(\eta\text{-}C_5H_5)\}_2]^{2+}$ at 1.17 V. The cyclic voltammogram also showed a second, irreversible, reduction wave at – 1.40 V. However, the peak current appeared

larger than those of the other redox processes described above, but the wave was close to that of the base electrolyte and may correspond to the initial formation of $[\{Co(\mu\text{-}NO)(\eta\text{-}C_5H_5)\}_2]^-$. In the presence of PPh_3, $[\{Co(\mu\text{-}NO)(\eta\text{-}C_5H_5)\}_2]$ was un-reactive but underwent instant metal-metal bond cleavage to give $[Co(PPh_3)(NO)(\eta\text{-}C_5H_5)]^+$. The voltammogram of $[\{Co(\mu\text{-}NO)(\eta\text{-}C_5H_5)\}_2][PF_6]$ revealed a one-electron reduction wave at 0.34 V corresponding to the couple $[\{Co(\mu\text{-}NO)(\eta\text{-}C_5H_5)\}_2]^+ - [\{Co(\mu\text{-}NO)(\eta\text{-}C_5H_5)\}_2]$. On adding one equivalent of PPh_3 a reaction occurred to give an orange-brown solution, a voltammogram showed another wave at – 0.43 V, due to the irreversible one-electron reduction to $[Co(PPh_3)(NO)(\eta\text{-}C_5H_5)]^+$ [19].

The halogen-bridged tricobalt clusters, $[Co_3Cp_3(\boldsymbol{\mu}_3\text{-}CPh)_2(\boldsymbol{\mu}\text{-}Cl)]PF_6 \cdot MeCN$ (**2**), $[Co_3Cp_3(\boldsymbol{\mu}_3\text{-}CPh)_2(\boldsymbol{\mu}\text{-}Br)]SbF_6$ (**3**), and $[Co_3Cp_3(\boldsymbol{\mu}_3\text{-}CPh)_2(\boldsymbol{\mu}\text{-}I)]SbF_6 \cdot CH_2Cl_2$ (**4**), were obtained from a reaction of a benzylidyne-capped tricobalt cluster, $[Co_3Cp_3(\boldsymbol{\mu}_3\text{-}CPh)_2]$ (**1**), with halogens ($X_2 = Cl_2$, Br_2 and I_2) in CH_2Cl_2. The compounds were characterized by X-ray diffraction, UV-Vis absorption spectra and cyclic voltammetry [20]. In a cyclic voltammogram of **1** in 0.1 M BuNCl/MeCN an oxidation wave was observed at $E_{pa} = -0.01$ V, for the oxidation of **1** to $\mathbf{1}^+$. On scan reversal an irreversible reduction wave appeared at $E_{pc} = -0.45$ V. The complexes, $\mathbf{2}^+$, $\mathbf{3}^+$, and $\mathbf{4}^+$ were studied by CV in CH_2Cl_2 with 0.1 M Bu_4NPF_6. In the oxidation of $\mathbf{2}^+$, a chemically reversible oxidation wave was observed at E_{pa} = 0.75 V versus Fc/Fc^+. Very similar oxidation waves to those of $\mathbf{2}^+$ were observed for $\mathbf{3}^+$ and $\mathbf{4}^+$. In the second scan, new redox waves were observed at $E_{pa} \sim 0.0$ V, which indicated that the oxidized species of **2** and **3** decompose slowly on a CV time-scale. In CH_3CN, $\mathbf{4}^+$ showed similar redox responses to those observed in CH_2Cl_2, but the oxidation waves of $\mathbf{2}^+$ and $\mathbf{3}^+$ were irreversible showing an E_{pa} of 0.71 and 0.72 V, respectively [20]. Reduction processes of the complexes in CH_2Cl_2 also resemble each other. An irreversible reduction wave was observed in the potential region of – 0.57 to – 0.60 V. The irreversible reduction of each complex exhibited a new chemically reversible redox couple at $E_{1/2} = -0.05$ V, which was the same as the oxidation potential of **1**. These results suggested that the reduction of the halogen-bridged complex reproduced the parent complex **1** [20].

The electrochemical properties of the redox mediator Co(III)/Co(II)$(dbbip)_2$ (dbbip = 2,6-bis(1'-butylbenzimidazol-2'-yl)pyridine) in a mixed acetonitrile/ethylene carbonate solvent have been studied by a range of techniques in order to determine the rate constants for electron transfer and the diffusion coefficients of the Co(II) and Co(III) species [21]. Cyclic

voltammogram of Co(II)$(dbbip)_2^{2+}$ in a mixture of 60 % ethylene carbonate/40 % acetonitrile at a Pt disk electrode revealed a quasi-reversible electrode process at E_p = 0.39 V, assigned to the couple Co(III)/Co(II). A plot of the peak current density, $j_{p,ox}$ versus the square root of the scan rate was used to estimate the diffusion coefficient of the Co(II) complex. The plots gave a value of 1.9×10^{-6} cm^2s^{-1} for the diffusion coefficient of the bulky Co(II)$(dbbip)_2^{2+}$ in the mixed solvent. The diffusion coefficient of Co(III) complex ion was obtained using Fick's first law and found to be equal to 1.1×10^{-6} cm^2/s^{-1} [21].

The electrochemical behaviour of monomeric [$Co_2(CO)_6$(alkyne)] derivative is well known [22]. At room temperature a one-electron diffusion controlled reduction process occurred at E_p = – 1.0 V and was followed by a fast chemical complications in CH_2Cl_2 at a Pt electrode. The chemical reversibility of the first process was enhanced by electron-withdrawing substituents (e.g. CF_3) or, to a lesser extent, by sterically demanding alkyne substituents [22]. At ambient temperatures [{$Co_2(CO)_6$}$_2$(PhC≡C–C≡CPh)] in CH_2Cl_2 the complex undergone an apparent single two-electron reduction at E_p = – 0.94 V and another ill-defined reduction wave was observed further at less negative potentials of ~ – 1.16 V. It was found that a fast chemical decomposition following the reduction prevented proper electrochemical analysis. It was also found that the two-electron peak at – 0.94 V gradually split into two one-electron peaks as the temperature was lowered. At – 80 °C both waves became reversible, as chemical complications were completely quenched, so that full chemical reversibility was achieved, as shown by the directly associated re-oxidation peaks [23].

1.3 THEORY OF ELECTROCHEMICAL FLOW CELLS

Detectors based on interactions between matter and an electrical current are another group of major detection systems in FIA [24]. Electrochemical detection relies on the transfer of electroactive species to the sensing surface. Because the sensor can only respond to species in its vicinity, their concentration should be representative of the average concentration in the bulk sample. This is strongly dependent on the characteristics of the hydrodynamic system and flow–cell used. Thus, the flow should be fully uniform, pulse–free, and the contact time of samples and standards with the sensor should be exactly the same. Kinetic

discrimination of any side reactions taking place at the sensor surface has a very favourable effect on selectivity [24].

The main assets of these detectors are their high sensitivity and selectivity which they exhibit over wide concentration ranges [24]. Unlike optical detectors, they measure no solution property, but rather respond to phenomenon occurring at the electrode surface; as a result, they are better candidates for miniaturization. Electrochemical detectors are compatible with a wide variety of cell shapes and volumes. Thus, some electrodes are embedded in the cell walls, other planar electrodes are adhered to them, and still others are of the open tubular type. Electrochemical flow cells are just as varied. They include the early cascading models, commercially available electrodes and recent designs with built–in electrodes. Also, electrodes can be placed in various positions (in the cavity, aligned with the flow direction, in combination with others such as ion–selective sensors for multi-determinations, etc.). In any case, the point measurement provided by electrodes should be representative of the mean analyte concentration in the sample [24].

The flow through electrochemical cell designed by Burguera and co-workers [25] was made from a polyethylene vial (45 cm long × 0.8 cm diameter filled with glass marbles) with an effective volume of 0.5 ml. Two parallel glassy carbon rods with a total surface of 1.5 cm^2 and of 2.0 cm^2 were used as working and counter electrodes, respectively. Between them, a 1.3 cm long Pt wire was inserted as a pseudo-reference electrode. To further reduce the inner volume of the cell to 0.5 ml, its body was filled with glass marbles of 2.0 mm of diameter [25].

A multianalyte flow electrochemical cell for boianalysis was constructed by Maestre and co-workers [26]. The upper and bottom parts of the cell were constructed from poly(methyl methacrylate), providing high-level precision for the assembly of both surfaces. The dimensions of the cell were 45 mm × 45 mm × 35 mm. A polyetheretherketone (PEEK) plastic gasket (0.10 mm thickness) between both parts determined a cell dead volume of 70 µL. The six working electrodes and the reference electrodes were located in the upper part. The inlet and the six outlets, corresponding to each working electrode, were placed in the bottom part of the cell. The radial arrangement of the working electrodes, all of which were equidistant from the inlet, guaranteed a laminar and identical hydrodynamic flow regime at the six electrodes. Next to each working electrode, but at the bottom block, the six outlets

were placed to prevent cross-talk from occurring and also to help contributing to identical hydrodynamic pressure across the electrodes. The location of the reference electrode, as well as the dimensions of the two platinum counter electrodes, prevented inadequate conductance of the cell solution. The reference electrode was an $Ag/AgCl_{sat}$ of the double liquid junction type. The refillable outer electrolyte solution served as salt bridge to prevent contamination of the reference element. This reference electrode was placed equidistantly from each working electrode [26].

A wall-jet electrochemical detector was designed and characterized by Jaenicke and co-workers [27]. The cell was manufactured from Perspex with an internal volume of ~ 4 cm^3. The working electrode was a glassy-carbon disk 3.0 mm diameter and 2.0 mm thickness (Tokai, Tokyo) which was press-fitted in a Teflon holder using an epoxy resin seal. The electrode was prepared by first polishing with abrasive paper (# 1200) followed by a final polish using 0.3 µm diamond paste until a mirror finish was obtained. A graphite disk (Johnson Matthey) with the same dimension as that of the working electrode was used as counter electrode. The reference electrode was Ag │AgCl │saturated KCl with a 'Dycor' polymer frit (Priceton Applied Research) as a liquid junction [27].

A modified Z-type flow-through cell for optical, electrochemical, and optoelectrochemical flow injection analysis measurements was designed and constructed by Haghighi and co-workers [28]. The body of the flow-through cell was machined from a block of Plexiglas. The flow cell had a 1 mm i.d. and was 20 or 10 mm long, so the volume of the cell was 16 or 8 µl, respectively. Two platinum sheets (0.1 mm thick) were placed on both ends of the flow cell. A 1 mm i.d. hole was provided in each of these platinum sheets for transmission of light. Both ends of the cell cavity were enclosed by two transparent glass windows. The two platinum sheets were used as working and auxiliary electrodes with an electrochemically active area of approximately 3 mm^2. The reference electrode, a saturated calomel electrode (SCE), was placed downstream in an overflow tube. The cell holder was made of aluminium and was designed on the basis of the shape of the cell compartments of the spectrophotometer. For spectrophotometric measurements in which organic solvent was passed through the flow cell, the body of the flow cell was machined from stainless steel [28].

The home-made electrochemical flow-through cell was designed and modified for flow injection analysis system by Masawat and co-workers [29]. The materials used were polymethylmethacrylate or Perspex (A.C.S. Xenon Company Ltd, Thailand) as a working block (19 mm thickness), stainless steel (Sahakol Machining, Chiang Mai, Thailand) as an auxiliary block, home-made poly(ethyleneterephthalate) or PET (23 – 25 µm thickness) as a spacer or gasket, 5H and 2B pencil lead (2 mm in diameter, Steadtler®) with only 5 mm each in length of pencil lead was connected with silver wire (1 mm in diameter, 5 cm in length) using conductive epoxy (Chemtronics®, USA) so that electrical contact can be made to the pencil lead working electrode, and a 1 mm in diameter, 5 cm in length of silver wire (99.9%, Prolabo, France) as a reference electrode. The Perspex body was drilled in the centre and then was inserted with a piece of pencil lead which was drilled in the small length at the other end. The silver wire was covered at one end with a small amount of conductive epoxy and was inserted immediately into the drilled hole to connect with a piece of pencil lead, then another silver wire was inserted in the drilled hole of Perspex body near the one which was inserted first [29].

A simple and versatile cell suitable for spectroscopic and spectroelectrochemical studies in the ultraviolet, visible, and infrared regions has been described [30]. Among the cell's generally beneficial traits are its continuously adjustable path length, high degree of chemical compatibility, ease of assembly and disassembly, and wide spectra range. Regarding SEC applications, the cell permits adequate control of the OTE (optically transparent working electrode) potential and exhibits a relatively short exhaustive electrolysis time. The cell body was constructed from threaded glass connectors and a Teflon stopcock assembly purchased from Ace Glass, Inc. The minimum liquid sample volume of the cell is ~10 mL when the minimum path length configuration is employed. A 10 mm × 13 mm platinum screen (Aesar, 80-mesh) welded to a Pt lead at the end of a sealed Pyrex tube was employed as the OTE in spectroelectrochemical studies. Platinum auxiliary and quasi-reference electrodes were isolated in fritted Pyrex tubes (Ace Glass, C porosity) [30].

Economou and co-workers have designed a thin layer electrochemical cell with a flow channel thickness of 0.2 mm, for the detection of Co(II) by chemiluminescence [31]. The flow cell consisted of a glassy carbon rod (3 mm in diameter) as a working electrode, a home-made Ag/AgCl as a reference electrode positioned opposite a working electrode and a

glassy carbon rod as a counter electrode was positioned downstream, near the outlet of the cell [31].

On-line electrochemistry/mass spectrometry was used to study the complex mechanism of electrochemical oxidation of N,N-dimethyl-p-phenylenediamine in aqueous electrolytes in the pH range 1.4 – 9.7 using a radial flow electrochemical cell [32]. The electrochemical flow cell consisted of two cylindrical Delrin blocks separated by a 50 µm Teflon spacer. The electrochemical flow cell consisted of a Pt disk electrode (1.6 mm diameter) as a working electrode pressed into the lower block. The electrolyte flowed in a radial, inward direction. The auxiliary and reference electrodes were both Ag | AgCl | 1 M KCl aqueous electrodes separated from the flow of the electrolyte by 2 µm PEEK frits. The volume of the compartment of the working electrode, which was the volume of electrolyte located between the working electrode and the wall of the central tube, was only 0.1 µL [32].

An electrochemical cell was developed to enable flow analysis with voltammetric detection using a hanging mercury drop electrode (HMDE) [33]. The flow cell was made from a piece of cylindrical extruded acrylic (Perpex) with a length of 2.5 cm and a diameter of 1.5 cm. The cylindrical piece was flattened at the bottom to allow the positioning of a Teflon support with a mirror for visual inspection of the mercury drop. A flow-channel was drilled through the Perpex with a diameter of 0.7 mm and a length of 1cm (volume 4 µL). The capillary of the working electrode was inserted in the flow cell from the top, perpendicular to the reference and counter electrodes. The reference electrode was a silver wire (1 cm length; 0.5 mm diameter) and the chloride in the seawater was used as a counter ion. The counter electrode was a platinum wire (1 cm length; 0.46 mm diameter). The counter electrode and reference electrode were inserted in 3 mm diameter nylon 6-6 screws and screwed into the Perpex cell with holes leading to the flow-cell [33].

The voltammetric flow cell was designed for operation in a manner compatible with FIA [34]. The flow cell was machined from a 7-mm thick Perspex plate. It had a volume of < 4 µL and accommodated three electrodes: the working electrode was a mercury hemisphere which protruded from the bottom of the flow channel; the reference electrode consisting of a Ag | AgCl wire bathed in saturated potassium chloride was placed in a Pasteur pipette with an asbestos fibre junction; the auxiliary electrode was a stainless steel syringe needle which also served as solution outlet. A suction pipette with an asbestos fibre junction; the auxiliary

electrode was held in place by a screw and silicone rubber washer. The distance between the inlet and the surface of the working electrode (*d*, ca. 3 mm) was a critical parameter and was, therefore, kept constant during all experiments [34].

Janata and co-workers have designed a flow-through cell and characterized it using the combination of FIA and cyclic voltammetry [35]. The flow cell consisted of a mercury microelectrode as a working electrode, a Ag | AgCl (in saturated KCl) as a reference electrode, a steel rod tube as an auxiliary electrode and outlet, a sample inlet, a mercury reservoir, and drop-size adjustment. The microelectrode was placed just below the orifice of the inlet tube. This arrangement ensured that any part of the sample plug comes into contact with the electrode surface only once. The replacement of the mercury drop was done by simply gently knocking off the old drop and then forming a new drop. The used up mercury was allowed to accumulate at the bottom of the cell compartment from where it was removed periodically [35].

1.4 THEORY OF ELECTRON TRANSFER CHAIN (ETC) CATALYSIS (ELECTROCATALYSIS) REACTIONS

Electrocatalysis or electron transfer chain (ETC) catalysis is the catalysis of reactions by electrons without net current flow (as opposed to redox catalysis, which means catalysis of reduction or oxidation by redox mediators, thus involving a net current flow) [36]. The theory of electrocatalysis was first applied to an organometallic system by Feldberg, who also set up the method of finite differences for the computer simulation of kinetic analysis of the electrochemical data [37].

ETC catalysis has been shown to be a very efficient way to perform organic, inorganic and organometallic reactions such as ligand exchange, isomerization, chelation, decomplexation, insertion, extrusion, and oxidative addition. The coupling of electrocatalysis with organometallic catalysis was also shown to be efficient for alkyne polymerization. The simplest organometallic reaction, ligand exchange, has been the most studied one [36].

Electrocatalysis has been efficiently practiced using either an electrode in a preparative electrolysis cell or a redox reagent as an initiator (electrocatalyst). It is thus extremely useful

to have at hand a library of redox reagents and knowledge of their redox potentials [38]. The chain induction can be affected by an oxidant (anode, 17e complex such as ferricinium, organic or inorganic oxidant) or by a reducing agent (cathode, 19e complex such as Cp_2Co or $CpFe(C_6R_6)$ (R = H or Me), or organic or inorganic reducing agent). Ligand exchange reactions have been electrocatalyzed for mono- and polynuclear complexes. Note that 19e intermediates or transition states are involved in both types of electrocatalysis induced by an oxidizing or by a reducing agent [36].

The principle of ETC catalysis involves an initiation step, which is induced by an electron or a hole of an electron [38]. This electron can be provided via an electrode or via a catalytic amount of a judiciously chosen redox couple. It is followed by the propagation step which may include many chemical steps. The cross electron transfer step closes the catalytic cycle regenerating the radical obtained at the first stage of the initiation step. Side reactions due to the high reactivity of 17- and 19-electron radicals may also disrupt the system at any stage [38].

Let us say for example, one wishes to check the electrocatalytic reaction A → B, say a ligand exchange reaction [36]. The cyclic voltammogram of a reactant A, gives a wave for A which may be reversible or not (at least a certain degree of reversibility should be observable on lowering the temperature and at high scan rate). In the presence of added ligand L^1, the CV of A will show the appearance of a new wave due to the reaction product, B ($A + L^1 \rightarrow B - L^2$). If the wave of A is a cathodic one ($A \rightarrow A^-$), setting the potential at this wave or scanning through this wave generates A^- in the vicinity of the cathode. This explains the observation of a CV wave for B. Meanwhile the wave for A is profoundly affected: since A^- reacts rapidly with L^1 to give B, its concentration in the neighbourhood of the cathode is strongly diminished and can reach zero (depending on the relative rates of the scan and of the propagation reaction of A^- with L^1). A is also consumed by the cross redox reaction ($A + B^- \rightarrow A^- + B$); hence, its intensity is also diminished. In this case the wave of B is located at a more negative potential than that of A. If a ligand exchange reaction is electrocatalyzed by a small anodic current, the CV wave normally observed in the absence of the ligand is modified in the presence of this ligand and a new wave due to the reaction product appears at a more positive potential. This behaviour is characteristic of electrocatalysis and gives an idea of the rate of both propagation steps [36].

Ligand substitution of metal carbonyls plays a key role in the catalytic sequences of a variety of important processes leading to carbon monoxide fixation. The conventional associative and dissociative mechanisms for such exchanges are usually considered to involve even-numbered, 16- and 18-electron intermediates [39]. Ligand exchange in metal carbonyls and their derivatives has received extensive mechanistic scrutiny. Electrocatalysis of ligand exchange is best illustrated by examining the effect of an extremely small anodic current upon solutions of metal carbonyls containing added nucleophiles [40].

The role of 19-electron intermediates or transition states in oxidatively induced electrocatalytic ligand exchange reactions was first demonstrated by Kochi [41], in his study of the manganese complex [$MeCpMn(CO)_2$]. The exchange of the ligands MeCN, pyridine, and THF by the less electron-releasing ligands phosphines, phosphates, and isonitriles is possible because cross ET propagation step is exergonic [41].

A cyclic voltammogram of $MeCpMn(CO)_2(MeCN)$ revealed a reversible one-electron wave at E_p = 0.22 V, in acetonitrile at a Pt microelectrode [41]. In the presence of PPh_3, a CV revealed another reversible one-electron wave at E_p = 0.55 V and the wave at E_p = 0.22 V for the reactant [R = $MeCpMn(CO)_2(MeCN)$] became irreversible. The anodic peak current for $MeCpMn(CO)_2(MeCN)$ continued to decrease in magnitude in proportion to the concentration of PPh_3, and the diffusion current fell to near zero in the presence of very high concentrations of PPh_3. It was concluded that addition of PPh_3 led to the substitution product [P = $MeCpMn(CO)_2(PPh_3)$], which occurred at E_p = 0.55 V. In other words the anodic process leading to the depletion of $MeCpMn(CO)_2(MeCN)$ away from the electrode surface, results in the concomitant formation of $MeCpMn(CO)_2(PPh_3)$. The electrochemical process involved was [41]:

$$[MeCpMn(CO)_2(MeCN)]^+ + PPh_3 \rightarrow [MeCpMn(CO)_2(PPh_3)]^+ + MeCN \qquad (1.17)$$

A cyclic voltammogram of a monopyridine complex $(py)W(CO)_5$ in acetonitrile consisted of a single irreversible wave at E_p = 1.01 V. However, after addition of 20 equivalent moles of tert-butyl isocyanide to a solution containing 1.0×10^{-3} M $(py)W(CO)_5$, a CV wave at E_p = 1.01 V disappeared and a new irreversible wave appeared at E_p = 1.18 V corresponding to a substitution product, $(t\text{-BuNC})W(CO)_5$. When smaller amounts of tert-butyl isocyanide

were employed, both waves, at E_p = 1.01 V and 1.18 V were observed on a cyclic voltammogram. The electrochemical processes involved were [42]:

$$(py)W(CO)_5 \rightarrow [(py)W(CO)_5]^+ + e^- \qquad (1.18)$$

The electrocatalytic substitution of the monopyridine and monoacetonitrile complexes of tungsten carbonyl, (py)W(CO)$_5$ (E_p = 1.01 V) and (MeCN)W(CO)$_5$ (E_p = 1.02 V), by triphenylphosphine were found to be more difficult to interpret solely on the basis of the CV experiments [42], since their anodic waves were not cleanly separated from the anodic wave of triphenylphosphine which occurred at E_p = 1.3 V. In the presence of added PPh_3, the anodic wave at E_p = 1.02 V for (MeCN)W(CO)$_5$ was absent. However, the cyclic voltammogram of (py)W(CO)$_5$ appeared to be unaffected by the presence of added triphenylphosphine. In neither case the CV wave corresponding to the product (PPh_3)W(CO)$_5$ could not be clearly discerned, owing to the presence of the phosphine wave. Nonetheless, preparative scale electrolysis demonstrated that both complexes undergo ligand substitution with PPh_3 at the electrode potentials [42].

The thermodynamic parameters governing the electron transfer chain catalyzed substitution of triphenylphosphine or iodide on CpFe(CO)$_2$I have been studied [43]. The reaction is driven by the much higher stability of the triphenylphosphine complex relative to the iodide complex, and proceeds to completion even though the electron transfer which propagates the catalytic chain is endergonic. A cyclic voltammogram of CpFe(CO)$_2$I in CH_2Cl_2 at a platinum disk electrode, revealed a chemically irreversible wave at E_p = – 1.64 V. Another irreversible wave at E_p = – 2.24 V was also observed on a CV of CpFe(CO)$_2$I, which was assigned to the formation of a dimer, [CpFe(CO)$_2$]$_2$. The chemical irreversibility of the reductions of CpFe(CO)$_2$-halide complexes was established to be the result of rapid dissociation of the halide following electron transfer. And the formation of I^- was confirmed by the observation of two oxidation peaks on the reverse CV scan at ca. 0.0 and + 0.1 V, corresponding to the two-step oxidation of iodide to triiodide and then iodide. In the presence of PPh_3, a cyclic voltammogram revealed an irreversible wave at E_p = – 1.53 V for the formation of product CpFe(CO)$_2$(PPh_3), and a wave at E_p = – 2.24 V was also observed. On scan reversal a new anodic peak, which was not present on the CV wave of CpFe(CO)$_2$I was observed at E_p = + 0.95 V and was found to match that observed for PPh_3 alone [43].

Direct electroreduction of alkyl and aryl halides is mostly performed at potentials which are more negative than – 2 V. But the picture changes radically when complexes of certain transition metals, capable of reacting with aryl- or alkyl-halides (RX) and forming more readily reducible compounds, were introduced into the electrolyte solution. The reductive dehalogenation of RX can in this case be conducted at considerably more positive potentials, most often at those of the regeneration of the metal complex active with respect to RX [44].

The complexes which are catalytically active with respect to RX can be tentatively subdivided into three groups: phosphine, tetraazamacrocyclic and polypyridyl complexes [44]. Electrochemical behaviour of solutions of NiX_2L_2 (X = Cl, Br, I; L = PPh_3) in N-methylpyrrolidinone depends on the nature and concentration of the halide ions (X^-); the concentration of L and the presence of ethylene. Reduction of the dissociated nickel (II) species leads to soluble zerovalent complexes only when Ni(II) is complexed to both phosphine and halide ions. Additions of Cl^- to solutions of $NiCl_2$ lead to formation of $NiCl_3^-$ or $NiCl_4^{2-}$, which are no longer electroactive. In the absence of ethylene the electroreduction of Ni(II) yields successfully Ni(I) and Ni(0) complexes of the type $Ni(0)L_3$. In the presence of ethylene the total reduction of NiX_2L_2 can be achieved in the absence of added L leading directly to the Ni(0) species $NiL_2C_2H_4$. The zerovalent complexes may exist in the anionic forms $Ni(0)L_3X^-$ and $Ni(0)L_2C_2H_4X^-$ depending on the nature and concentration of X [45].

Cyclic voltammetry of nickel (II) perchlorate was studied in 0.1 M TBAP in acetonitrile. In the presence of added PPh_3, it yielded an octahedral complex $[Ni^{II}(PPh_3)_2(MeCN)_4]^{2+}$, which was reduced directly in a two-electron process to $[Ni^0(PPh_3)_4]$. Another one-electron anodic peak, reversible in character, was observed on the reverse scan and was due to the oxidation of the obtained nickel(0) to $[Ni^I(PPh_3)_4]^+$ which was further oxidized at the second irreversible anodic peak, thus restoring the nickel(II) initially present. In the presence of added C_3H_5Br, three new processes appeared, one was associated with a nickel(II) cathodic peak which shifted to less negative potentials, and another two anodic peaks were due to catalytic oxidation of free bromide ions in the presence of triphenylphosphine. However, the anodic peaks relative to the stepwise oxidation of nickel(0) nearly disappeared. Further additions of C_3H_5Br only caused a progressive increase in the new cathodic peak which also took on a sigmoid shape. The overall reduction process was summarized as follows [46]:

$$[Ni^{II}(PPh_3)_2(MeCN)_4]^{2+} + 2e^- + 2PPh_3 - 4MeCN \rightarrow [Ni^0(PPh_3)_4] \quad (1.19)$$

$$[Ni^0(PPh_3)_4] + C_3H_5X - 3PPh_3 \rightarrow C_3H_5Ni^I(PPh_3)X + PPh_3 \rightarrow C_3H_5Ni^I(PPh_3)_2X \quad (1.20)$$

Cyclic voltammetry of $[Rh(PPh_3)_3]^+$ in the absence of excess PPh_3, at low scan rate (0.02 Vs^{-1}) showed two reversible one-electron reduction processes at E_p = – 1.40 V and – 1.73 V and an irreversible anodic peak was also present on scan reversal at E_p = – 0.85 V. Increasing the scan rate to 0.2 Vs^{-1}, lead to a decrease in peak current of the couple at – 1.73 V, and another reversible couple appeared at more negative potentials of – 1.90 V, and also an anodic peak at – 0.85 V decreased in magnitude [47]. At very high scan rate of 5.0 Vs^{-1}, two-well defined one-electron reversible processes appeared at – 1.40 V and – 1.90 V. Thus, it appeared that $[Rh(PPh_3)_3]^+$ was reduced in two reversible steps to $[Rh(PPh_3)_3]$ and $[Rh(PPh_3)_3]^-$, and a species, responsible for the anodic process at – 0.85 V was tentatively formulated as $[Rh(PPh_3)_2]_x$. In the presence of added free PPh_3, a rather complicated cyclic voltammogram of $[Rh(PPh_3)_3]^+$ became quite simple. $[Rh(PPh_3)_3]^+$ was reduced in two one-electron reversible steps at – 1.20 V and – 1.73 V. The second reduction potential was fixed at – 1.73 V, whilst the first one was affected by an increase in concentration of PPh_3, which made it shift positively by 60 mV per decade of concentration. This implied that the reduction process accompanied by coordination of a fourth phosphorus ligand. Since the UV-Vis spectrum of $[Rh(PPh_3)_3]^+$ was not modified by addition of PPh_3 up to 0.1 M concentration, coordination of the fourth ligand must take place after reduction of $[Rh(PPh_3)_3]^+$. The overall reduction process proposed was as follows [47]:

$$[Rh(PPh_3)]^+ + e^- \leftrightarrow Rh(PPh_3)_3 + PPh_3 \leftrightarrow Rh(PPh_3)_4 \quad (1.21)$$

The electrochemistry of (OMC)Rh(PPh_3) and (OMC)Co(PPh_3) was investigated in the presence of excess PPh_3 to determine the fate of the bound PPh_3 axial ligand after electrooxidation or electroreduction of each complex [16]. Cyclic voltammetry of (OMC)Co(PPh_3) revealed three reversible one-electron oxidation peaks in benzonitrile (PhCN) at E_p = 0.19 V, 0.76 V, and 1.54 V and two reduction waves at E_p = – 0.86 V and – 1.92 V. Both the first oxidation peak at 0.19 V and the two reduction peaks were unaffected by PPh_3 addition to solution, even after addition of 100 equivalent of PPh_3. The second oxidation peak at 0.76 V became irreversible after addition of 1.0 equivalent of PPh_3 to solution, and no further changes were observed up to addition of 500 equivalent of PPh_3, the

highest concentration investigated. The third oxidation at 1.54 V could not be investigated in the PhCN/PPh_3 mixtures due to an oxidation of PPh_3, which occurred at a more positive potential [16].

Cyclic voltammetry of (OMC)Rh(PPh_3) revealed three oxidation peaks in benzonitrile (PhCN) at E_p = 0.21 V, 0.66 V and 1.42 V and in addition two reduction peaks at E_p = – 1.27 V and – 1.34 V. Several changes were observed in the cyclic voltammograms of (OMC)Rh(PPh_3) in PhCN as PPh_3 was added to solution. The first oxidation process at 0.21 V, shifted negatively in potential while the second oxidation process at 0.66 V, became irreversible. The third oxidation at 1.42 V could not be investigated in the PhCN/PPh_3 mixtures due to an oxidation of PPh_3, which occurred at a more positive potential. Addition of PPh_3 also resulted in an increased anodic current for a reduction peak at – 1.34 V, resulting in the formation of rhodium complex $[(OMC)Rh(PPh_3)_2]^+$. The proposed electrochemical reaction was as follows [16]:

$$[(OMC)Rh^{III}(PPh_3)]^+ + PPh_3 \leftrightarrow [(OMC)Rh^{III}(PPh_3)_2]^+ \qquad (1.22)$$

The anodic peak current for the process at – 1.34 V increased with an increase in PPh_3 concentration. The ratio of anodic to cathodic peak current for process at – 1.34 V also depends upon the scan rate, which was 0.23 at 0.02 Vs^{-1} and 0.90 at 20 Vs^{-1} in the presence of 500 equivalent of PPh_3 [16].

1.5 RESEARCH AIMS AND OBJECTIVES

The overall objectives of this dissertation were as follows:

- Testing of the three flow-through cells designed and developed by Cukrowski [48] that should allow us to gain on-line, in a closed system, fundamental information about the cobalt organometallic compounds that are used as catalysts in industrial streams in non-aqueous solutions.
- Development of a method for correction of an uncompensated resistance using ferrocene as a model compound in batch solutions.
- Determine the experimental parameters to be used in each design of a flow cell (i.e., the influence of flow rate and scan rate) using ferrocene. This will enable us to

establish which flow cell will be used for fundamental studies and which for analytical purposes. Study the influence of on-line mixing on the CV curves and use the established methodologies for quantitative analysis on-line.

- Use of $CoCl_2(PPh_3)_2$ as a cobalt standard aimed to provide the quantitative information on the amount of cobalt organometallic compounds that are used as catalysts in industrial streams, since it was fairly stable. Since it is known that most cobalt catalysts are not stable under common room conditions under which the monitoring system is envisaged to operate.
- Study the electrochemical properties of $CoCl_2(PPh_3)_2$ and identify species present in solution during its oxidation, since the anodic reactions of $CoCl_2(PPh_3)_2$ were never studied using electrochemical techniques.
    - Synthesis of $CoCl_2(PPh_3)_2$ and characterisation using elemental analysis and Infrared (IR) spectroscopy.
    - Investigate the influence of a kind of working electrode material used on recorded voltammograms.
    - Establish sensitivity of voltammetric measurements towards traces of moisture present in a background solution.
    - Identify the oxidation reactions observed from the voltammograms.
    - Electrochemically monitored titration of $CoCl(PPh_3)_3$ with chloride to investigate the binding ability of chloride.
    - Electrochemically monitored titration of $CoCl_2(PPh_3)_2$ with PPh_3 using Cyclic Voltammetry (CV) to investigate the electrocatalytic properties of the complex and establish if it is possible to monitor the free PPh_3 in organic solvents in the presence of organometallic compounds containing cobalt.
    - Investigate use of ferrocene as a possible internal standard to be used during electrochemical measurements of $CoCl_2(PPh_3)_2$.
    - Determine the number of electrons involved in each electrode process observed from the voltammograms of $CoCl_2(PPh_3)_2$.
- Determine a diffusion coefficient of ferrocene in a mixture of acetonitrile and pentanol (1:1).

1.6 SUMMARY OF CHAPTERS

This dissertation contains six chapters, including the current chapter (Chapter 1). In Chapter 1 (Introduction) a detailed literature review and the aims and objectives of this research project were presented.

In Chapter 2 the theory associated with the electrochemical techniques employed in the dissertation were discussed in detail.

In Chapter 3 the experimental procedures employed for each electrochemical technique and the types of instruments used including the instrumental parameters were presented. The reagents and electrodes used were also listed.

Chapters 4 and 5 contain results and discussion regarding the preliminary studies using ferrocene and the electrochemical properties of dichlorobis(triphenylphosphine)cobalt(II), $CoCl_2(PPh_3)_2$.

Chapter 6 contains the conclusions achieved from the results obtained.

Other results were also presented in an Appendix section A and B whilst references were provided at the end of the dissertation.

CHAPTER 2 THEORY OF EXPERIMENTAL TECHNIQUES EMPLOYED

In this chapter, a theory of the basic concepts of electrochemical techniques employed in this work is reviewed. The interest in characterization of electrode mechanisms has motivated the development of a multitude of electrochemical techniques. These techniques enable the sequence of reactions to be determined and the rate constant(s) of the homogeneous chemical reactions to be measured. Such information is deduced from the effect of the coupled chemical reactions on the response signal to a particular excitation signal that is impressed on the electrode. Spectroscopic techniques (UV-visible, IR, NMR and ESR) have been effectively coupled with electrochemistry to enable monitoring of homogeneous chemical reactions. Intermediates and products can sometimes be identified from their spectra [2].

Electrochemistry has proven to be a valuable technique for generating reactive oxidation states and studying the attendant solution chemistry of such electrogenerated species. The ease of oxygen removal from electrochemical cells greatly facilitates the study of oxygen-sensitive species which are electrogenerated. Small quantities of valuable materials can be studied with ease. Very rapid reactions can be monitored since some electrochemical techniques are capable of measuring reactions up to the limit of diffusion-controlled rates. Electrochemistry often has an additional advantage over traditional chemical approaches in that the solution is not complicated by a reagent added to generate the redox state of interest [2].

2.1 CYCLIC VOLTAMMETRY (CV)

Cyclic Voltammetry (CV) is perhaps the most effective and versatile electroanalytical technique available for the mechanistic study of redox systems [2]. It enables the electrode potential to be rapidly scanned in search of redox couples. Once located, a couple can then be characterized from the potentials of peaks on the cyclic voltammogram and from changes caused by variation of the scan rate. CV is often the first experiment performed in an electrochemical study. The repetitive triangular potential excitation signal for CV causes the

potential of the working electrode to sweep back and forth between two designated values (the switching potentials). Although the potential scan is frequently terminated at the end of the first cycle, it can be continued for any number of cycles, hence the terminology cyclic voltammetry. A scan in which the potential is becoming increasingly positive is termed a positive scan and a scan in which the potential is becoming increasingly negative is a negative (even though the potential may actually be positive). The scan profile used in a particular experiment is generally determined by the location of the redox couple of interest [2].

CV has the further attraction of providing information not only on the thermodynamics of redox processes but also on the kinetics of heterogeneous electron-transfer reactions and coupled chemical reactions. The characteristic shapes of the voltammetric waves and their unequivocal position on the potential scale virtually fingerprint the individual electrochemical properties of redox systems. For this reason the method has been labelled "electrochemical spectroscopy" [49].

The cells for voltammetric experiments usually comprise a three-electrode arrangement, with working and counter-electrodes sufficiently spaced, while the reference electrode is brought close to the working electrode surface with a Haber-Luggin capillary to minimize IR loss. In particular, in case of organic solvents and high scan rates, uncompensated resistance with the resulting IR drop and double layer effects may affect the voltammograms. The IR drop distorts the linear *E/t* curve, usually assumed in CV. Of course, in turn, the current is affected. Thus, the IR compensation or correction is strongly recommended [50].

The IR correction is then the potential drop between electrode and the capillary tip from the salt bridge (note that there is no potential drop between the capillary tip and the reference electrode itself, since only minute ($< 10^{-12}$ A) currents flow in the reference electrode circuit) [51]. It is obviously essential that the electrolyte conductivity should not vary with capillary position, that the current flow should be uniform and that no substantial electrolyte concentration profile should be set up in the diffusion layer, which can best be achieved with highly conductive concentrated electrolyte. Experimental determination of the IR drop is always possible. Earlier work involved the systematic variation of tip-electrode distance and extrapolated the resultant measurement to zero separation, but nowadays the current-

interrupt method is most commonly employed. This exploits the fact that, on interrupting the current, the IR contribution to the potential drops immediately to zero, whereas the electrode potential falls only relatively slowly (in the order of ms) owing to the large double-layer capacitance. The potential change can be measured with a storage oscilloscope or by utilizing an appropriate electronic circuit within the potentiostat; IR compensation can be built into the potential control by a variety of means, yielding automatically corrected values of the electrode potential [51].

Another significant problem in cyclic voltammetry is the possibility of dissolution of the counter electrode [51]. The potentiostat will force an equal and opposite current through the counter electrode as the working electrode, and a small amount of metal at the counter electrode may dissolve and re-deposit on the working electrode. For this reason, a counter electrode of the same material as the working electrode is usually employed during electrochemical investigations on gold, platinum etc. Cyclic voltammograms of a much more complex form are found for more complex electrochemical processes such as the oxidation of organic substances, especially in cases where the solution is unstirred, and the CV shows a sensitive dependence on the type of electroactive substance in the electrolyte, the electrolyte itself, and the electrode material. The existence of multiple peaks often reflects the build-up and dissolution of chemisorbed inhibitor layers on the electrode surface, for example, the inhibiting effect of a build-up of oxide layer on platinum on the oxidation of small organic molecules [51].

Applicability of voltammetric techniques is in some cases limited due to several factors. In a background electrolyte solution, we will observe oxidation or reduction of electrolyte components, the electrode material itself, or impurities in the electrolyte at certain potentials. These processes define the *accessible potential window*, and the observable electrode reactions should yield voltammetric signals well inside this window to allow analysis without interferences of background contributions [50].

If voltammetry is used for analytical purposes, an extremely large electrode area or volume ratio is often chosen to increase sensitivity, e.g., in inverse voltammetry or when working with thin-layer cells. Under these conditions, diffusion is no longer semi-infinite but finite, i.e., the thickness of the diffusion layer is limited by the volume, and this changes the characteristics of the diffusion gradient. In a voltammetric experiments the measurable

current at the working electrode has two components; one for the heterogeneous charge transfer and one for the mass transport. However, there are two exceptions: the reversible and the irreversible case [49].

❖ **Reversible System.**

An example of an electrochemical reversible system is the simplest possible one-electron oxidation or reduction of a chemical species in solution at the working electrode (WE). The rate of heterogeneous charge transfer is so high that a dynamic equilibrium is established at the phase boundary. The Butler-Volmer equation [eq. (2.1)] is reduced to the Nernst equation [eq. (2.2)], i.e., the surface concentrations depend only on the actual electrode potential and are no longer influenced by heterogeneous kinetic effects. The current, as a measurable quantity for the charge flux at the electrode surface, is influenced solely by mass transport, the slowest step (diffusion control). The characteristic shape of the cyclic voltammogram is a result of the potential-dependent changes in the surface concentrations of the redox system and the simultaneous diffusion processes [49].

$$j_A(0,t) = \frac{i}{nFA}$$
$$= C_A(0,t)k^o \exp[-\alpha nF/RT(E - E^o)] - C_B(0,t)k^o \exp[(1-\alpha)\, nF/RT\,(E - E^o)] \quad (2.1)$$

$$E = E^o - \frac{RT}{nF} \ln Q \quad (2.2)$$

where, j_A is a flux of species A (mol $s^{-1}cm^{-2}$); k° is a standard heterogeneous rate constant (cm/s); α is a cathodic transfer coefficient, $1 - \alpha$ is an anodic transfer coefficient, and Q is a reaction quotient. The other variables were defined in the previous chapter and in the list of symbols.

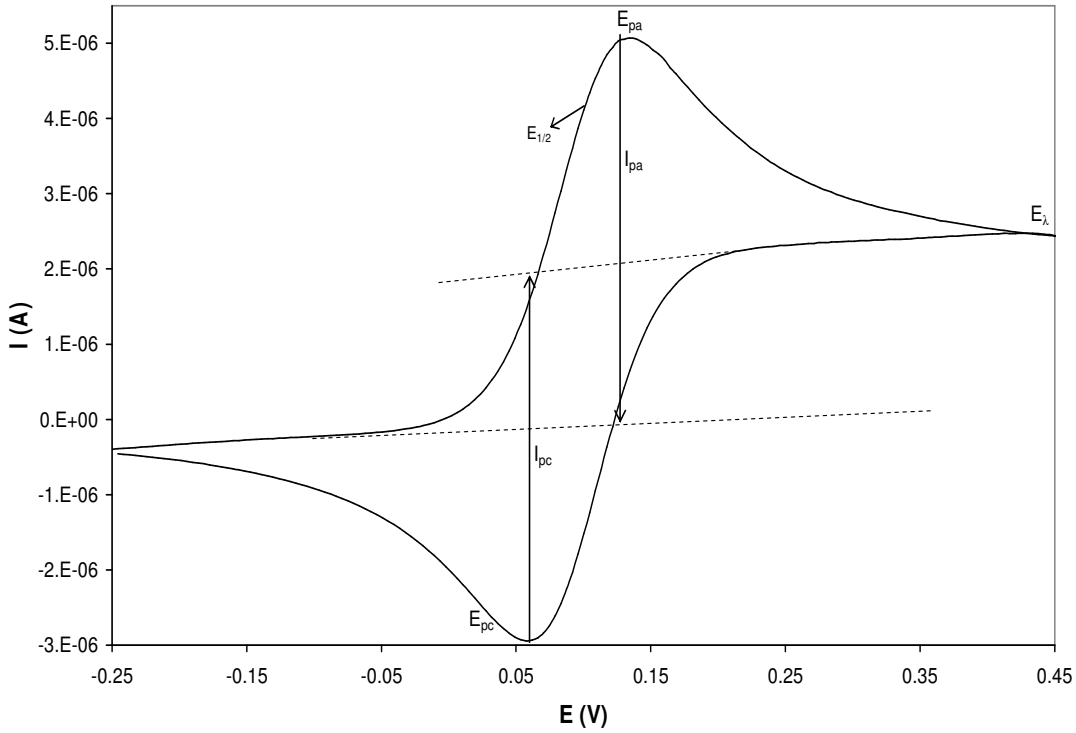

Figure 2.1 Cyclic voltammetric curve of a reversible charge transfer obtained to show how the CV parameters were evaluated. E_λ = switching potential, $E_{1/2}$ = half-wave potential, E_{pa} and E_{pc} = anodic and cathodic peak potential, I_{pa} and I_{pc} = anodic and cathodic peak current.

The most important parameters are the two peak potentials E_{pa} and E_{pc} as well as the peak currents I_{pa} and I_{pc} (Fig. 2.1). For reversible charge transfer (α = 0.5) without coupled chemical reactions, $I_{pa}/I_{pc} = 1$ and $\Delta E_p = 59 / n$ mV (at 25 °C) [49].

The peak current for a reversible electron transfer is given by the Randles-Sevčik equation (at 25 °C):

$$i_p = 2.686 \times 10^5 \; n^{3/2} C D^{1/2} v^{1/2} A \qquad (2.3)$$

where, n = number of moles (mol^{-1}); C = concentration of the oxidized or reduced species in a bulk solution (mol cm^{-3}); D = diffusion coefficient (cm^2 s^{-1}); v = scan rate (V s^{-1}) and A = area of the WE electrode (cm^2). The peak current is proportional to the square root of the scan rate.

❖ **Irreversible System**

Charge transfer at the electrode is extremely slow. Depending on the potential, only one of the cathodic or anodic heterogeneous reactions has a measurable rate. Thus, the current is largely controlled by the rate of the charge-transfer reaction (charge-transfer control). Since the surface concentrations at the electrode are dependent on the heterogeneous reaction and are far removed from thermodynamic equilibrium, one speaks of an irreversible process. Under such conditions, the Nernst equation does not apply. Furthermore, this means that the measured potential values cannot be compared with thermodynamic equilibrium potentials [49].

❖ **Quasi-reversible System.**

Both the charge transfer and the mass transport determine the current. The Nernst equation is only approximately satisfied. The charge transfer is therefore termed quasi-reversible [49].

❖ **Multielectron Transfer Processes.**

Multielectron transfer usually takes place in separate steps. Depending on the separation between the theoretical potentials of the redox reactions, several cases have to be distinguished. If the separation of the potentials between redox transfers is large, the resulting cyclic voltammogram consists of two typical, additively superimposed, one-electron transfer waves [49]. Also, the second electron transfer might take place at potentials negative to the first, giving rise to two overlapped one-electron peaks. Often there is a chemical reaction upon reduction or oxidation, giving rise to an ECE process with an apparent multielectron transfer [52].

Figure 2.2 presents a typical example of a two-step redox process of cobalt-tetra-{2-(2-thienyl)ethoxy}phthalocyanine [CoTETPc]. The first wave corresponds to oxidation of Co^{II}TETPc to Co^{III}TETPc which was followed by complex oxidation, Co^{III}TETPc to $[Co^{III}TETPc]^{+}$. In this Figure a multielectron overall response arises. The product of the first electron-transfer reaction (process I) undergoes a second electron-transfer step (process II) at potentials more positive than that for the first step [4].

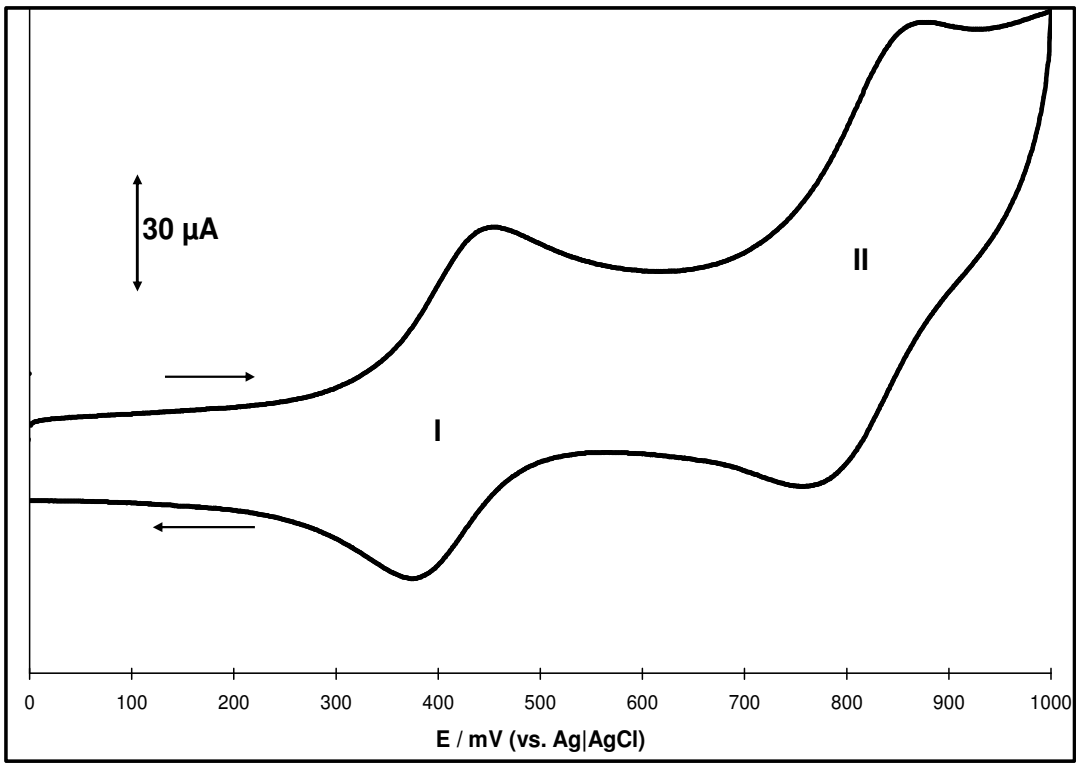

Figure 2.2 Cyclic voltammogram of two-electron transfer process obtained using 5 mM CoTETPc; in DMF containing 0.1 M $TBABF_4$, at a scan rate of 100 mV/s, obtained from Ref [53].

❖ **Electron Transfer with Coupled Chemical Reactions**

One of the most intriguing aspects of electrochemistry involves the homogeneous chemical reactions that often accompany heterogeneous electron-transfer processes occurring at the electrode-solution interface. The addition or removal of an electron from a molecule generates a new redox state, which can be chemically reactive. A variety of mechanisms, some of which involve complicated sequences of electrode and chemical reactions, have been characterized [2].

2.2 CHRONOAMPEROMETRY

In Chronoamperometry a current through a working electrode is recorded as a function of time, while the constant potential is applied to this electrode. During the experiment the electrode is stationary and usually the electrolyte is not agitated, but is at rest. The derivation of the response began at a potential step from a value at which no current flows, to one at which the diffusion-limited current passes [50]. The response of the current to this

perturbation will be a sharp change from zero current followed by relaxation to a value close to zero, the final steady state magnitude that is determined by the flow of species to the electrode surface (Figure 2.3). Hence this varies according to electrode geometry and solution convection [50].

For a uniformly accessible planar electrode, the diffusion process is known as semi-infinite linear diffusion, since it can be assumed to occur only in one dimension perpendicular to the electrode surface. The observed current depends directly on the observed concentration gradient at the electrode surface [50].

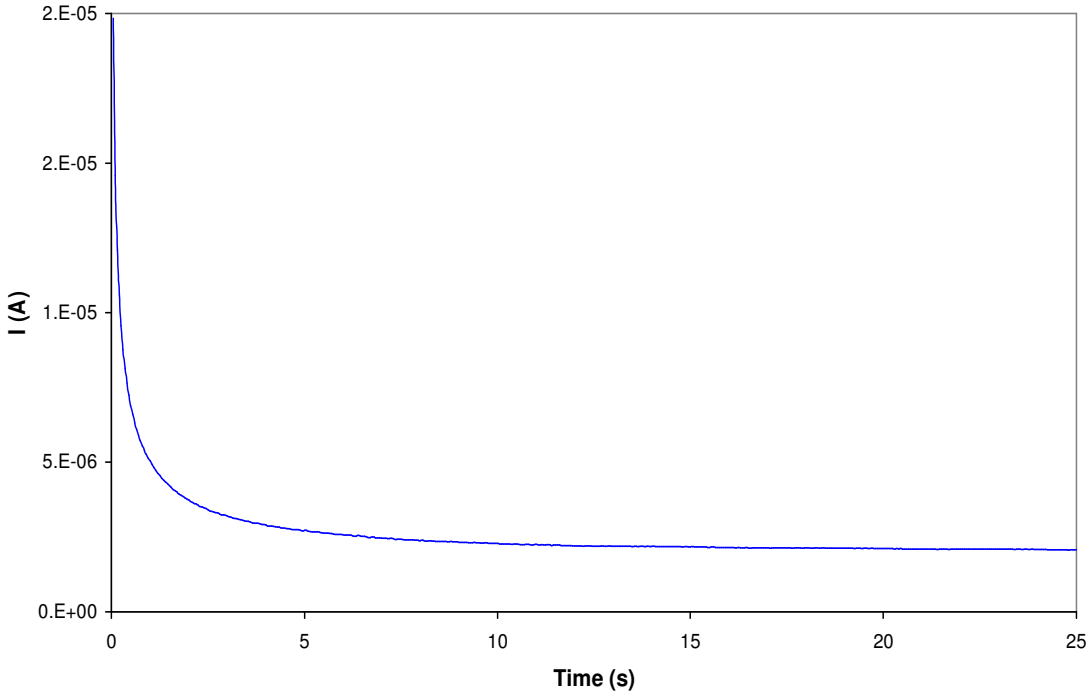

Figure 2.3 Potential step chronoamperometric response of a 7.7×10^{-4} mol/l ferrocene solution in 0.05 M TBAHFP in acetonitrile.

In fact, the current decays smoothly from an initial value at $t = 0$ and approaches zero with increasing the time as described by the Cottrell equation for a planar electrode [2]:

$$i_t = \frac{nFACD^{1/2}}{\pi^{1/2} t^{1/2}} \tag{2.4}$$

where, i_t = current of time (t), A

n = number of electrons, mol^{-1}

F = Faraday's constant, 96485 A.s

A = electrode area, cm^2

C = concentration of electroactive species, mol/cm^3

D = diffusion coefficient of electroactive species, cm^2/s

Hence, the current is inversely proportional to the square root of time. The Cottrell equation states that the product $it^{1/2}$ should be a constant for a diffusion-controlled reaction at a planar electrode. Deviation from this constancy can be caused by a number of situations, including nonplanar diffusion, convection in the cell, slow charging of the electrode during the potential step, and coupled chemical reactions. For each of these cases the variation of $it^{1/2}$, when plotted against t, is somewhat characteristic [2].

Chronoamperometry has proven useful for the measurement of diffusion coefficients of electroactive species. An average value of $it^{1/2}$ over a range of time is determined at an electrode the area of which is accurately known and with a solution of known concentration. The diffusion coefficient can then be calculated from $it^{1/2}$ via the Cottrell equation. Although the electrode area can be physically measured, a common practice is to measure it electrochemically by performing the chronoamperometric experiment on a redox species whose diffusion coefficient is known. The value of A is then calculated from $it^{1/2}$. Such an electrochemically measured surface area takes into account any unusual surface geometry that may be difficult to measure geometrically [2].

If the heterogeneous electron transfer of the redox species with the electrode itself is slow, the current after the potential step is necessarily less than in a system in which the electron transfer is rapid. This aspect of electrochemistry has been used for the measurement of heterogeneous rate constants. The behaviour of $it^{1/2}$ as a function of time can be influenced substantially by the presence of chemical reactions that are coupled to the electrode process. Consequently, characteristic variations of $it^{1/2}$ vs. t have been effectively utilized for the quantitative study of such homogeneous chemical reactions [2].

2.3 FLOW INJECTION ANALYSIS (FIA)

Years ago scientists involved with making analytical measurements had very limited and primitive equipment at their disposal. Light sources were flames and the sun. Most wavelength dispersions or discrimination were performed using filters or prisms. The detectors, in many cases, were the eyes or eventually photographic films. The readout devise was a person capable of evaluating the observed signals. Data evaluation was again a person. The sample was collected by a person and filtered, diluted, and in general handled by a person using volumetric glassware, like pipettes and volumetric flasks. All measurements were slow, tedious, and required a great deal of skill on the part of the analysts in order to ensure precise and accurate results [54].

Any measurement in a chemical laboratory involving liquid materials comprises the following operations: solution handling, analyte detection, data collection and computation of results. Nowadays, there is no shortage of computers and sophisticated detectors to aid chemists in performing data collection and computation of results, but solution handling requires an arsenal of skills, which a practicing chemist has to master, since mixing, decanting, pipetting, and other volumetric operations are still performed manually, even in the most advanced laboratories, using tools that were designed more than 200 years ago [55]. It might seem that robots would be suitable tools for automation of such manual tasks; but, it is likely that their impact will remain limited to repetitive operations like weighing of pulverized materials, mechanization of sample injection into chromatographic columns, handling of radioactive materials, or sample preparation. Because manual handling using robots requires extensive programming and active feedback control, the use of robots is justified only if large series of repetitive operations is to be handled over prolonged periods [55].

Truly, there seems to be no way of resolving the problem of automated solution handling other than by manual operations, as long as we think in terms of batch operations, a concept in which generations of chemists have been trained. Therefore, in freshmen courses, as well as in advanced research laboratories, beakers, flasks, and volumetric glassware are still the standard tools of the trade, coexisting with the electronics of advanced detectors and computers [55].

In flow injection analysis (FIA) the sample is injected directly into a moving stream without the addition of air (Fig. 2.4). The sample-reagent zone mixes and reacts as it moves downstream towards the detector; the degree of dispersion is controlled by a variety of factors, their impact being specific to the analytical system in use. It is the control of this dispersion which is at the heart of the technique and coupled with short, highly reproducible retention times and provides the potential for sampling rates up to 200 per hour [24]. Figure 2.5 below shows an amperometric response obtained from multiple injections of various concentrations of ferrocene solution in the flow cell using FIA system, using a continuous-flow method.

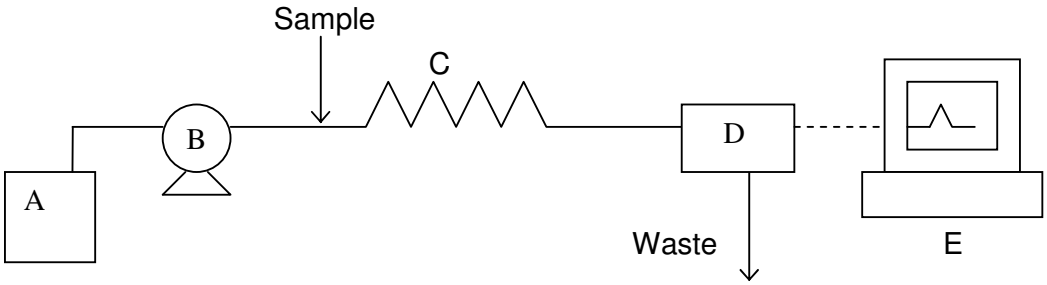

Figure 2.4 Schematic representation of a typical flow injection analysis system. A = background electrolyte solution, B = Pump, C = mixing coil, D = detector and E = computer.

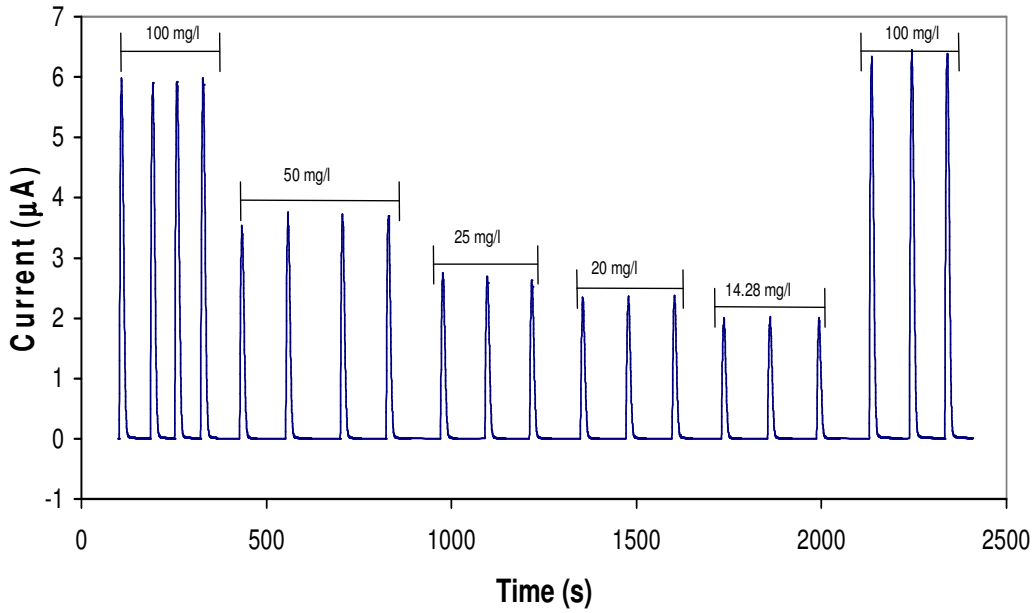

Figure 2.5 Typical detector output of an FIA system into which a ferrocene solution of various concentrations is repeatedly injected.

According to the type of flow used, flow methods can be classified as: (i) segmented-flow, (ii) continuous-flow, and (iii) stopped-flow methods [56]. The term 'stopped-flow methods' is applied to kinetic methods involving mixing of the sample and the reagents in the detector cell in order to perform periodic measurements for monitoring reaction development. This type of method is rarely considered to be of the automatic type. We should note that the 'continuous-flow' concept does not exclude occasionally stopping the flow (for example, to allow the reaction to proceed without increasing sample dispersion in the carrier). Continuous-flow methods are also kinetic methods: measurements are performed during the course of the reaction without the need to wait for equilibrium to be reached. Therefore, some continuous-flow methods frequently include halting of the flow. In segmented-flow methods the flowing stream is segmented by air bubbles that are primarily intended to avoid carry-over between successively processed samples [56].

The three basics of FIA, as defined by Růžička and Hansen, are reproducible timing (which leads to the reproducible physical conditions), sample injection and controlled dispersion. Dispersion is described as the amount that the chemical signal is reduced by injecting a sample plug into an FIA system [54]. This is represented mathematically by

$$D^{*} = C^{\circ} / C^{\max} \tag{2.5}$$

where D^{*} is the dispersion coefficient at the peak maximum produced by the ratio between C°, the concentration of a pure dye, and $C^{\max}$, the concentration of that same injected dye as it passes through the detector [54].

The experimental conditions usually involved in FIA result in incomplete mixing of the injected sample plug with the carrier stream, with two important consequences, (i) mixing is time-dependent, and therefore occurs to different extents at different points along the flow-line, (ii) the extent of mixing is highly reproducible from sample to sample. Thus, the technique gives rise to the creation of a time-dependent concentration gradient of sample within the carrier streams. The physical foundations of FIA are related to dispersion, which is defined as the dilution undergone by a sample volume injected into the flowing stream. The dispersion is characterized by the concentration profile adopted by a zone or plug inserted at a given point in the system without stopping the flow [57].

There are two mechanisms contributing to the dispersion of the injected sample,

(i) Convective transport, occurring under laminar flow conditions (Fig. 2.6). This yields a parabolic velocity profile with sample molecules at the tube walls having zero linear velocity and those at the centre of the tube having twice the average velocity [57].

(ii) Diffusional transport, due to the presence of concentration gradients in the convective transport regime, gives rise to axial and radial diffusion (Fig. 2.6). The former, due to horizontal concentration gradients at the leading and trailing edges of the injected sample zone contributes insignificantly to the overall dispersion, whereas the latter, resulting from concentration differences perpendicular to the direction of the flow makes an important contribution to the overall dispersion. If the flow is considered to be made up of a large number of superimposed fluid cylinders travelling convectively at different speeds, radial diffusion tends to balance concentrations in such a manner that the molecules located at the tube walls tend to move to the centre, whereas those at the centre travel outwards. This process is of transcendental importance in accounting for the fact that every sample injected maintains its integrity. Indeed, this motion slows down convective transport, thus hindering progressive dilution of the zone in the carrier stream [57].

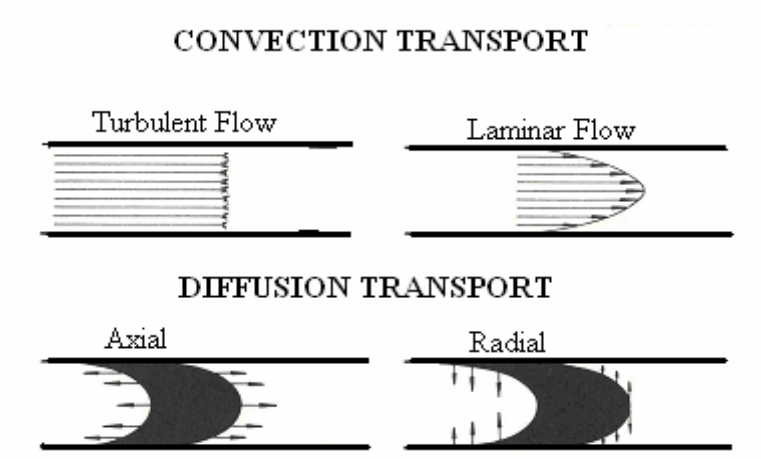

Figure 2.6 Types of transport mechanisms present in a closed system.

Flow operations are much easier to automate, since they replace the mechanical handling of oddly shaped (and often fragile) containers by sequential movements of liquids in tubes.

Flow operations are much easier to miniaturize by using small bore tubing, and the micro volumes are conveniently manipulated and metered by pumping devices, which (unlike pipettes) are not affected by surface tension (or by shaking hands) [55]. Flow operations are much easier to control in space and time, since using closed tubing avoids evaporation of liquids, provides exactly repeatable path(s) through which measured solutions move, and provides an environment for a highly reproducible mixing of components and formation of reaction products. Flow operations are very versatile, since flows can be mixed, stopped, restarted, reversed, split, recombined, and sampled, while contact times with selected sections of reactive or sensing surfaces can be precisely controlled. Finally, flow operations allow most detectors and sensors to be used in a more reproducible manner than when used in batch operations and by hand-as is obvious to anyone who has used both conventional and flow-through cuvettes [55].

While many of the advantages of flow operations have been exploited in chromatography, why has the batch approach not yet been replaced by flow systems in all areas of laboratory practice? The reason must be tradition, and the fact that most chemists are used to thinking in terms to batch operations, where homogeneous mixing is thought to be the only reproducible way to bring reactants together and where the homogeneously mixed solution is regarded as the only suitable form in which a reproducible measurement can be taken [55].

FIA technique can be applied to agriculture, water and soil analysis, environmental laboratories, biochemistry, biotechnology, pharmaceuticals, clinical laboratories and in food and feed, and in process and quality control [54]. Predominantly FIA has been applied to colorimetric methods using well established chemistries also found on both air segmented and discrete analysis systems. Such analysis can be simple involving no more than the addition of the sample to the moving reagent/carrier stream or involve dialysis; solvent extraction; multiple reagent addition as intermediate steps. Improved sensitivity can be achieved from a stopped flow technique, on line pretreatment etc, but at the expense of sampling rate. FIA can also be applied to other detection systems e.g. ion selective electrodes or as a means of sample introduction to Atomic Absorption Spectrophotometry [24].

Modern electrochemistry offers a wide range of methods that can be used for continuous or discrete measurements in flowing liquids. The combination of flow injection analysis and cyclic voltammetry is attractive because of the flexibility of the former and the diagnostic power of the latter. Recently developed flow injection techniques with controlled dispersion offer a unique possibility to prepare solutions under controlled conditions in flowing systems [58]. Two classes of electrochemical measurement are employed in flow detection: one class is based on charge transfer between a liquid or gaseous phase containing the analytes and a solid or immiscible liquid phase that is electrically conductive or semi conductive, and includes the most common potentiometric, voltammetric and coulometric detection techniques, and the other class involves the measurement of the electrical properties of liquids, i.e. the electrical conductivity and relative permissivity [58].

There are many designs of flow-through detectors described in the literature, mainly for continuous, on-line monitoring and for chromatographic applications [58]. The best design for both solid-state and polarographic detectors involves a geometry in which the fluid stream points at a right angle to the electrode surface or a disk upon which the fluid system stream impinges perpendicularly. For the polarographic detectors, the best geometry is that the fluid and mercury streams are at right angle to each other. The two kinds of detectors then perform equally well [59]. Figure 2.7, shows an example of a cyclic voltammetric curve of ferrocene solution in a flowing solution, using a kind of detector cell where the fluid stream points at a right angle to the electrode surface.

Flowers and Callender, designed and characterized a transmittance cell (volume 10 ml) for ultraviolet, visible, and infrared spectroscopy and spectroelectrochemistry [30]. Cyclic voltammograms were measured at various scan rates for ~ 1.5 mM ferricyanide in 0.1 M KNO_3. A rather severe edge effect manifested the voltammograms due to exposure of the thin layer to the bulk solution about its entire perimeter. Separation of the cathodic and anodic peaks was observed to increase from ~ 50 to 100 mV as the scan rate was increased from 1 to 4 mV/s. This was likely a result of ohmic drop across the optically transparent working electrode due to the resistance of the thin layer solution. Despite these shortcomings, the quality of the voltammograms indicated that the cell design permitted reasonably accurate control of the optically transparent working electrode [30].

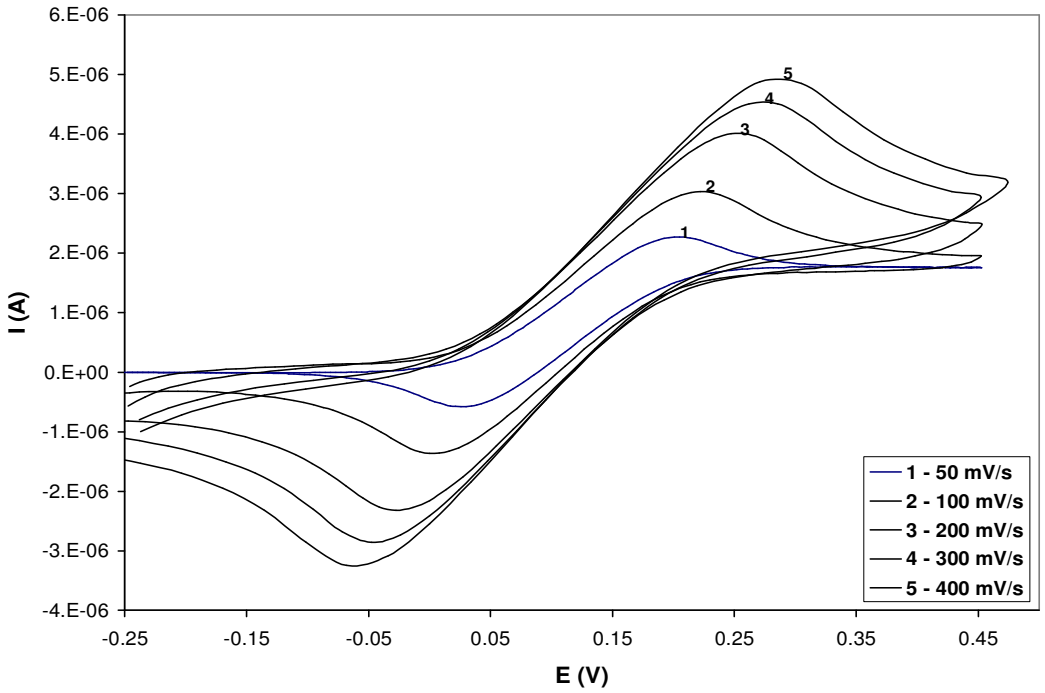

Figure 2.7 Cyclic Voltammograms of a 50 mg/l Ferrocene in 0.01 M TBAHFP in acetonitrile on a Pt disk electrode at various scan rates, using a flow-through cell, at a flow rate of 1 ml/min.

Chen and Long designed a flow micro-cell (volume 5 µL) and characterized it using cyclic voltammetry of potassium hexacyanoferrate(III) at various scan rates [60]. A separation of the cathodic and anodic peaks from 26 to 89 mV was observed, when the scan rate was increased from 2 to 18 mV/s. They found that the edge effect of the flow micro-cell was less than that previously reported by Flowers and Callender [30], the symmetry of the cyclic voltammogram for this thin layer cell was improved and the IR drop was decreased. The quality of the data demonstrated that the flow microcell can be successfully used for electrochemical studies [60].

CHAPTER 3 EXPERIMENTAL

This chapter describes in general the experimental procedures employed for each electrochemical technique and the types of instruments used including the instrumental parameters. The description of the three flow cells is included, the reagents and types of electrodes used. The synthetic procedure of the two cobalt organometallic complexes is also presented.

3.1 REAGENTS AND ELECTRODES

3.1.1 Reagents

- Tetrabutyl ammonium hexaflourophosphate ($TBAPF_6$), and ferrocene were purchased from Fluka and used without further purification.
- Acetonitrile C.P (99 %) was purchased from Sigma-Aldrich and purified by distillation over P_2O_5 (98 %, from Riedel-deHaën).
- Pentanol (99 %) was purchased from Fluka and purified by distillation over dried potassium carbonate (99.85 %, from Ssangyong) (dried at 125 °C).
- Acetone A.R (99.8 %), from Promark Chemicals was used as received.
- Methanol A.R (99.5 %) and Hexane C.P (96 %) were purchased from Radchem Laboratory Supplies and used as received.
- Tetrahydrofuran A.R (99.8 %), from Lab-Scan Analytical Sciences was use as received.
- Ethanol (99.5 %), from Merck was used as received.
- Ethyl acetate, ACS reagent (99.5 %); petroleum ether; Hydranal-Coulomat AD (reagent for coulometric Karl Fischer titration for cells without diaphragm), were purchased from Riedel-deHaën and used as received.
- Cobalt (II) chloride hexahydrate ($CoCl_2.6H_2O$) was purchased from Riedel-deHaën and dried in an oven to a blue color before use.
- Nitric acid C.P (HNO_3, 55 %), from Bio-zone chemicals was used as received.
- Sodium tetrahydroborate ($NaBH_4$, 98 %), and $AgNO_3$ were purchased from Saarchem and used as received.
- Triphenylphosphine was purchased from Sigma-Aldrich and used as received.

- Bis-(triphenylphosphine)dichlorocobalt(II) $[CoCl_2(PPh_3)_2]$ and chlorotris-(triphenylphosphine)cobalt(I) $[CoCl(PPh_3)_3]$ were synthesized using the literature method [61 – 62].

3.1.2 Electrodes

- Platinum disk, glassy carbon, silver disk, and gold disk electrodes, each 2 mm in diameter, were purchased from Metrohm, Switzerland.
- Steel rod tube outlet (1/16 x 0.040 x 5 cm), from Upchurch Scientific, Anatech.
- Platinum sheet electrode was from Metrohm, Switzerland.
- Autolab dummy Cell, from Echo Chemie, Netherlands.

3.2 APPARATUS

3.2.1 Flow Injection Analysis

The flow injection apparatus consisted of two Dosimats (Metrohm), with a 10 and a 5 ml exchange units, a PEEK mixing tee (25 x 23 x 20 mm in size), a six-port Hamilton injection valve, and a flow cell. The tube length between the injectors and the mixing tee was 40 cm Teflon tubing (2 mm ID, Metrohm). The tube length between the mixing tee and the manifold and the manifold and the detector were both 15 cm Teflon tubing (2 mm ID, Metrohm). The solutions were degassed by bubbling with argon before pumping through the flow injection analysis system. The descriptions of the three flow cells designed by Cukrowski [48] are as follows:

- **Flow Cell 1**

The flow–by electrochemical cell body was made of a rectangular piece of PEEK (49 x 32 x 25 mm in size). The flow cell consisted of a platinum disk electrode (2 mm diameter) as a working electrode, a gold disk electrode (2 mm diameter) as a counter electrode and a $Ag \mid AgNO_3$ (0.01 M) in acetonitrile as a reference electrode, connected to a frit as a liquid junction, and two bores (inlet and outlet) and a spacer. In this flow cell, the working electrode was positioned in such a way that the fluid stream points at a right angle to the electrode surface. The counter and the reference electrode were facing each other at opposite

positions. The working electrode and the spacer were also facing each other, and the spacer was used to vary the flow cell volume.

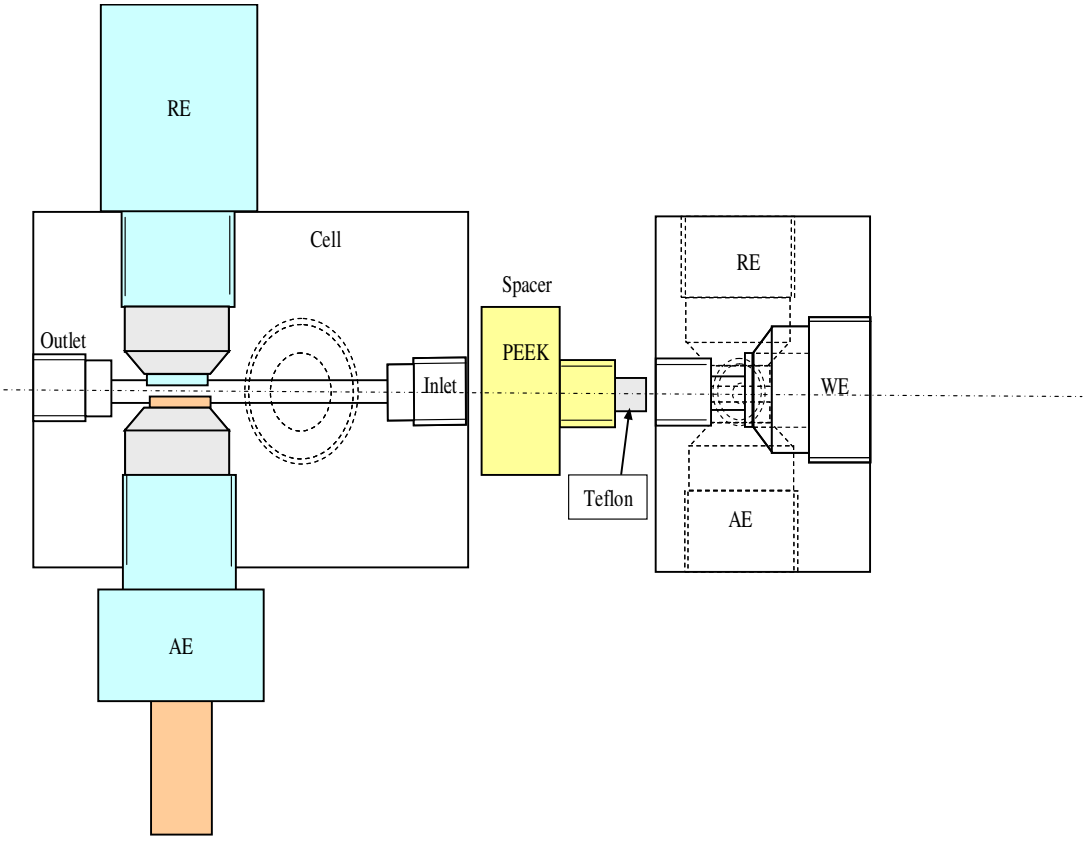

Figure 3.1 Diagram of the representative electrochemical flow–by cell 1, where WE = working electrode, RE = reference electrode and AE = auxiliary electrode.

- **Flow Cell 2**

The electrochemical flow cell was a wall-jet type. The cell body was made of a rectangular piece of PEEK (42 x 32 x 25 mm in size). The flow cell consisted of the same electrodes as those described in flow cell 1. The only difference between the two flow cells was the position of the inlet tube with respect to the working electrode. In this flow cell the working electrode was facing the inlet tube. This arrangement ensures that any part of the sample plug comes into contact with the working electrode surface only once. And also an inlet tube was incorporated inside a spacer.

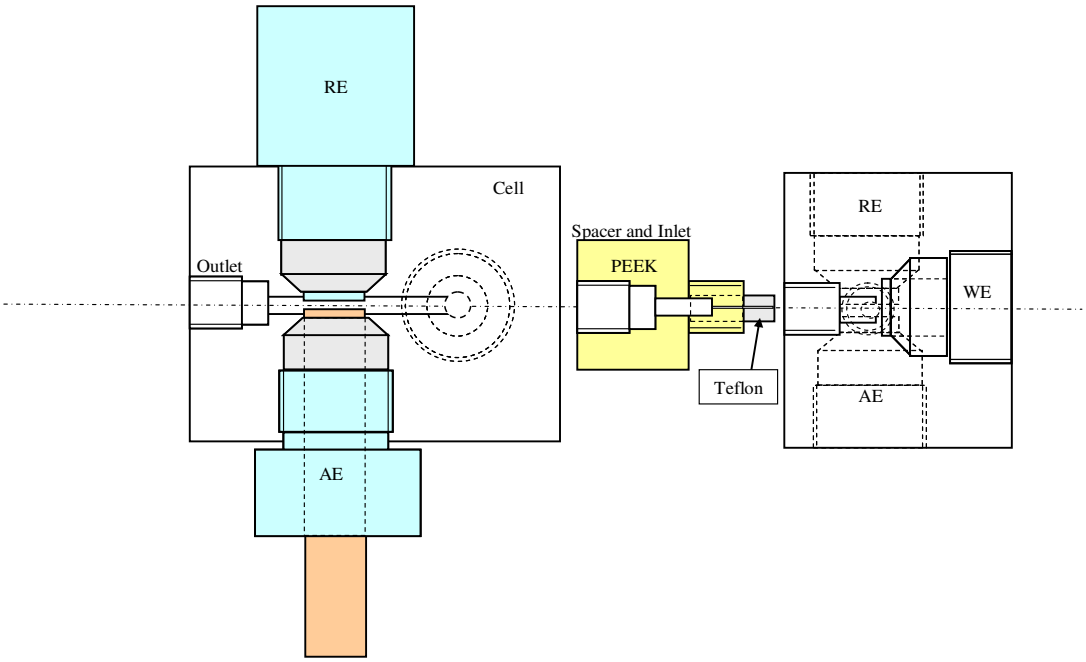

Figure 3.2 Diagram of the electrochemical wall–jet cell 2, with a gold disk as a counter electrode.

Flow Cell 3

The electrochemical flow cell was a wall-jet type. The cell body was made of a rectangular piece of PEEK (42 x 27 x 25 mm in size). The position and type of the counter electrode in this flow cell differs from that of flow cell 2. The counter electrode was a steel rod tube and it was positioned perpendicular to the reference electrode, and it served as a solution.

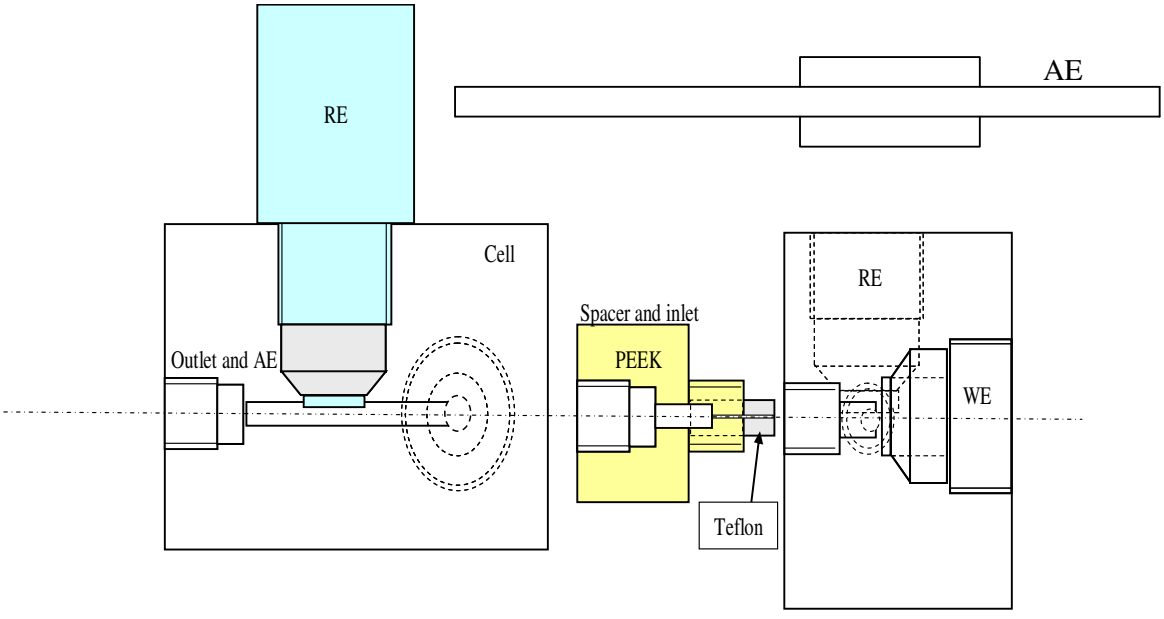

Figure 3.3 Diagram of the electrochemical wall–jet cell 3, with the steel rod tube as a counter electrode.

3.2.2 Cyclic Voltammetry (CV) and Chronoamperometry

An Autolab Type II system (Eco Chemie, Utrech, Netherlands) connected to a model VA Stand 663 (Metrohm, Herisau, Switzerland) was used for all experiments. The instrument was controlled by PC via GEPS version 4.8 software. All electrochemical experiments were carried out at room temperature using a three-electrode cell. The working electrodes were either a Pt disk; gold disk or a glassy carbon disk (all from Metrohm, each with diameter of 2 mm). The counter electrode was a Pt sheet. The reference electrode consisted of a silver wire immersed in a solution of silver nitrate (0.01 M) in acetonitrile. The reference electrode was immersed in a Luggin capillary salt bridge containing 0.1 M TBAHFP dissolved in a desired background solvent. The distance between the Pt disk working electrode and the tip of the salt bridge was ~ 1 mm to minimize ohmic drop. The stability of the reference electrode was checked periodically against a 0.77 mM ferrocene solution in the solvent of interest by measuring the change in peak potential, ΔE_p, of $Fe^{2+}Cp_2/Fe^{3+}Cp_2$ after measurement of the current-potential curve of the investigated compound. All potentials have been referenced to the $Fe^{2+}Cp_2/Fe^{3+}Cp_2$ couple. The standard IR drop correction facility of the instrument was used to minimize the effects of resistance in the electrolyte, using the resistance value obtained with ferrocene.

3.2.3 Digital Fitting and Simulation

Theoretical cyclic voltammograms were fitted using the Fit and Simulation option located in the Analysis menu of the Data Presentation window obtained from a GPES version 4.8 software. A reversible model was selected and a model name was set to Fit. The number of exchanged electrons was set to 1, temperature to 298 K and the initial guesses of the parameters were obtained. The Full Fit control parameter was selected followed by a Fast Fit and the fitted curve was saved.

3.2.4 Karl Fischer Titration

A Hydranal-Coulomat AD reagent for coulometric titration for cells without diaphragm was used. The reagent contains methanol, imidazole, sulfur dioxide and diethanolamine. The instrument used for moisture determination was 831 KF Coulometer (Metrohm), and a 728 magnetic stirrer (Metrohm). This instrument consisted of a generator electrode, a platinum wire electrode (with two wires), a 300 ml titration vessel, a stirrer bar and a keyboard.

3.2.5 UV-Visible Spectroscopy

A Perkin Elmer UV-Vis (Lambda E2 201) spectrometer was used. The experimental parameters were as follows: scan speed = 400 nm/min; path length = 10 mm; response = medium and data range = 190 – 800 or 500 – 800 nm.

3.2.6 Infrared Spectrum

The IR spectra were obtained from KBr disks. The disks were run on the Perkin Elmer (RX 1 FT-IR system) spectrum using 32 scans at 2.0 cm^{-1} resolution and in the region 400 to 4000 cm^{-1}.

3.2.7 Nuclear Magnetic Resonance (NMR) Spectroscopy

Room-temperature ^{31}P NMR measurements of the free ligand, and complex were performed on a Bruker ARX 300. H_3PO_4 ($\delta = 0$) was used as an internal standard for ^{31}P spectrum.

3.2.8 Other Equipment

- Hyprez Five-Star 1µm synthetic diamond paste for use on IMP cloth was purchased from IMP Sampling Analysis.
- Diamond extender blue, used as a lubricant with synthetic diamond paste was purchased from IMP Sampling Analysis.
- An IMP polishing cloth was purchased from IMP Sampling Analysis.
- A DPA-2 polishing wheel was from Struers.
- Whatman filter paper (44 Ashless Circles 110 mm diameter), from Sigma-Aldrich.
- Magnetic stirrer hot plate was purchased from Metrohm.
- A PTFE magnetic stirrer bar.
- A PTFE magnetic retriever rod.
- Drying Oven Series 2000, with a maximum temperature of 250 °C was purchased from Apollo Scientific.
- Precision balance (Mettler Toledo, 4 decimal places in grams), was purchased from Microsep, Switzerland.
- 763 Dosimats and exchange units were purchased from Metrohm, Switzerland.
- A six port distribution valve (model-R77810) and valve head (model-R36719) were purchased from Hamilton, Switzerland.

- PEEK material was purchased from Metrohm, Switzerland.
- Teflon tubing's were purchased from Metrohm, Switzerland.
- Millipore (Milli-Q Synergy), water supply system capable of producing ultra pure water with a resistivity of 18.2 M Ω cm was purchased from Microsep.
- Argon UHP gas (minimum purity 99.999 %), from Afrox Scientific.

3.3 SYNTHESIS

3.3.1 Synthesis of Bis-(triphenylphosphine)-dichlorocobalt(II) [$CoCl_2(PPh_3)_2$]

$CoCl_2(PPh_3)_2$ solid was prepared by dissolving 2.4007 g of dried $CoCl_2$ in 60 ml of ethanol and heated at 60–70 °C. 8.0003 g of triphenylphosphine was also dissolved in 60 ml of ethanol and heated at 60–70 °C. The hot ethanol solutions of $CoCl_2$ and triphenylphosphine were mixed slowly. The complexes began to precipitate before the mixing was complete. After complete mixing the hot solution was allowed to cool for about 2 minutes, filtered using canular technique while still warm, and the crystalline products were washed several times with ethanol and finally with ethyl acetate. The products were then dried in vacuum [61 – 62]. The solid product was blue and it was stored in a desiccator over $CoCl_2$. Yield = 4.4 g (66 %). Anal. Calcd for $CoCl_2(PPh_3)_2$ ($CoC_{12}H_{10}P_2Cl_2$): C, 66.06; H, 4.62; Found: C, 65.80; H, 4.60. IR (KBr) v/cm^{-1}: 3364m, 3047s [ν(C–H)], 1658mw, 1480s [m ν(C–C)], 1434vs [n ν(C–C)], 1303m, 1181vs, 1164s [c δ(C–H) ip], 1096s [q X-sens], 1070s [d δ(C–H) ip], 1028m [b δ(C–H) ip], 997s [p ring], 920 m [l δ(C–H) oop], 843m [g δ(C–H) oop], 744s [f δ(C–H) oop], 708vs [v δ(C–C) oop], 520s [y X-sens], 498s [y X-sens], 456m, 439m [t X-sens], 420w [[t X-sens]. UV-Vis [acenonitrile/pentanol (1:1)] λ_{max}/nm: 297, 591, 678 nm.

3.3.2 Synthesis of chlorotris(triphenylphosphine)cobalt(I) [$CoCl(PPh_3)_3$]

Cobalt (II) chloride hexahydrate (2.4006 g) and triphenylphosphine (8.0004 g) were added to ethanol (60 ml), and the mixture was vigorously stirred at 60–70 °C for 30 min to form blue $CoCl_2(PPh_3)_2$. The mixture was cooled to 30 °C, and sodium tetrahydridoborate was added (total of 0.3206 g, added in 10 small portions) over ca. 10 min. The reaction mixture turned dark-green, and finally minute brown crystals were formed. The crystals of

chlorotris(triphenylphosphine)cobalt(I) were vacuum-filtered under argon, washed with ethanol, water, ethanol, and petroleum ether, and dried under vacuum [62]. Yield = 5.1 g (57 %). Anal. Calcd for $CoCl(PPh_3)_3$ ($CoC_{54}H_{45}P_3Cl$): C, 73.59; H, 5.15; Found: C, 68.17; H, 4.75. IR (KBr) v/cm^{-1}: 3542m, 3418m, 3047s [*v*(C–H)], 1974mw, 1811mw, 1583m [k *v*(C–C)], 1479s [m v(C–C)], 1434vs [n v[C–C], 1307m, 1282mw, 1189vs, 1154s [c *δ*(C–H)], 1119vs, 1090s [q X-sens], 1070s [d *δ*(C–H) ip], 1025m [b *δ*(C–H) ip], 997s [p ring], 918m [l *δ*(C–H) oop], 852m [g *δ*(C–H) oop], 742s [f *δ*(C–H) oop], 722vs, 693vs [v *δ*(C–C) oop], 618w [s *δ*(C–C) ip], 541vs, 507m [y X-sens], 484s [y X-sens], 406m [w *δ*(C–C) oop].

3.4 SOLUTION PREPARATION

3.4.1 Background Electrolyte Solution

- 0.3874 g (1 mmol) TBAHFP salt was weighed and transferred into a 20 ml volumetric flask. 10 ml of acetonitrile was added to the flask to dissolve the salt. Pentanol was later added to the mark to make up a 20 ml background electrolyte solution.

3.4.2 Salt Bridge Solution

- A 0.3874 g (1 mmol) of TBAHFP salt was weighed and transferred into a 10 ml volumetric flask. 5 ml of acetonitrile was added to the flask to dissolve the salt. Pentanol was later added to the flask to the mark to make up a 10 ml solution.

3.4.3 Reference Electrode Solution

- A 0.0425 g (0.25 mmol) of $AgNO_3$ salt was weighed and transferred into a 25 ml volumetric flask. Acetonitrile was added to dissolve the salt. Once dissolution was complete, the flask was filled to the mark with acetonitrile, to make up a 0.01 M solution. The reference electrode solution was prepared weekly. The reference electrode was stored in a 0.01 M $AgNO_3$ solution in acetonitrile (solution was changed weekly).

3.4.4 Analyte (i.e. Ferrocene, $CoCl_2$, etc.) Solution

- For example, a 0.05×10^{-3} mol/l analyte stock solution was prepared by weighing a required mass of solid and transferring it into a 20 ml volumetric flask and diluting it with the background solvent (i.e. mixture of acetonitrile and pentanol (1:1)) containing the supporting electrolyte.

3.5 PROCEDURE

3.5.1 Cleaning of Electrodes and Cells

- A titration vessel and a Luggin-capillary salt bridge were rinsed first with deionised water, followed by nitric acid (0.5 M), then rinsed with deionized water and finally dried by rinsing with acetone (three times), wiped with a filter paper. During repeats of experiments the cell was rinsed with a background solvent and dried with acetone.
- The flow cells were rinsed first with deionized water, followed by rinsing quickly with nitric acid (0.5 M) (to avoid swelling of the cells, since they were made of PEEK material), then rinsed thoroughly with deionized water and finally dried by rinsing with acetone (three times). During repeats of experiments, the cell was cleaned by passing the background electrolyte solution into the cell, and scanning the CV at the same potential range, until no redox features indicating the presence of the studied electroactive species can be detected.
- A Pt sheet auxiliary electrode was cleaned in the similar manner as the salt bridge.
- The reference electrode was rinsed with acetone and wiped with a filter paper.
- The Pt disk working electrode was cleaned by polishing with a 1 µm diamond paste mixed with diamond extender blue, using a polishing cloth. The disk electrode was mantled on a polishing wheel and rolled for several minutes over a wet polishing cloth, until it was shiny. It was then rinsed with deionized water, followed by a 0.5 M HNO_3 acid, deionized water, and finally rinsed with acetone (three times) and wiped with a filter paper.
- During repeats of experiments, the electrodes were removed from the solution, carefully rinsed with a background solvent, dried with acetone and scanned over the

same potential range in the same background electrolyte solution, until no redox features indicating the presence of the studied electroactive species were detected.

3.5.2 Karl Fischer Titration

- A 5 ml syringe was used to suck the distilled solvent from the flask.
- The syringe was weighed.
- The start button form the KF instrument was pressed, and 2 ml of the solvent in a syringe was added into the KF cell, the syringe was weighed again and the obtained mass (i.e. the mass of a 2 ml solution) was entered into the KF parameters using a keyboard.
- The enter button was pressed to resume the titration and the results were recorded on the KF screen.

3.5.3 CV in Stationary Solution

- An electrochemical cell was filled with 20 ml of a background electrolyte solution.
- The cell was equipped with all the electrodes. All necessary electrical connections between the electrodes and the potentiostat were made.
- The solution was purged, by bubbling with argon for approximately 10 minutes. The argon was turned off during measurement, but a blanket of argon was maintained over a solution.
- The CV parameters were set as follows.

  (a) Ferrocene:

  - $E_{start} = -0.25$ V
  - $E_{sweep} = +0.45$ V
  - $E_{final} = -0.25$ V
  - E_{step} and Scan Rate = 0.004 V (50 mV/s).

  (b) $CoCl_2(PPh_3)_2$:

  - $E_{start} = 0$ V
  - $E_{sweep} = +1.8$ V
  - $E_{final} = 0$ V
  - E_{step} and Scan Rate = 0.004 V (50 mV/s).

- Before adding the analyte to the background solution, the background curves were recorded. These curves were subtracted later from the curves in the presence of the analyte.
- The background electrolyte solution was stirred between measurements in order to restore initial conditions, but it was not stirred during the experiment.
- A desired amount of the analyte was injected into the cell and the CV for the redox couple was recorded.
- The solution was purged between measurements.

3.5.4 Chronoamperometry in Stationary Solution

- Chronoamperometric curves were recorded immediately after recording a cyclic voltammogram (i.e. from the same solution).
- Before measurement of any chronoamperometric curves, each compound was first evaluated using cyclic voltammetry; the potentials determined by CV were used to set the potential limits for the chronoamperometry experiments.
- Example of the chronoamperometric experiment:
    - The background current of the electrode was recorded in 0.05 M TBAHFP in acetonitrile (20 ml), applying the constant potential.
    - The potential was stepped from –0.2 to 0.2 V.
    - A desired amount of ferrocene was injected into the cell, and current was recorded as a function of time at an appropriate potential.
    - The background curve was subtracted from the ferrocene curve.
    - The Cottrell plot of current versus the square root of time was constructed, and the slope was determined using linear regression analysis.
    - The electrochemically active area of the electrode was determined from the slope and the diffusion coefficient for ferrocene obtained from the literature (D = 2.37 x 10^{-5} cm^2/s, at 24 °C [63]).
    - After the determination of the electrode area, the cell and electrodes were cleaned as described in section 3.3, and the same procedure as above was repeated to determine the diffusion coefficients of the other compounds.
    - Chronoamperometric parameters in mixture of acetonitrile and pentanol (1:1) were set as follows:

(a) Ferrocene:

- Standby Potential = – 0.2 V
- Number of Potential Steps = 1
- Applied Potential = 0.25 V
- Duration Time = 25 s
- Sample Time = 0.01 s

(b) $CoCl_2$:

- Standby Potential = 0.2 V
- Number of Potential Steps = 1
- Applied Potential = 1.0 V
- Duration Time = 25 s
- Sample Time = 0.01 s

(c) $CoCl_2(PPh_3)_2$:

- Standby Potential = 0.2 V
- Number of Potential Steps = 1
- Applied Potential = 1.1 V
- Duration Time = 25 s
- Sample Time = 0.01 s

3.5.5 Combination of FIA and CV.

- 200 ml of a background electrolyte solution was added into a 250 ml bottle and connected to a dosimat (with a 10 ml exchange unit).
- A 100 ml solution of an analyte was added into another 250ml bottle and connected to another dosimat (with a 5 ml exchange unit).
- The two solutions were degassed by bubbling with argon before pumping through the flow injection analysis system.
- Then the background solution was pumped through the cell at a flow rate of 1 ml min^{-1} and the CV obtained.
- Both the background solution and the sample solution were pumped at a flow rate of 4 ml min^{-1} each to afford a total flow rate of 8 ml min^{-1}, to the mixing tee where they were mixed.
- After leaving the mixing tee, the mixed sample and background solution passed through a length of tubing and went to waste.

- They were then pumped at a flow rate of 0.5 ml min^{-1} each to afford a total flow rate of 1 ml min^{-1}, to the detector.
- The analyte was oxidized at the platinum disk working electrode in the flow cell. After travelling through the flow cell, the stream exited the cell, flowed past a reference and counter electrode, and then was delivered to waste.
- The CV was then obtained on a flowing solution.
- The flow was then stopped for a few seconds and the CV was obtained in a stopped flowing solution.

3.6 ELECTROCHEMICAL DATA ANALYSIS

- Peak current ratios for peaks of nearly reversible redox couples, where obtained from:

  i_{pa} / i_{pc} (3.1)

- For the evaluation of the separation of peak potentials the equation below was used,

  $\Delta E_p = E_{pa} - E_{pc}$ (3.2)

- ΔE_p was also used for the measurement of the reversibility of the charge transfer. For a fully reversible system, it was given by,

  $\Delta E_p = 2.3RT/nF = 59/n$ mV (25 °C) (3.3)

- The half-wave potential was determined from the following equation,

  $E_{1/2} = E_{pa} - \Delta E_p/2 = (E_{pa} + E_{pc})/2$ (3.4)

- Analysis of the chronoamperometry data was done by fitting the current-time data to the Cottrell equation (eq. 2.4) using i versus $t^{-1/2}$ graph.
- The slope of this plot was obtained.
- The active electrode area was calculated by substituting the value of $it^{1/2}$ into the Cottrell equation.
- The same working electrode was immediately used to determine the diffusion coefficient of ferrocene (in another solvent) and that of cobalt compounds studied.
- The values of $it^{1/2}$ and the active electrode area were then substituted into the Cottrell equation and the diffusion coefficient was calculated.
- The number of electrons involved was determined from the slope of a Cottrell plot of $i\pi^{1/2}/FACD^{1/2}$ vs. $t^{-1/2}$.

CHAPTER 4 PRELIMINARY STUDIES INVOLVING FERROCENE

This chapter will focus on the preliminary studies involving ferrocene as a model compound using electrochemical techniques. Ferrocene/ferrocinium couple will be used as a reference electrode potential during the studies involving cobalt organometallic compounds. In this chapter the value of resistance present in solvent mixtures that will be used in the study of cobalt organometallic compounds will be measured using ferrocene as an electroactive species. This value will then be used to correct the IR voltage drop present in solutions when studying the electrochemical properties of cobalt organometallic compounds. The effect of electrolyte concentration on the peak potential separation value will also be evaluated in this chapter. The effect that electrode positioning has on the cyclic voltammogram will also be evaluated in a flowing solution using three different types of electrochemical flow cells designed by Cukrowski [48] during the course of this project. This was done by investigating the influence of solution flow-rate and scan rate on the appearance of the voltammogram and also investigating the possibility of sample/reagent mixing on-line.

Typical experimental conditions of CV were as follows, unless otherwise stated:

- Platinum (Pt) disk was used as a working electrode (WE).
- Acetonitrile was used as a background solvent.
- Tetrabutyl ammonium hexafluorophospate ($TBAPF_6$) was used as a supporting electrolyte.
- An analyte concentration of 7.7×10^{-4} mol/l was employed.
- A scan rate was 50 mV/s.
- Only the third (or last) CV scan was used for analysis.
- All measurements were made at room temperature.

4.1 A MEASUREMENT OF UNCOMPENSATED RESISTANCE PRESENT IN VOLTAMMOGRAMS OF FERROCENE

The oxidation of ferrocene is widely used in cyclic voltammetric studies in highly resistive organic solvents as a means of reference electrode potential calibration, because of its presumed ideal reversible behaviour [64]. It has become common procedure to add ferrocene, typically in the range 0.5-1.0 mM concentration, to the electrolyte solution when cyclic voltammetry is practised in non-aqueous solvents. The main purpose of this preliminary work is to make use of the resistive distortion present in the ferrocene voltammogram to determine a reliable value of the uncompensated resistance, which in turn will be used to correct for IR voltage drop present in the voltammogram of the compound of interest. This was done by introducing increasing amounts of resistance into the cyclic voltammetric program until a good match was found between the theoretical and the experimental voltammogram. This method can also be used to confirm that the ferrocene process is indeed behaving in the ideal manner required for both reference potential and resistance calibration procedures to be valid. The uncompensated resistance in a cell is that resistance which, when multiplied by the total cell current, gives the difference in potential between the solution at the surface of the working electrode (but outside the electrical double layer) and the solution at the tip of the reference electrode probe [65].

In this work ferrocene is investigated over the appropriate range of scan rate and at various concentrations. IR drop correction was applied until the properties of the cyclic voltammograms adhere to the criteria for reversibility: difference between half-peak and peak potentials ($E_{pa} - E_p/2$) equalling 56.5 mV, difference between the anodic and cathodic peak potentials ($E_{pa} - E_{pc} = \Delta E_p$) of about 59 mV (with some dependence on switching potential), peak potentials that are independent of scan rate (numerical criteria are for a one-electron reaction at 298 K) [65], the peak current that is directly proportional to the square root of scan rate ($I_p/v^{1/2} = k$) and the ratio between anodic and cathodic peak current (I_{pa}/I_{pc}) must be equal to one. The solvent used in this experiment is a mixture of acetonitrile and pentanol (1:1 volume ratio), with 0.05 M tetrabutyl ammonium hexaflourophosphate ($TBAPF_6$) as supporting electrolyte.

A typical cyclic voltammogram with resistance compensation for the oxidation of ferrocene is given in Figure 4.1 below. The diamonds curve is the theoretical current-potential curve

for a reversible one-electron process whilst the bold line is the experimental current-potential curve obtained using Ferrocene after IR voltage drop correction. The theoretical CV curve was obtained using a digital fitting and simulation method (the procedure is given in the experimental section chapter 3). The resistance compensation was adjusted in this case by using the method described in the above paragraph. The agreement between experiment and theory indicates that the instrumental compensation has introduced no significant distortion in the data.

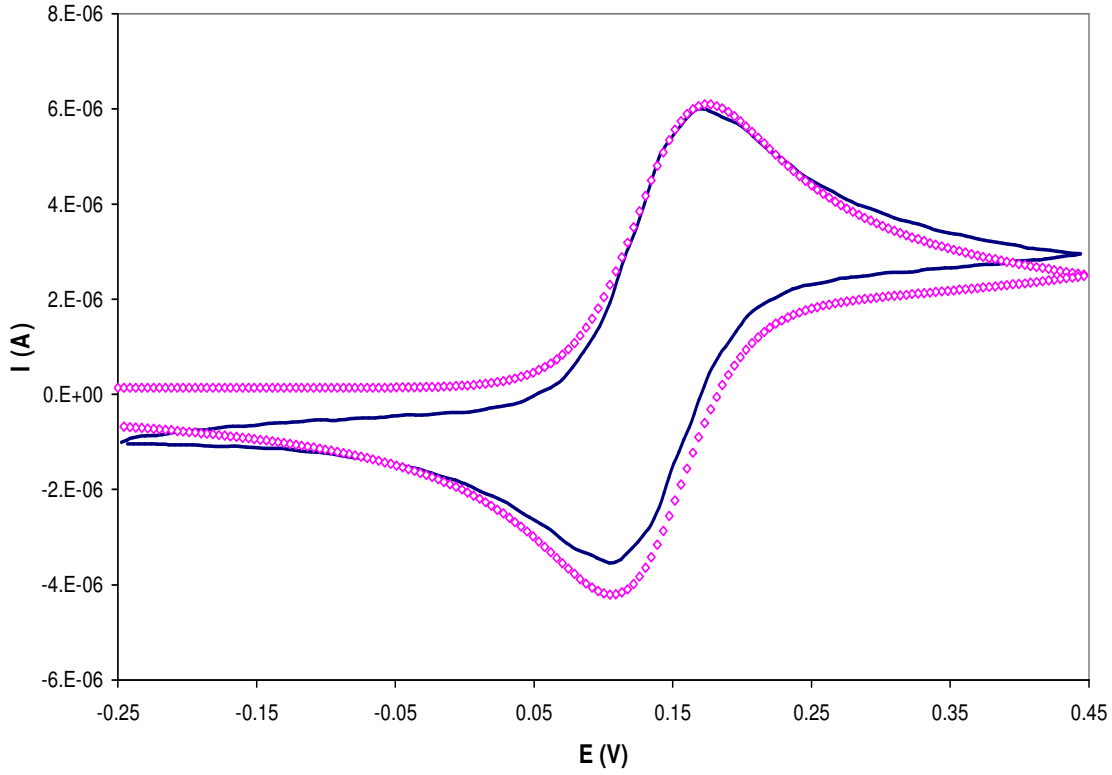

Figure 4.1 Comparison of a theoretical (diamonds) and experimental (solid line) corrected for IR with, R = 2200 Ω) CV curves of ferrocene.

Under the same conditions with no compensation, the curve resulted in large ΔE_p of about 86 mV at low scan rates of 100 mV/s (Figure 4.2). Data from 8 experiments for scan rates between 0.05 and 0.5 V/s were analysed and several important parameters describing the shape of the voltammograms were obtained. The data is summarised in Table 4.1 and 4.2.

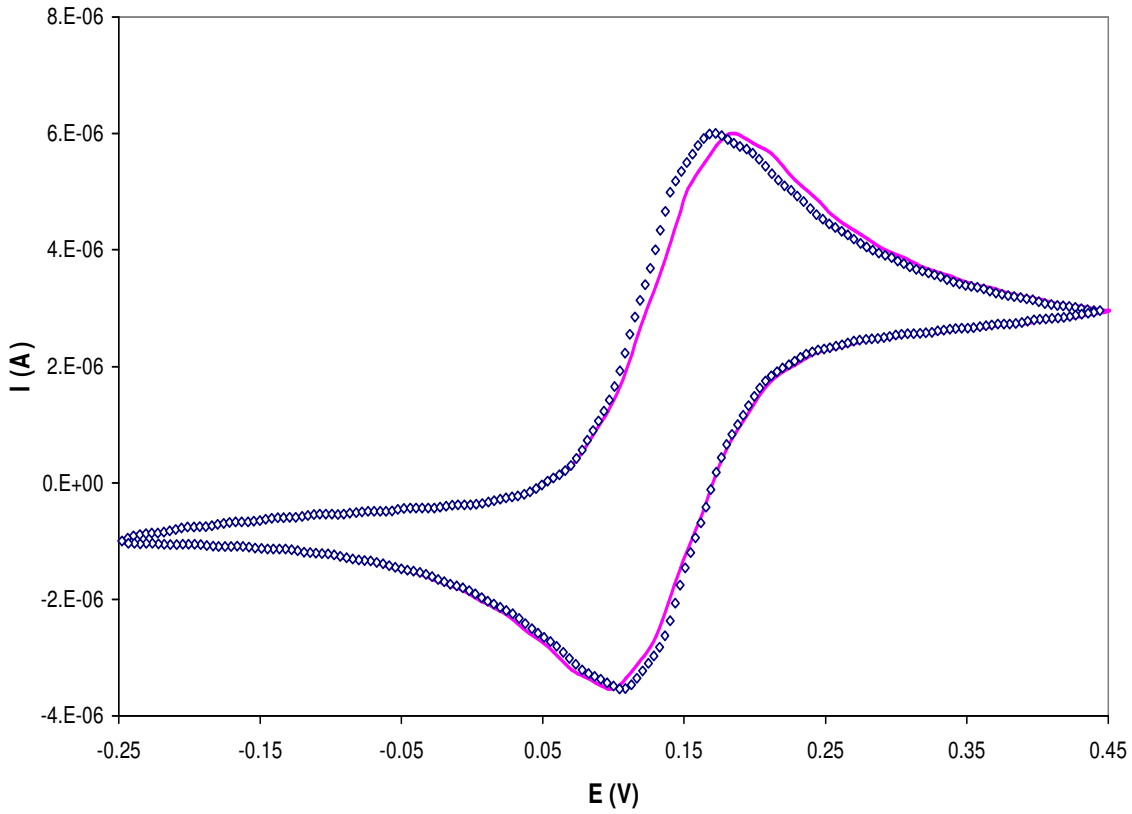

Figure 4.2 Comparison of an experimental uncorrected (solid line) and corrected for IR with R = 2200 Ω (diamonds) CV curves of ferrocene.

ΔE_p remains constant up to scan rates of 500 mV/s, a fact attesting to the accuracy of the compensation (Table 4.2). Uncompensated voltammograms obtained under the same conditions showed peak potential shifts of 8 mV at 500 mV/s (Table 4.1). $E_{pa} - E_p/2$, I_{pa}/I_{pc}, and ΔE_p values are all in accord with theory. Anodic peak current over square root of scan rate ($I_{pa}/v^{1/2}$) remained constant regardless of scan rate, which is ideal for a reversible one-electron transfer process.

Table 4.1 Analysis of data obtained from CV curves of ferrocene after background subtraction.

Scan rate, v (V/s)	E_{pa} (V)	E_{pc} (V)	ΔE_p (mV)	I_{pa} (A)	I_{pc} (A)	I_{pa}/I_{pc}	$I_{pa}/v^{1/2}$ [A/(V/s)$^{1/2}$]	$E_{pa}-E_p/2$ (mV)
0.05	0.182	0.100	82	3.60×10^{-6}	3.58×10^{-6}	1.00	1.6×10^{-5}	57
0.075	0.186	0.100	86	4.50×10^{-6}	4.48×10^{-6}	1.00	1.6×10^{-5}	60
0.100	0.186	0.100	86	5.22×10^{-6}	5.19×10^{-6}	1.00	1.6×10^{-5}	60
0.150	0.186	0.100	86	6.38×10^{-6}	6.36×10^{-6}	1.00	1.6×10^{-5}	60
0.200	0.190	0.100	90	7.37×10^{-6}	7.34×10^{-6}	1.00	1.6×10^{-5}	62
0.250	0.190	0.100	90	8.25×10^{-6}	8.25×10^{-6}	1.00	1.6×10^{-5}	63
0.400	0.190	0.100	90	1.04×10^{-5}	1.09×10^{-5}	0.95	1.6×10^{-5}	63
0.500	0.190	0.100	90	1.16×10^{-5}	1.20×10^{-5}	0.97	1.6×10^{-5}	63

Table 4.2 Analysis of data obtained from CV curves of ferrocene after background subtraction and after correction of IR voltage drop using an R value of 2200 Ω.

v (V/s)	E_{pa} (V)	E_{pc} (V)	ΔE_p (mV)	I_{pa} (A)	I_{pc} (A)	I_{pa}/I_{pc}	$I_{pa}/v^{1/2}$ [A/(V/s)$^{1/2}$]	$E_{pa}-E_p/2$ (mV)
0.05	0.173	0.113	60	3.60×10^{-6}	3.58×10^{-6}	1.00	1.6×10^{-5}	54
0.075	0.173	0.113	60	4.50×10^{-6}	4.48×10^{-6}	1.00	1.6×10^{-5}	54
0.100	0.173	0.113	60	5.22×10^{-6}	5.19×10^{-6}	1.00	1.6×10^{-5}	54
0.150	0.173	0.113	60	6.38×10^{-6}	6.36×10^{-6}	1.00	1.6×10^{-5}	54
0.200	0.173	0.113	60	7.37×10^{-6}	7.34×10^{-6}	1.00	1.6×10^{-5}	54
0.250	0.173	0.113	60	8.25×10^{-6}	8.25×10^{-6}	1.00	1.6×10^{-5}	54
0.400	0.173	0.113	60	1.04×10^{-5}	1.09×10^{-5}	0.95	1.6×10^{-5}	54
0.500	0.173	0.113	60	1.16×10^{-5}	1.20×10^{-5}	0.97	1.6×10^{-5}	54

4.2 CV OF FERROCENE IN A FLOWING SOLUTION

We needed to analyse the compounds of interest in a closed system by combining flow injection analysis and cyclic voltammetry technique. Combination of flow injection analysis and cyclic voltammetry is attractive because of the flexibility of the former and the diagnostic power of the latter [35]. In order to do this we first determined the suitable flow rate, scan rate, and a type of flow cell to use in order to obtain important parameters from a CV curve. Ferrocene was used as a model compound for this study since it is a well-studied compound that behaves reversibly. The flow rate and the scan rate are the two important parameters. Their influence on the appearance of the voltammogram is examined in detail using the three flow cells designed in our group by Cukrowski [48]. Full descriptions of the

cell designs are presented in the experimental section (Chapter 3). CV's of ferrocene were obtained first in a stationary solution before obtaining them in a flowing solution.

The effect of concentration of the supporting electrolyte was evaluated in order to make an educated decision on which concentration to use in a flowing solution. This was done with the aim of minimizing the cost of an electrolyte since high concentrations of background electrolyte will demand huge amounts of supporting electrolytes (bearing in mind that large amounts of electrolytes will be consumed daily during monitoring). Ferrocene was also investigated in this solvent over a wide range of scan rates and at various concentrations and IR drop correction was applied until the properties of the cyclic voltammograms adhere to the criteria for reversibility.

4.2.1 Studies in a Stationary Solution.

First we looked at the effect of supporting electrolyte concentration to determine a suitable concentration to be used for the preliminary studies of ferrocene in a flowing solution; the electrolyte concentrations investigated were 0.01 M and 0.05 M. Table 4.3 and 4.4 present tabulated results of the peak current separations before and after IR drop correction with R = 6200 Ω over a wide range of scan rates and on samples containing 50 and 100 mg/l concentration of ferrocene using 0.01 M $TBAPF_6$ as supporting electrolyte concentration.

Data from 9 experiments for scan rates between 0.05 and 0.5 V/s were analysed and several important parameters describing the shape of the voltammograms were obtained (Table 4.3 and 4.4). From Table 4.3 before IR voltage drop correction, ΔE_p increases with increase in scan rate and concentration of ferrocene at high scan rates (300 mV/s). At low scan rates of up to 200 mV/s and at a concentration of 50 mg/l, ΔE_p remains constant but is above 59 mV. $E_{pa} - E_p/2$ is 55 mV, I_{pa}/I_{pc} ratio is close to one and $I_{pa}/v^{1/2}$ remained constant. Increasing the scan rate to above 200 mV/s resulted in an increase in ΔE_p, $E_{pa} - E_p/2$ and decrease in $I_{pa}/v^{1/2}$ values. Increasing the concentration to 100 mg/l resulted in a huge increase in ΔE_p, $E_{pa} - E_p/2$ and decrease in $I_{pa}/v^{1/2}$ values at all studied scan rates. The ratio between anodic and cathodic peak current is far from unity.

Table 4.3 Analysis of data obtained from CV curves of ferrocene in acetonitrile containing 0.01 M $TBAPF_6$ after background subtraction.

Conc. (mg/l)	v (V/s)	E_{pa} (V)	E_{pc} (V)	ΔE_p (mV)	I_{pa} (A)	I_{pc} (A)	I_{pa}/I_{pc}	$I_{pa}/v^{1/2}$ [A/(V/s)$^{1/2}$]	$E_{pa}-E_p/2$ (mV)
50	0.05	0.135	0.053	82	1.80×10^{-6}	1.75×10^{-6}	1.03	8.0×10^{-6}	55
	0.075	0.135	0.053	82	2.20×10^{-6}	2.18×10^{-6}	1.01	8.0×10^{-6}	55
	0.100	0.135	0.053	82	2.53×10^{-6}	2.50×10^{-6}	1.01	8.0×10^{-6}	55
	0.125	0.135	0.053	82	2.84×10^{-6}	2.79×10^{-6}	1.02	8.0×10^{-6}	55
	0.150	0.135	0.053	82	3.10×10^{-6}	3.04×10^{-6}	1.02	8.0×10^{-6}	55
	0.200	0.135	0.053	82	3.60×10^{-6}	3.55×10^{-6}	1.01	8.0×10^{-6}	55
	0.300	0.139	0.053	86	4.20×10^{-6}	4.18×10^{-6}	1.00	7.7×10^{-6}	57
	0.400	0.143	0.045	98	4.77×10^{-6}	4.73×10^{-6}	1.00	7.5×10^{-6}	62
	0.500	0.143	0.045	98	5.26×10^{-6}	5.24×10^{-6}	1.00	7.4×10^{-6}	62
100	0.050	0.147	0.049	98	3.49×10^{-6}	3.08×10^{-6}	1.13	1.6×10^{-5}	63
	0.075	0.156	0.045	111	4.10×10^{-6}	3.38×10^{-6}	1.21	1.5×10^{-5}	66
	0.100	0.160	0.045	115	4.63×10^{-6}	3.84×10^{-6}	1.21	1.5×10^{-5}	68
	0.125	0.160	0.045	115	5.00×10^{-6}	4.15×10^{-6}	1.21	1.4×10^{-5}	68
	0.150	0.164	0.041	123	5.35×10^{-6}	4.44×10^{-6}	1.21	1.4×10^{-5}	70
	0.200	0.169	0.041	128	5.95×10^{-6}	4.98×10^{-6}	1.20	1.3×10^{-5}	72
	0.300	0.173	0.036	137	6.97×10^{-6}	5.92×10^{-6}	1.18	1.3×10^{-5}	74
	0.400	0.177	0.032	145	7.73×10^{-6}	6.73×10^{-6}	1.15	1.2×10^{-5}	76
	0.500	0.182	0.032	150	8.27×10^{-6}	7.18×10^{-6}	1.15	1.2×10^{-5}	80

Introduction of IR drop correction only improved the ΔE_p value, which remained constant with increase in scan rate with a value of 60 mV (Table 4.4). The $E_{pa} - E_p/2$ deviated from a theoretical value by about 5 mV at all studied scan rates at a concentration of 50 mg/l and deviated by 4 mV at a concentration of 100 mg/l. The deviation in a ($E_{pa} - E_p/2$) value from 56 mV predicted for the process controlled only by diffusion, may be due to overcompensation resulting in a steep curve. The peak current ratio remained unchanged after compensation, so was the value of $I_{pa}/v^{1/2}$.

Table 4.4 Analysis of data in Table 4.3, obtained from CV curves of ferrocene after correction of IR voltage drop using an R value of 6200 Ω.

Conc. (mg/l)	v (V/s)	E_{pa} (V)	E_{pc} (V)	ΔE_p (mV)	I_{pa} (A)	I_{pc} (A)	I_{pa}/I_{pc}	$I_{pa}/v^{1/2}$ [A/(V/s)$^{1/2}$]	$E_{pa}-E_p/2$ (mV)
50	0.050	0.120	0.060	60	1.80×10^{-6}	1.75×10^{-6}	1.03	8.0×10^{-6}	51
	0.075	0.120	0.060	60	2.20×10^{-6}	2.18×10^{-6}	1.01	8.0×10^{-6}	51
	0.100	0.120	0.060	60	2.53×10^{-6}	2.50×10^{-6}	1.01	8.0×10^{-6}	51
	0.125	0.120	0.060	60	2.84×10^{-6}	2.79×10^{-6}	1.02	8.0×10^{-6}	51
	0.150	0.120	0.060	60	3.10×10^{-6}	3.04×10^{-6}	1.02	8.0×10^{-6}	51
	0.200	0.120	0.060	60	3.60×10^{-6}	3.55×10^{-6}	1.01	8.0×10^{-6}	51
	0.300	0.120	0.060	60	4.20×10^{-6}	4.18×10^{-6}	1.00	7.7×10^{-6}	51
	0.400	0.120	0.060	60	4.77×10^{-6}	4.73×10^{-6}	1.00	7.5×10^{-6}	51
	0.500	0.120	0.060	60	5.26×10^{-6}	5.24×10^{-6}	1.00	7.4×10^{-6}	51
100	0.050	0.122	0.062	60	3.49×10^{-6}	3.08×10^{-6}	1.13	1.6×10^{-5}	52
	0.075	0.122	0.062	60	4.10×10^{-6}	3.38×10^{-6}	1.21	1.5×10^{-5}	52
	0.100	0.122	0.062	60	4.63×10^{-6}	3.84×10^{-6}	1.21	1.5×10^{-5}	52
	0.125	0.122	0.062	60	5.00×10^{-6}	4.15×10^{-6}	1.21	1.4×10^{-5}	52
	0.150	0.122	0.062	60	5.35×10^{-6}	4.44×10^{-6}	1.21	1.4×10^{-5}	52
	0.200	0.122	0.062	60	5.95×10^{-6}	4.98×10^{-6}	1.20	1.3×10^{-5}	52
	0.300	0.122	0.062	60	6.97×10^{-6}	5.92×10^{-6}	1.18	1.3×10^{-5}	52
	0.400	0.122	0.062	60	7.73×10^{-6}	6.73×10^{-6}	1.15	1.2×10^{-5}	52
	0.500	0.122	0.062	60	8.27×10^{-6}	7.18×10^{-6}	1.15	1.2×10^{-5}	52

Increasing the electrolyte solution concentration to 0.05 M, results in improved results. Table 4.5 presents data before IR voltage drop correction for scan rates between 0.05 and 0.5 V/s; ΔE_p remains constant but is above 59 mV. The $E_{pa} - E_p/2$ value is 55 mV and I_{pa}/I_{pc} is close to one; this is all in accord with theory at all studied scan rates and concentrations.

Table 4.5 Analysis of data obtained from CV curves of ferrocene in acetonitrile containing 0.05 M $TBAPF_6$ after background subtraction.

Conc. (mg/l)	v (V/s)	E_{pa} (V)	E_{pc} (V)	ΔE_p (mV)	I_{pa} (A)	I_{pc} (A)	I_{pa}/I_{pc}	$I_{pa}/v^{1/2}$ [A/(V/s)$^{1/2}$]	$E_{pa}-E_p/2$ (mV)
50	0.050	0.130	0.062	68	1.80×10^{-6}	1.82×10^{-6}	0.99	8.0×10^{-6}	55
	0.075	0.130	0.062	68	2.20×10^{-6}	2.20×10^{-6}	1.00	8.0×10^{-6}	55
	0.100	0.130	0.062	68	2.55×10^{-6}	2.62×10^{-6}	0.97	8.0×10^{-6}	55
	0.125	0.130	0.062	68	2.85×10^{-6}	2.83×10^{-6}	1.00	8.0×10^{-6}	55
	0.150	0.130	0.062	68	3.10×10^{-6}	3.12×10^{-6}	0.99	8.0×10^{-6}	55
	0.175	0.130	0.062	68	3.36×10^{-6}	3.31×10^{-6}	1.01	8.0×10^{-6}	55
	0.200	0.130	0.062	68	3.60×10^{-6}	3.55×10^{-6}	1.01	8.0×10^{-6}	55
	0.300	0.130	0.062	68	4.41×10^{-6}	4.37×10^{-6}	1.01	8.0×10^{-6}	55
	0.400	0.130	0.062	68	5.09×10^{-6}	5.05×10^{-6}	1.01	8.0×10^{-6}	55
	0.500	0.130	0.062	68	5.66×10^{-6}	5.54×10^{-6}	1.02	8.0×10^{-6}	55
100	0.050	0.130	0.062	68	3.61×10^{-6}	3.58×10^{-6}	1.00	1.6×10^{-5}	55
	0.075	0.130	0.062	68	4.41×10^{-6}	4.42×10^{-6}	1.00	1.6×10^{-5}	55
	0.100	0.130	0.062	68	5.08×10^{-6}	5.05×10^{-6}	1.00	1.6×10^{-5}	55
	0.125	0.130	0.062	68	5.65×10^{-6}	5.66×10^{-6}	1.00	1.6×10^{-5}	55
	0.150	0.130	0.062	68	6.10×10^{-6}	6.05×10^{-6}	1.00	1.6×10^{-5}	55
	0.200	0.130	0.062	68	7.00×10^{-6}	6.96×10^{-6}	1.00	1.6×10^{-5}	55
	0.300	0.130	0.062	68	8.52×10^{-6}	8.50×10^{-6}	1.00	1.6×10^{-5}	55
	0.400	0.130	0.062	68	9.96×10^{-6}	9.94×10^{-6}	1.00	1.6×10^{-5}	55
	0.500	0.130	0.062	68	1.15×10^{-5}	1.14×10^{-5}	1.00	1.6×10^{-5}	55
200	0.050	0.130	0.062	68	6.88×10^{-6}	7.04×10^{-6}	0.98	3.1×10^{-5}	55
	0.075	0.130	0.062	68	8.56×10^{-6}	8.66×10^{-6}	0.99	3.1×10^{-5}	55
	0.100	0.130	0.062	68	9.93×10^{-6}	1.00×10^{-5}	0.99	3.1×10^{-5}	55
	0.125	0.130	0.062	68	1.11×10^{-5}	1.12×10^{-5}	0.99	3.1×10^{-5}	55
	0.150	0.130	0.062	68	1.21×10^{-5}	1.22×10^{-5}	0.99	3.1×10^{-5}	55
	0.200	0.130	0.062	68	1.40×10^{-5}	1.40×10^{-5}	1.00	3.1×10^{-5}	55
	0.300	0.130	0.062	68	1.69×10^{-5}	1.69×10^{-5}	1.00	3.1×10^{-5}	55
	0.400	0.130	0.062	68	1.95×10^{-5}	1.94×10^{-5}	1.00	3.1×10^{-5}	55
	0.500	0.130	0.062	68	2.19×10^{-5}	2.16×10^{-5}	1.00	3.1×10^{-5}	55

Correction of IR drop only improved the ΔE_p value, which remained constant with increase in scan rate and concentration and had a value of 60 mV (Table 4.6 and 4.7). The $E_{pa} - E_p/2$ deviated from a theoretical value of 56 mV by about 3 mV at all studied concentrations.

Table 4.6 Analysis of data in Table 4.5 obtained from CV curves of ferrocene after correction of IR voltage drop using an R value of 3000 Ω.

Conc. (mg/l)	v (V/s)	E_{pa} (V)	E_{pc} (V)	ΔE_p (mV)	I_{pa} (A)	I_{pc} (A)	I_{pa}/I_{pc}	$I_{pa}/v^{1/2}$ [A/ (V/s)$^{1/2}$]	$E_{pa}-E_p/2$ (mV)
50	0.050	0.126	0.066	60	1.80×10^{-6}	1.82×10^{-6}	0.99	8.0×10^{-6}	53
	0.075	0.126	0.066	60	2.20×10^{-6}	2.20×10^{-6}	1.00	8.0×10^{-6}	53
	0.100	0.126	0.066	60	2.55×10^{-6}	2.62×10^{-6}	0.97	8.0×10^{-6}	53
	0.125	0.126	0.066	60	2.85×10^{-6}	2.83×10^{-6}	1.00	8.0×10^{-6}	53
	0.150	0.126	0.066	60	3.10×10^{-6}	3.12×10^{-6}	0.99	8.0×10^{-6}	53
	0.175	0.126	0.066	60	3.36×10^{-6}	3.31×10^{-6}	1.01	8.0×10^{-6}	53
	0.200	0.126	0.066	60	3.60×10^{-6}	3.55×10^{-6}	1.01	8.0×10^{-6}	53
	0.300	0.126	0.066	60	4.41×10^{-6}	4.37×10^{-6}	1.01	8.0×10^{-6}	53
	0.400	0.126	0.066	60	5.09×10^{-6}	5.05×10^{-6}	1.01	8.0×10^{-6}	53
	0.500	0.126	0.066	60	5.66×10^{-6}	5.54×10^{-6}	1.02	8.0×10^{-6}	53
100	0.050	0.126	0.066	60	3.61×10^{-6}	3.58×10^{-6}	1.00	1.6×10^{-5}	53
	0.075	0.126	0.066	60	4.41×10^{-6}	4.42×10^{-6}	1.00	1.6×10^{-5}	53
	0.100	0.126	0.066	60	5.08×10^{-6}	5.05×10^{-6}	1.00	1.6×10^{-5}	53
	0.125	0.126	0.066	60	5.65×10^{-6}	5.66×10^{-6}	1.00	1.6×10^{-5}	53
	0.150	0.126	0.066	60	6.10×10^{-6}	6.05×10^{-6}	1.00	1.6×10^{-5}	53
	0.200	0.126	0.066	60	7.00×10^{-6}	6.96×10^{-6}	1.00	1.6×10^{-5}	53
	0.300	0.126	0.066	60	8.52×10^{-6}	8.50×10^{-6}	1.00	1.6×10^{-5}	53
	0.400	0.126	0.066	60	9.96×10^{-6}	9.94×10^{-6}	1.00	1.6×10^{-5}	53
	0.500	0.126	0.066	60	1.15×10^{-5}	1.14×10^{-5}	1.00	1.6×10^{-5}	53

Table 4.7 Analysis of data obtained from CV curves of ferrocene after background subtraction and after correction of IR voltage drop using an R value of 1000 Ω.

Conc. (mg/l)	v (V/s)	E_{pa} (V)	E_{pc} (V)	ΔE_p (mV)	I_{pa} (A)	I_{pc} (A)	I_{pa}/I_{pc}	$I_{pa}/v^{1/2}$ [A/ (V/s)$^{1/2}$]	$E_{pa}-E_p/2$ (mV)
200	0.050	0.122	0.062	60	6.88×10^{-6}	7.04×10^{-6}	0.98	3.1×10^{-5}	53
	0.075	0.122	0.062	60	8.56×10^{-6}	8.66×10^{-6}	0.99	3.1×10^{-5}	53
	0.100	0.122	0.062	60	9.93×10^{-6}	1.00×10^{-5}	0.99	3.1×10^{-5}	53
	0.125	0.122	0.062	60	1.11×10^{-5}	1.12×10^{-5}	0.99	3.1×10^{-5}	53
	0.150	0.122	0.062	60	1.21×10^{-5}	1.22×10^{-5}	0.99	3.1×10^{-5}	53
	0.200	0.122	0.062	60	1.40×10^{-5}	1.40×10^{-5}	1.00	3.1×10^{-5}	53
	0.300	0.122	0.062	60	1.69×10^{-5}	1.69×10^{-5}	1.00	3.1×10^{-5}	53
	0.400	0.122	0.062	60	1.95×10^{-5}	1.94×10^{-5}	1.00	3.1×10^{-5}	53
	0.500	0.122	0.062	60	2.19×10^{-5}	2.16×10^{-5}	1.00	3.1×10^{-5}	53

The amount of resistance required for compensation of curves at high concentrations of ferrocene (200 mg/l) was smaller than the amount required for low concentrations. The

resistance amount required for compensation was only 1000 Ohm. This shows that analyte made significant contribution to the overall conductivity of solution that most likely resulted in migration current. Therefore, for any rigorous studies involving e.g. mechanisms of electrochemical reaction, either the concentration of the supporting electrolyte would have to be increased or concentration of the analyte (i.e. ferrocene) would have to be decreased.

4.2.2 Studies in a Flowing Solution.

Here we investigated the effect of scan rate and flow rate on the appearance of a cyclic voltammogram using different flow cells. The main difference in these flow cells was positioning of electrodes. The performances of the flow through cells were evaluated by cyclic voltammetry using ferrocene as an analyte. First we analysed the CV curves obtained using the so-called flow-by cell, whereby the background electrolyte solution is flowing along the working electrode. The reference and counter electrodes were facing each other and so were the outlet and inlet tubes.

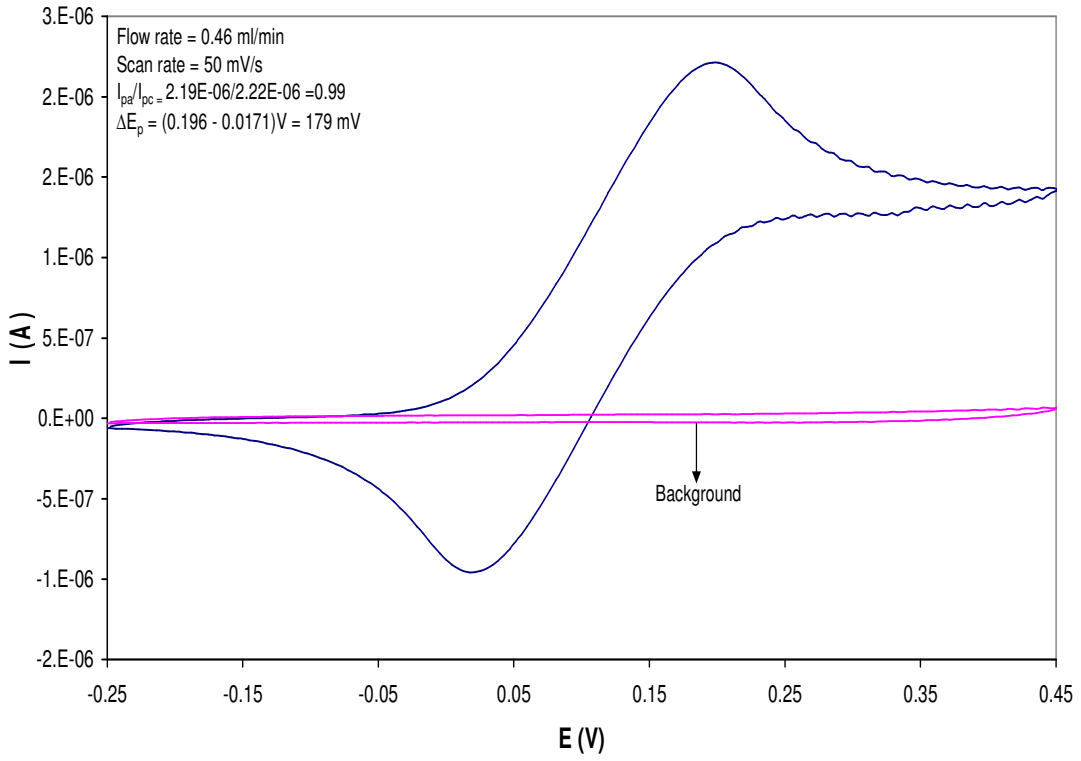

Figure 4.3 CV curve of a 50 mg/l ferrocene obtained using a flow-by electrochemical cell, flow rate = 0.46 ml min^{-1}.

The employed concentration of the supporting electrolyte ($TBAPF_6$) was 0.01 M. A low concentration of electrolyte solutions was used to minimize cost and because the amount of resistance introduced could be corrected for. Figure 4.3 shows a cyclic voltammogram of ferrocene at a scan rate of 50 mV/s and a flow rate of 0.46 ml min^{-1}. Well-defined anodic and cathodic peaks were observed from the CV curve. The anodic wave represents the oxidation of $Fe^{2+}Cp_2$ to $Fe^{3+}Cp_2$, while the cathodic wave represents the reduction of $Fe^{3+}Cp_2$ to $Fe^{2+}Cp_2$ (the reverse reaction).

Table 4.8 Data of peak potential separations and peak current ratio obtained from a 50 mg/l ferrocene stock solution at different scan rates and flow rates using a flow-by cell 1.

		Before IR drop correction				After IR drop correction		
Flow rate (ml min^{-1})	v (V s^{-1})	E_{pa} (V)	E_{pc} (V)	ΔE_p (mV)	I_{pa}/I_{pc}	E_{pa} (V)	E_{pc} (V)	ΔE_p (mV) [R = 34000 Ω]
0.00	0.050	0.183	0.00427	178	0.99	0.120	0.060	60
	0.100	0.206	0.0159	190	0.99	0.120	0.060	60
	0.200	0.233	0.0412	192	0.99	0.120	0.060	60
	0.300	0.262	0.062	200	0.98	0.120	0.060	60
	0.400	0.271	0.0677	203	0.98	0.120	0.060	60
0.46	0.050	0.196	0.0171	179	0.99	0.120	0.060	60
	0.100	0.214	0.0275	186	0.96	0.120	0.060	60
	0.200	0.247	0.0412	206	0.91	0.120	0.060	60
	0.300	0.262	0.0476	214	0.86	0.120	0.060	60
	0.400	0.271	0.0510	220	0.85	0.120	0.060	60
0.98	0.050	0.201	0.0256	175	0.99	0.120	0.060	60
	0.100	0.222	0.0159	206	0.99	0.120	0.060	60
	0.200	0.247	0.0275	219	0.98	0.120	0.060	60
	0.300	0.286	0.0476	238	0.94	0.120	0.060	60
	0.400	0.305	0.0577	247	0.89	0.120	0.060	60
1.52	0.050	0.214	0.0299	184	0.98	0.120	0.060	60
	0.100	0.230	0.0159	214	0.97	0.120	0.060	60
	0.200	0.247	0.0137	233	0.95	0.120	0.060	60
	0.300	0.284	0.0473	237	0.93	0.120	0.060	60
	0.400	0.304	0.0550	249	0.93	0.120	0.060	60

The CV curves obtained with increase in scan rate are presented in Appendix A (Figure A1 – A4). Increasing the flow rate and scan rate result in large potential separation between the anodic and cathodic peaks which can be interpreted in terms of IR drop due to the working

electrode and the reference electrode being far apart (Table 4.8). It is interesting to see that after IR drop correction (R = 34000 Ω) the ΔE_p value approached 60 mV for all studied scan rates as predicted for one-electron reversible charge transfer.

Figures 4.4 to 4.6 present comparisons of the CV curves of ferrocene obtained in a flowing solution, non-flowing solution in a flow cell and bulk solution in an open cell before and after IR voltage drop correction. This was done to see how the peak potential separation value vary in different solution types and how much resistance would be required in each CV to bring the peaks closer together (to ~ 60 mV). The amount of resistance used to bring the peak separation value to 60 mV was 34000 Ω in both the flowing and non-flowing solution and 6200 Ω in a bulk solution. The difference in IR is due to the geometry of the cells, namely the distance between the reference and the working electrode.

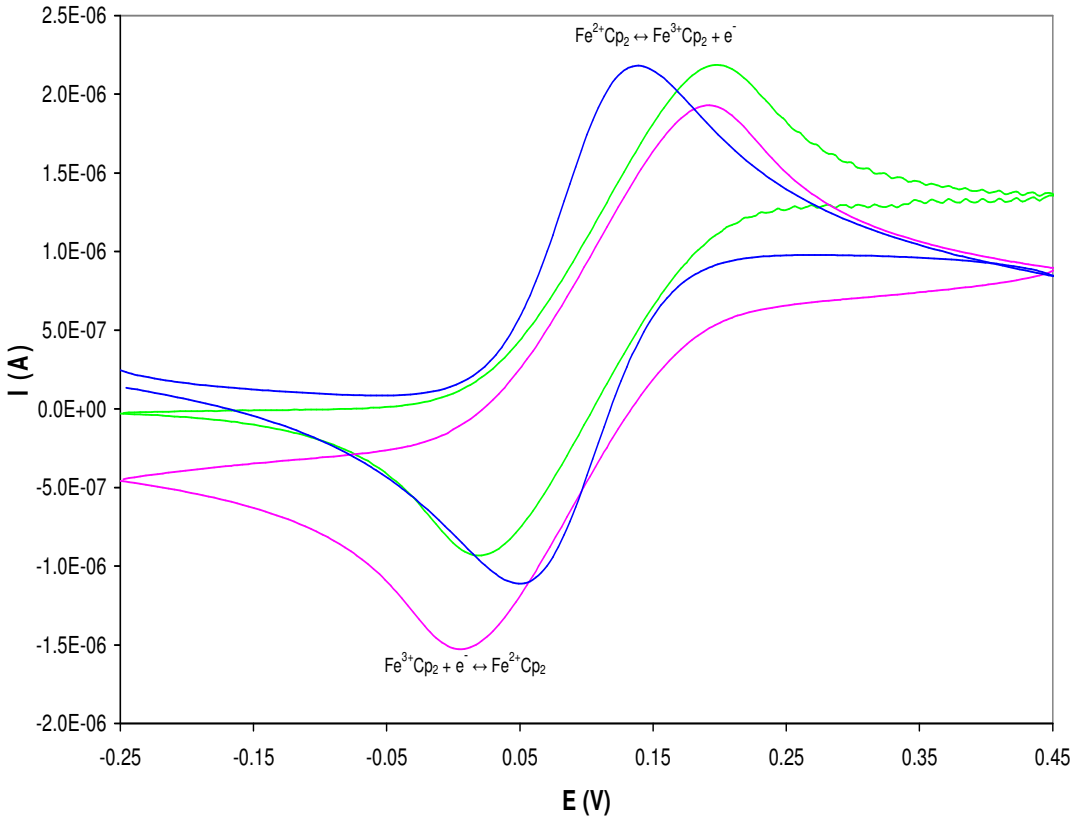

Figure 4.4 Comparison of the CV curves of a 50 mg/l ferrocene in a flowing (— 0.46 ml min^{-1}) and non-flowing (—) solution using a flow-by electrochemical cell and in a bulk solution (—) using an open cell.

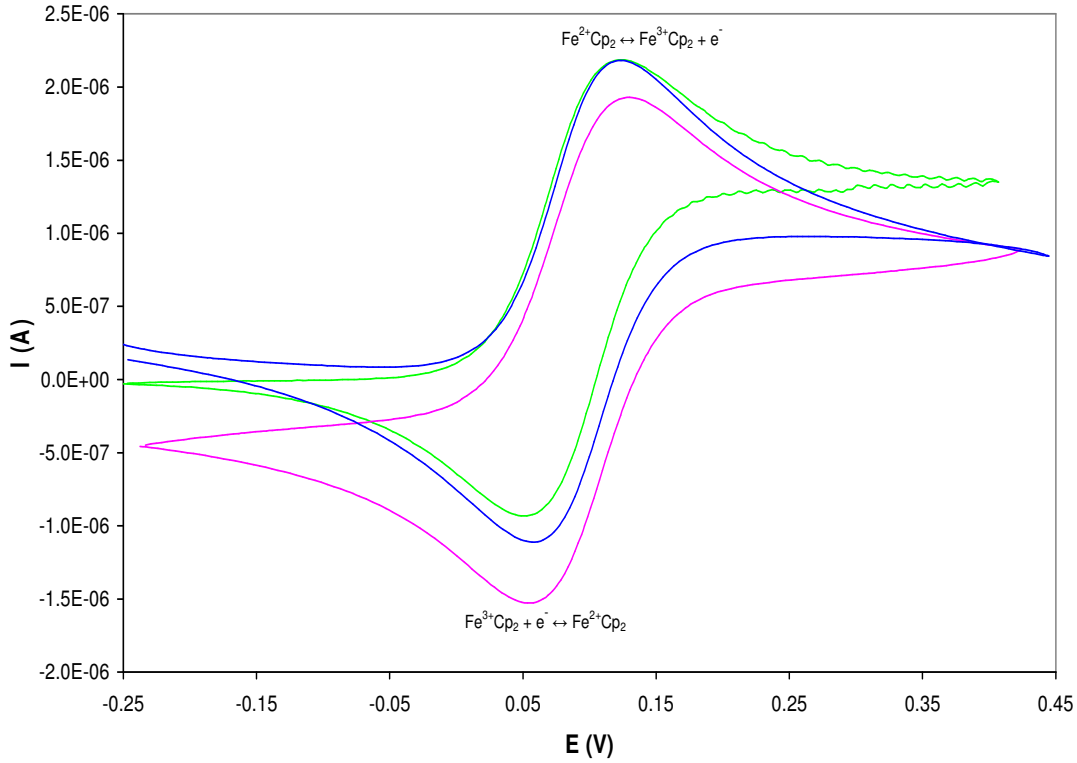

Figure 4.5 Comparison of the CV curves of ferrocene shown in Figure 4.4 after IR voltage drop correction.

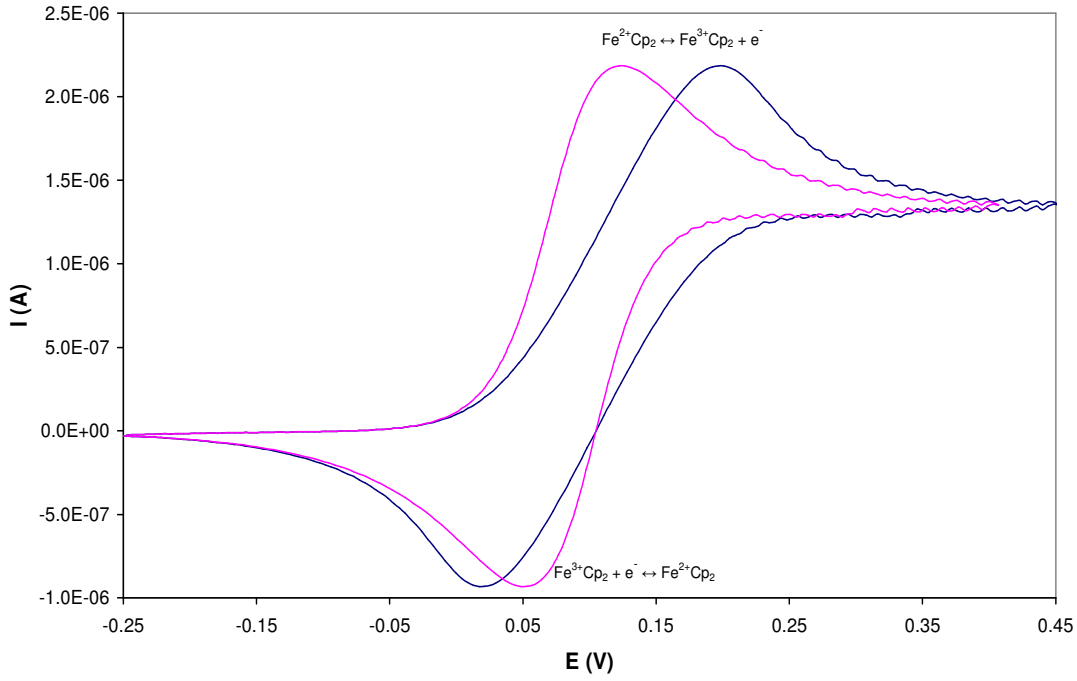

Figure 4.6 Comparison of CV curves of a 50 mg/l ferrocene in a flowing solution before (—) and after (—) IR voltage drop correction (R = 34000 Ω), flow rate = 0.46 ml min^{-1}.

Next, we repeated the above experiments of ferrocene in a flowing solution using a wall-jet type of a flow cell whereby the solution is flowing perpendicularly towards the working electrode. Two types of wall-jet flow cells were used in this study, with the main difference being a type of the auxiliary electrode used and its position in a flow cell as described in the experimental section chapter 3. Figures 4.7 and 4.8 show CV's of ferrocene in a flowing solution using two wall-jet flow cells at a flow rate 0.46 ml min^{-1}. CV exhibits a characteristic polarogram-like shape at slow scan rate (50 mV/s) and the reverse trace is almost superimposable on the forward trace, hence no peak-like responses are observed. In this respect the reverse trace yield no useful information as oxidized products are swept away from the electrode before they could eventually be reduced. This behaviour arises because in wall-jet cells a thin layer of stagnant solution is present adjacent to the electrode surface and flow is away from the electrode ensuring that a fresh solution is effectively brought to the electrode surface. Under such hydrodynamic conditions, the electrochemical process is controlled by both convection and diffusion.

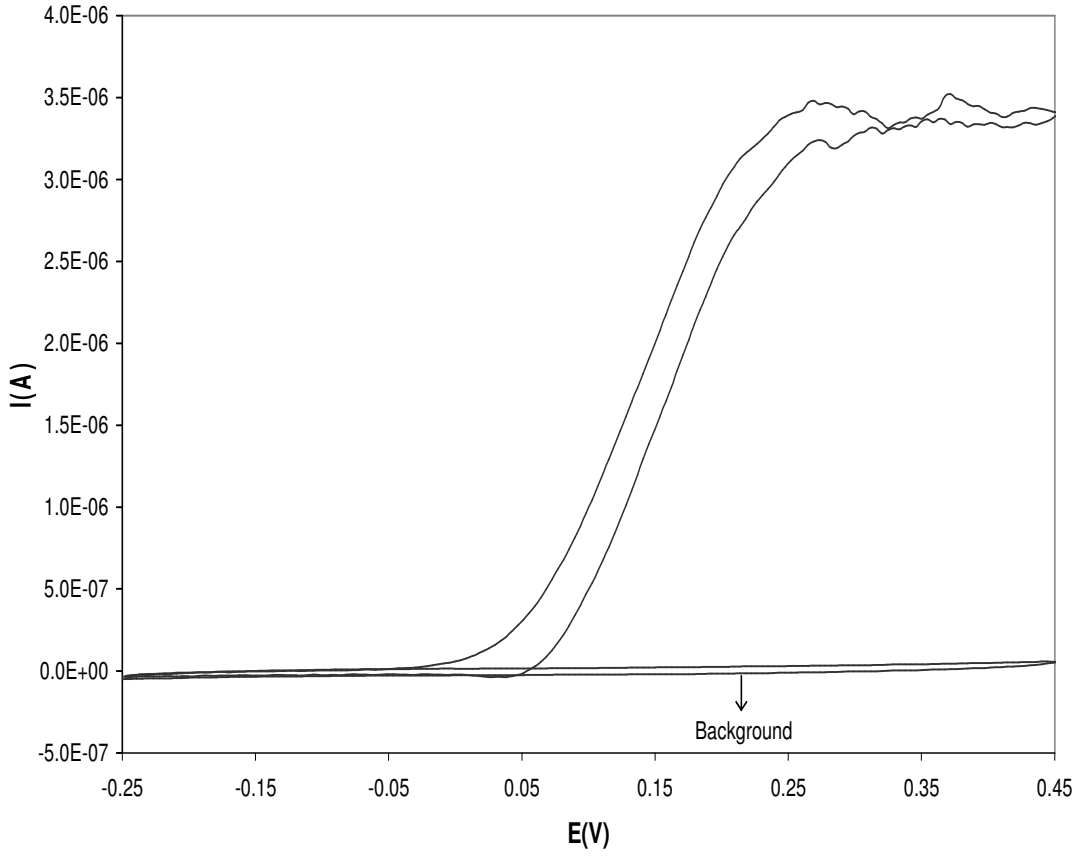

Figure 4.7 CV curves of a 50 mg/l ferrocene in a flowing solution using a wall-jet electrochemical cell with a gold-disk auxiliary electrode, flow rate = 0.46 ml min^{-1}.

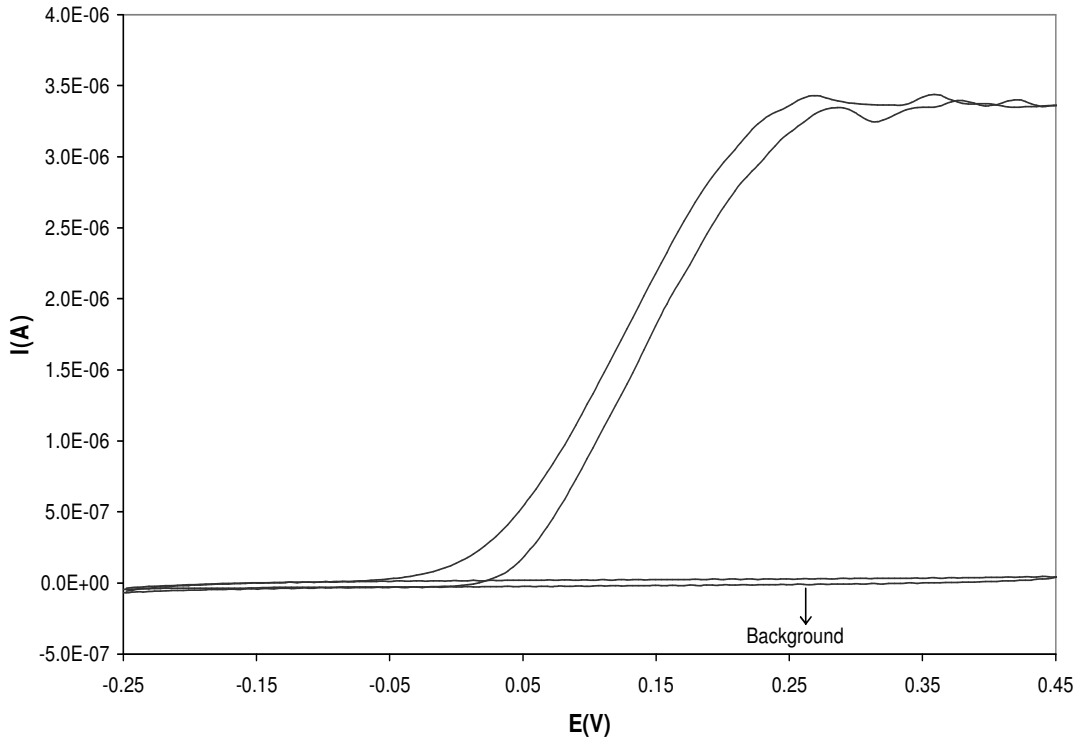

Figure 4.8 CV curves of a 50 mg/l ferrocene in a flowing solution using a wall-jet electrochemical cell with a steel rod tube auxiliary electrode and outlet, flow rate = 0.46 ml min^{-1}.

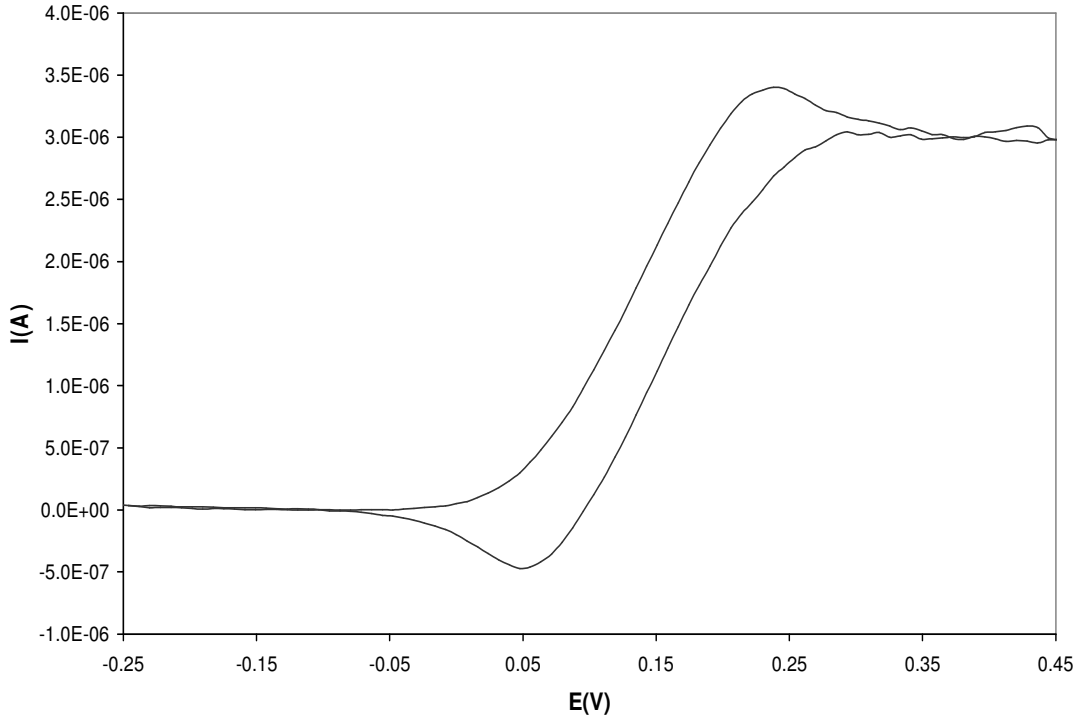

Figure 4.9 CV curves of a 50 mg/l ferrocene in a flowing solution using a wall-jet electrochemical cell with a gold-disk auxiliary electrode, flow rate = 0.46 ml min^{-1} and v = 100 mV/s.

As scan rate is increased to 100 mV/s, the voltammograms deviates a little from the typical polarogram shape, as a small peak component is present at the onset of the limiting current plateau (Figure 4.9).

Figure 4.10 shows the effect of increased scan rate on the cyclic voltammogram of ferrocene. As the scan rate is increased to above 100 $mV.s^{-1}$, the voltammograms deviate from a convection/diffusion-controlled polarogram shaped curve to nearly diffusion controlled peak-shaped curves. The peak intensity increased with increasing scan rate, while the anodic peak shifts towards higher potentials as expected due to IR drop. The oxidized compound will still be present in the stagnant layer attached to the electrode surface during the reverse scan, and the reversibly oxidized ferrocene clearly shows a reduction wave since increasing the scan rate results in a decrease of the diffusion layer thickness. There seems to be no significant difference between curves obtained in the two wall-jet flow cells, which confirms that the type and position of the auxiliary electrode does not play a significant role. The CV data obtained for the peak potential separations are summarised in Tables 4.9 and 4.10.

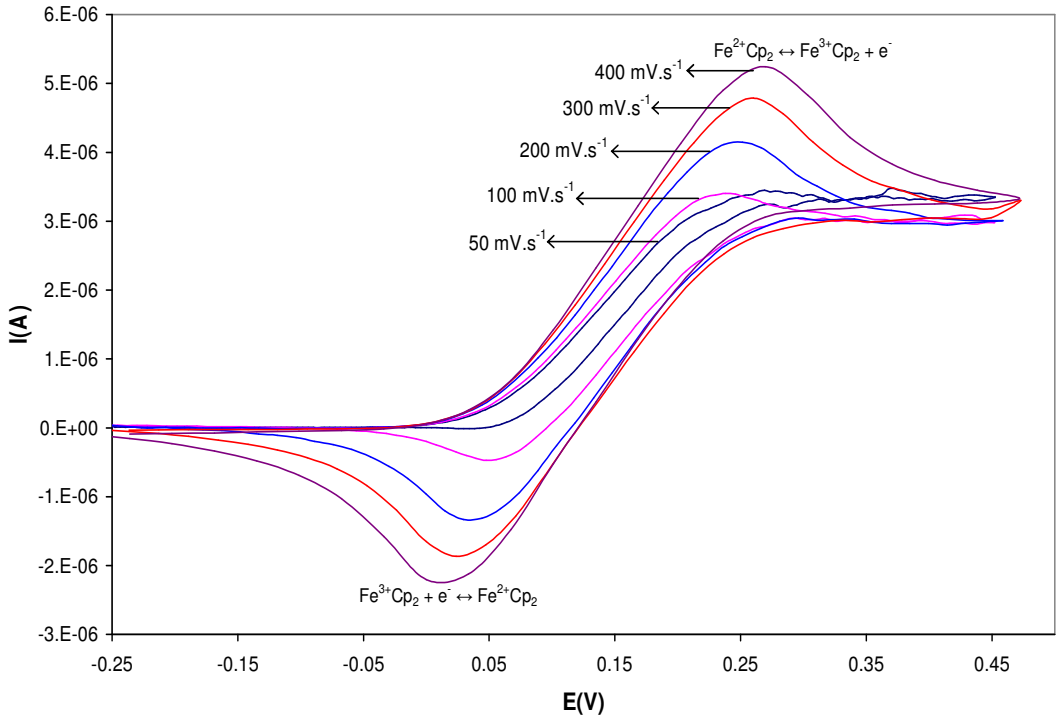

Figure 4.10 CV curves of a 50 mg/l ferrocene after background subtraction at different scan rates and a flow rate of 0.46 ml/min using a wall-jet electrochemical cell with a gold-disk auxiliary electrode.

Table 4.9 Data of peak potential separations and peak current ratio obtained from a ferrocene solution using a wall-jet flow cell with a gold disk auxiliary electrode.

Flow rate (ml min^{-1})	v (V s^{-1})	E_{pa} (V)	E_{pc} (V)	ΔE_p (mV)	I_{pa}/I_{pc}
0.46	0.050	–	–	–	–
	0.100	0.230	0.0476	182	0.97
	0.200	0.252	0.0296	222	0.97
	0.300	0.260	0.0237	236	0.97
	0.400	0.270	0.0000	270	0.99
0.98	0.050	–	–	–	–
	0.100	–	–	–	–
	0.200	–	–	–	–
	0.300	0.286	0.0238	262	1.03
	0.400	0.305	0.0000	305	0.99

– = *no peak was observed*

Table 4.10 Data of peak potential separations and peak current ratio obtained from ferrocene solution using a wall-jet flow cell with a steel rod tube auxiliary electrode.

Flow rate (ml min^{-1})	v (V s^{-1})	E_{pa} (V)	E_{pc} (V)	ΔE_p (mV)	I_{pa}/I_{pc}
0.46	0.050	–	–	–	–
	0.100	0.230	0.0159	214	1.0
	0.200	0.237	0.0148	222	1.0
	0.300	0.262	0.0238	238	0.99
	0.400	0.271	0.0310	240	0.99
0.98	0.050	–	–	–	–
	0.100	–	–	–	–
	0.200	–	–	–	–
	0.300	0.286	0.000	286	1.0
	0.400	0.305	0.000	305	1.0

– = *no peak was observed*

We arrived at the following conclusions from the above data:

- With all the flow cells it is possible to choose the experimental conditions that favour convection/diffusion-controlled (polarogram-shaped) voltammograms or diffusion-controlled (peak-shaped) voltammograms.
- The main distinguishing factor between the three home-made designs of the flow cells is that with the flow–by electrochemical cell 1, there is no convection, so

processes are controlled only by diffusion and results are very much similar to those obtained in the bulk solution in an open cell. It is obvious that diffusion-controlled electrochemical processes recorded here might change to mixed mode (convection and diffusion) at slow scan rates and increased flow rates. Flow-by cell is by far more versatile as it can be recommended for fundamental, mechanisms, speciation, quantitative and qualitative studies performed on-line.

- The wall-jet cells should be recommended for quantitative analysis as it generates significantly higher analytical signal when compared with the flow-by cell.

4.2.3 Investigations of the Possibility of Sample/Reagent Mixing On-Line Using Ferrocene in Acetonitrile Containing 0.01 M $TBAPF_6$.

The above flow injection analysis experiments were performed in solutions that were prepared in batch. We attempted to mix the electrolyte and sample solution on-line by incorporating a mixing T-piece onto our FIA system. During on-line mixing the mixing T-piece originated a reaction (mixing) zone that was subsequently carried through a six port manifold into the detector. The efficiency of the mixing approach is of importance for convenient reaction development, to improve the analytical signal and reproducibility. Before analysis, we performed an experiment over a range of resultant flow rates to see its effect on the anodic peak height. The resultant mixing flow rate is the total flow rate of the background electrolyte and the sample solution.

For example, if one desires to measure a CV curve of a 50 mg/l ferrocene solution from a 100 mg/l ferrocene stock solution on-line one will pump both the background and sample solution at a flow rate of 4 ml/min resulting in a mixed solution with a total flow of 8 ml/min to the cell.

$$Q/q = C/c$$

Where Q = is the total or resultant flow rate to the cell

q = is the sample solution flow rate to the mixing T-piece

C = is the concentration of the stock solution

c = is the concentration of the sample solution to the cell

Therefore: $q = Qc/C$

$$q = \frac{(8\ ml/\min) \times (50\ mg/l)}{100\ mg/l}$$

$$q = 4\ ml/\min$$

$$\therefore Background\ \ flow\ rate\ to\ the\ mixing\ T-piece = Q - q$$

$$= 8\ ml/\min - 4\ ml/\min$$

$$= 4\ ml/\min$$

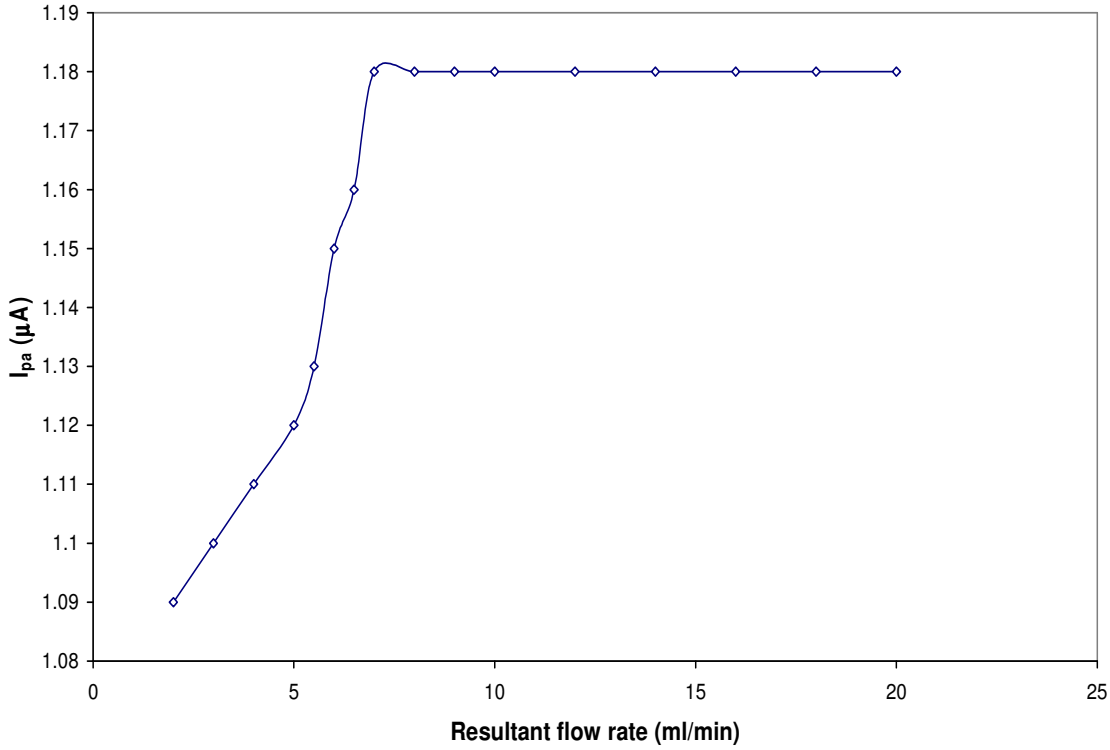

Figure 4.11 Plot of resultant flow rate vs. anodic peak current of ferrocene, v = 100 mV/s.

Figure 4.11 shows a plot of resultant mixing flow rate versus anodic peak current obtained in a ferrocene solution. The anodic peak current increased with an increase in mixing flow rate from 2 ml min^{-1} to 7 ml min^{-1} and remained constant from 7 ml min^{-1} to 20 ml min^{-1} (the highest studied mixing flow rate). It appears that from the resultant flow rate of 7 ml/min the stagnant layer remains constant as it has reached the smallest thickness, hence the signal does not increase further. From this data we decided to use 10 ml min^{-1} as the mixing flow rate in all experiments performed with on-line mixing.

The influence of on-line mixing on the CV curves of ferrocene was demonstrated by comparing the curve obtained with manual mixing to the one obtained with on-line mixing

(Figure 4.12). The peaks were enhanced when CV curves were recorded during on-line mixing and the analytical signal was improved. This behaviour arises because the solutions were prepared under controlled conditions with exclusion of moisture and any other particulate matters that can lead to contamination of solution. Comparison with a voltammogram obtained in a bulk solution (Figure 4.12, dotted curve) showed that the situation in a bulk solution approaches that in a flowing solution, when the analysed concentration of an analyte is prepared by hand using a syringe, in terms of signal intensity. It was not clear at this stage why the curve measured using an on-line mixing method was much higher or led to greater sensitivity as compared to those prepared in batch.

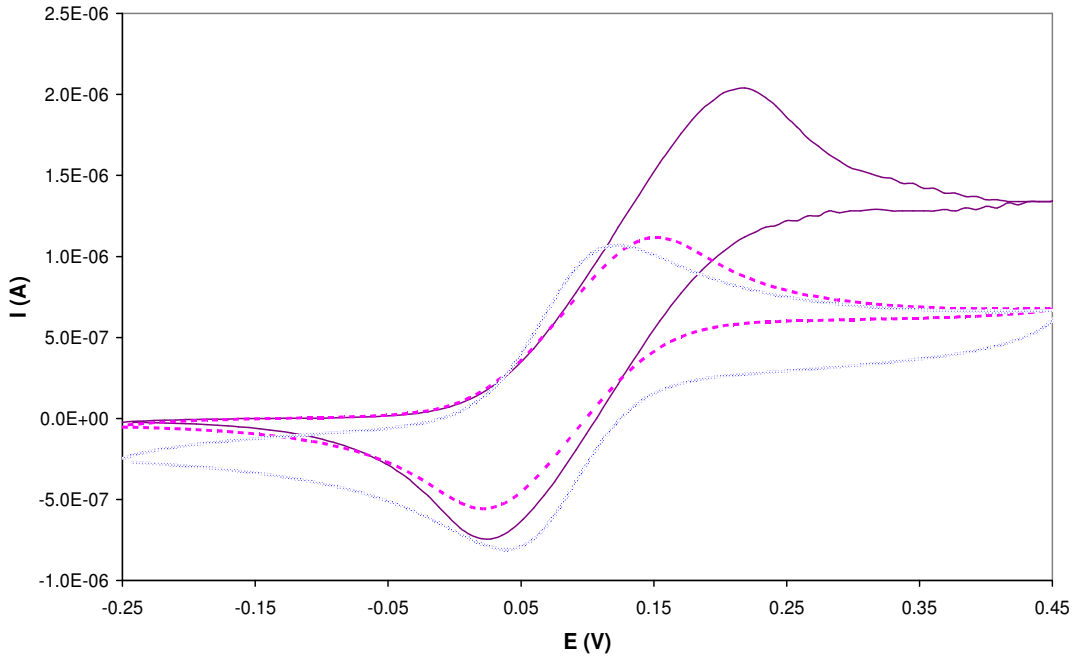

Figure 4.12 Comparison of the CV curves of a 20 mg/l ferrocene obtained in a flowing solution when the stock solution was prepared by hand (---) and using on-line (—) mixing technique, flow rate = 0.98 ml min^{-1} and v = 100 mV/s. The CV curve of 20 mg/l ferrocene obtained in a bulk solution (….) using an open cell at the same scan rate is also overlaid for comparison.

Quantitative analysis test of ferrocene at different concentrations was performed using on-line mixing approach. It must be noted that, one can prepare solutions of different concentrations by varying the flow rates of both the background and the sample solution.

Figures 4.13 and 4.14 shows CV curves obtained in different concentrations of ferrocene in a flowing solution with on-line mixing using a flow-by electrochemical cell. The peak intensity increases and the anodic peak shifts to higher potentials with an increase in

concentration. As a result the peak potential separation increased with an increase in concentration. This behaviour arises due to large IR voltage drop present in solution, which becomes significant in flowing solutions. Linearity was observed from a calibration curve constructed from CV curves obtained after background subtraction (Figure 4.15).

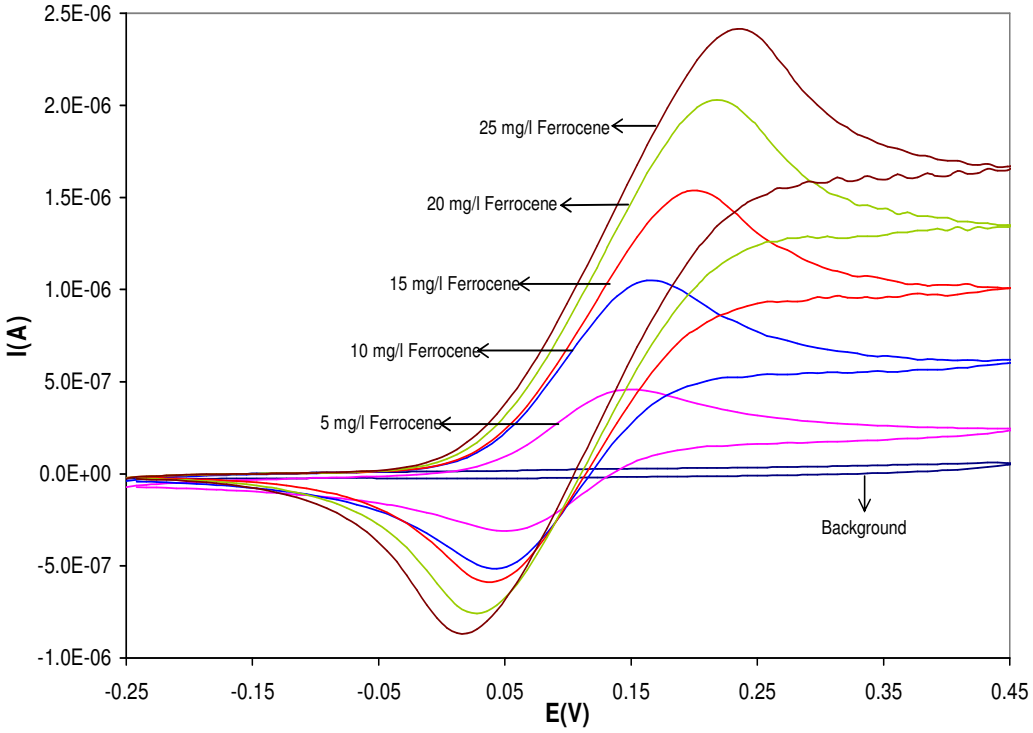

Figure 4.13 CV curves obtained from various concentrations of ferrocene in a flowing solution, flow rate = 0.98 ml min^{-1}, mixing rate = 10 ml min^{-1} and v = 100 mV/s.

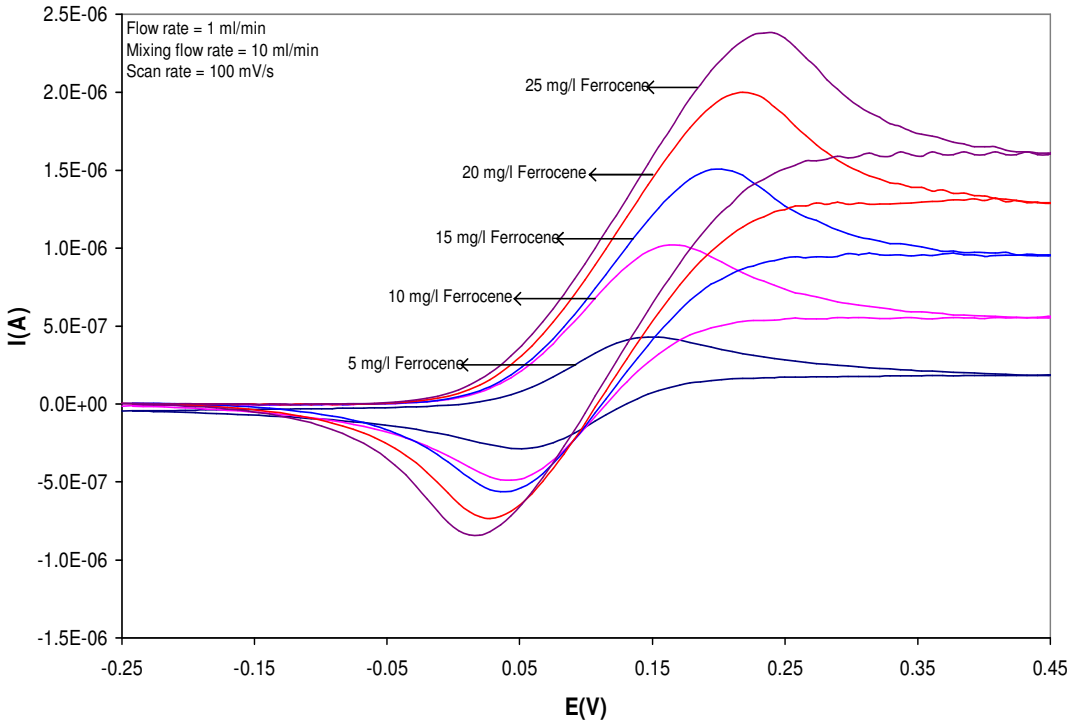

Figure 4.14 CV curves obtained in Figure 4.13 after background subtraction.

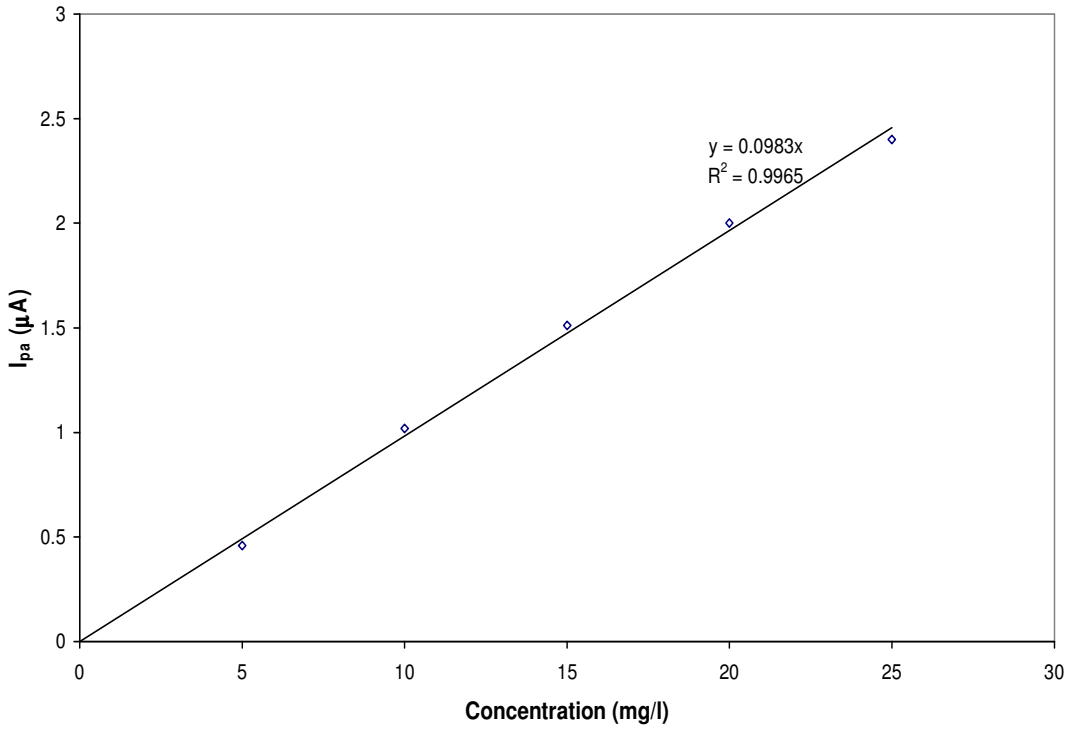

Figure 4.15 Calibration plot for data presented in Figure 4.14.

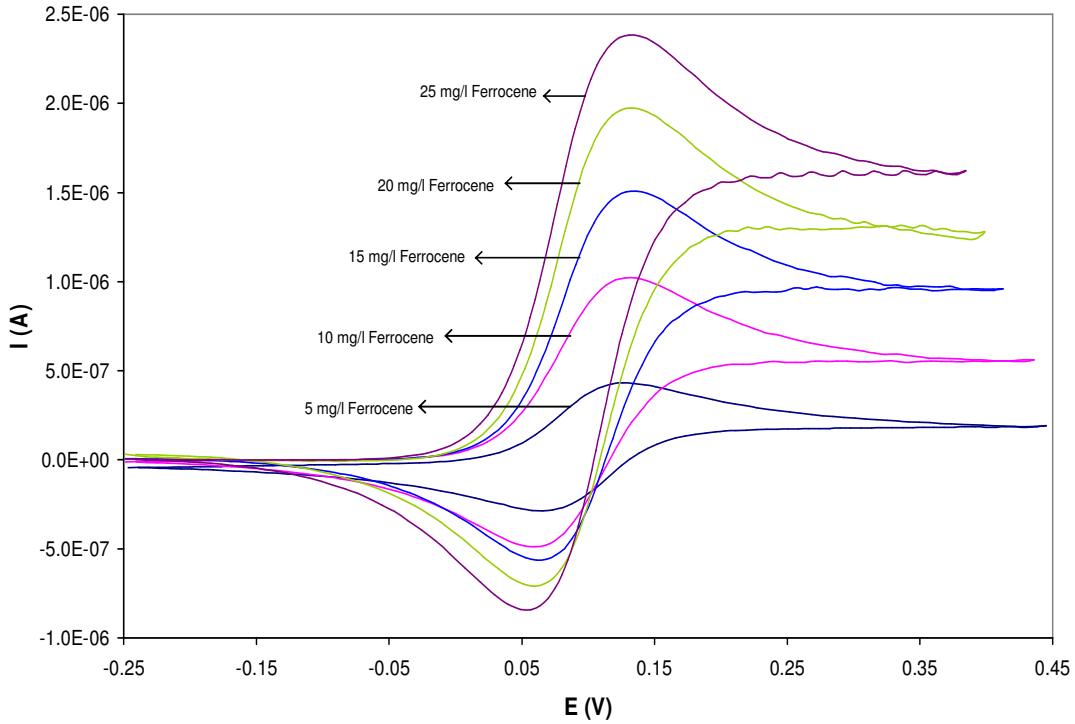

Figure 4.16 CV curves obtained in Figure 4.14 after IR voltage drop correction.

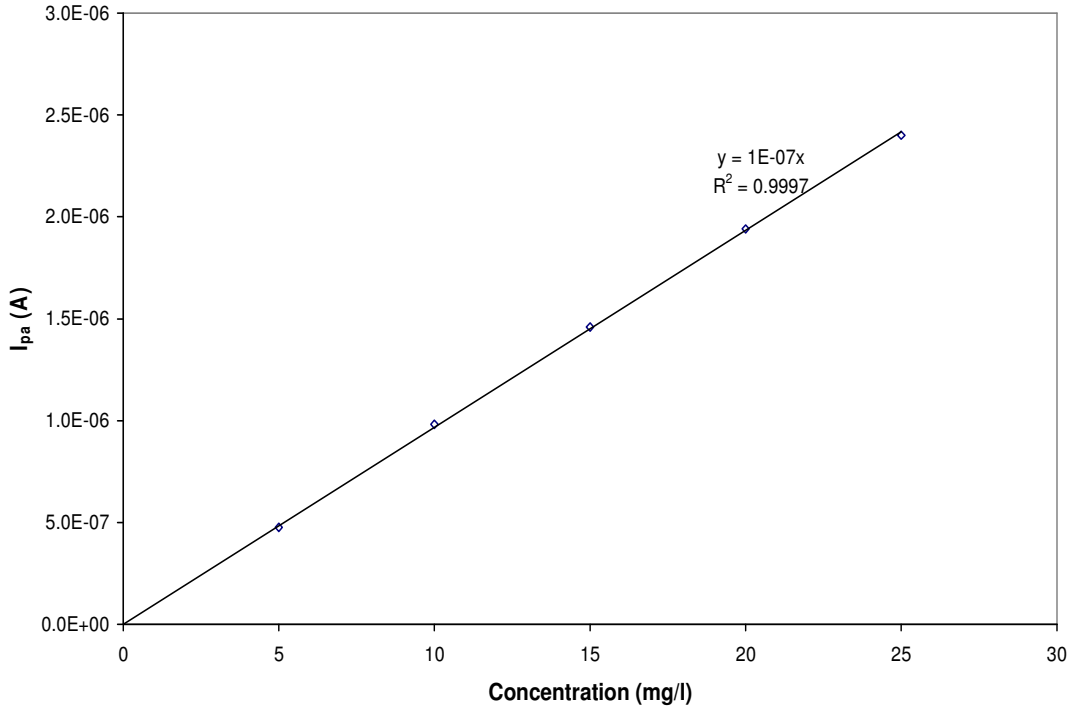

Figure 4.17 Calibration plot for data presented in Figure 4.16.

The CV curves obtained at different concentrations of ferrocene in Figure 4.14 where corrected for IR voltage drop with R = 34000 Ω and the new calibration plot was constructed. Figure 4.16 shows the CV curves obtained at different concentrations of ferrocene after IR voltage drop correction. The peak potential separation remained constant with increase in concentration. The calibration plot gave a linear relationship with concentration (Figure 4.17). IR voltage drop correction improved a calibration plot of ferrocene – almost a perfect straight line was obtained.

Most importantly, the anodic peak potential (E_{pa}) remained independent on the analyte concentration. This would allow applying constant potential, e.g. between 0.15 and 0.20 V for quantitative monitoring of the analyte. Without IR correction, it would be required to apply a large positive potential, which will vary with concentration of the analyte and might result in interferences from other oxidizable materials in cases where more than one compound is analysed or electroactive. It follows that IR drop plays a major role so one should redesign the cells to bring the reference electrode much closer to the working electrode to minimize IR drop and this can be achieved when using flow-by cell.